Wall-to-Wall Forest Mapping in Southeast and Southcentral Alaska: A New Application of the Gradient Nearest Neighbor Approach

by

Daniel R. Irvine

A PROJECT

submitted to

Oregon State University

in partial fulfillment of
the requirements for the
degree of

Master of Natural Resources in Forest Ecosystems and Society

Presented March 4, 2022
Commencement June 2022

ABSTRACT OF THE PROJECT OF

Daniel R. Irvine for the degree of Master of Natural Resources presented on March 4, 2022. Title: Wall-to-Wall Forest Mapping in Southeast and Southcentral Alaska: A New Application of the Gradient Nearest Neighbor Approach.

Boreal and temperate biomes host nearly half of the earth's forested ecosystems. The temperate rainforests of the Pacific coast of North America constitute nearly half of all temperate rainforests on earth. Along the northern extent of this region, the perhumid and sub-polar rainforests of southeast and southcentral Alaska are among the largest intact tracts of temperate rainforest in existence. These forests are globally significant for their role in storing and cycling carbon and are regionally and locally valued for their cultural significance, their provision of ecosystem services, and their economic importance. The cumulative impacts of historic management and uncertainties regarding future conditions under a changing climate have largely gone understudied in this important ecosystem. A relative dearth of spatially comprehensive information exists to describe detailed forest attributes at a resolution relevant for both informing management decisions and at an extent necessary to meet regional and national monitoring objectives.

This study demonstrates one approach to providing wall-to-wall forest attribute data across the forested areas of coastal southeast and southcentral Alaska using the Gradient Nearest Neighbor (GNN) method. I leverage field surveys from the USDA Forest Service Forest Inventory and Analysis (FIA) program collected across a 26-year timespan (1995-2020) with a set of spatially continuous environmental predictors and annual Landsat Timeseries (LTS) to produce spatially explicit 30-m predictions of forest structure and composition across the region. Spectral harmonization across sensors, a multi-step cloud masking procedure, and the spectral segmentation algorithm, LandTrendr, were implemented in Google Earth Engine (LT-GEE), to produce spatially complete annual imagery for model development. Model predictions were generally more precise and less biased in the boreal forest

biome of the western Kenai Peninsula, lending support for further exploration of the LandTrendr-GNN approach to broader monitoring efforts across Interior Alaska. In the coastal temperate rainforest ecoprovince, models tended to truncate distributions and overpredict some observation estimates, but overall agreement revealed relatively strong alignment with design-based estimates in this heterogeneous region.

Corresponding e-mail address: irvined@lifetime.oregonstate.edu

March 4, 2022

Acknowledgements

I am beyond grateful to my advisor, Dr. David Bell, and to my committee members, Matt Gregory and Dr. Robert Kennedy, for their efforts to help me develop and complete this project. Thanks especially to Dr. Bell for helping me to hone my research interests and focus, for always raising thoughtful questions, and for your tireless review of earlier drafts of this report. Mr. Gregory's patience for training a field biologist in python scripting and endless guidance and clarification through the technical aspects of imagery processing, model development, and nearest neighbor imputation and mapping were admirable. I also want to thank Dr. Harold Zald for his inspiration in the development and pursuit of this project, a longtime goal of mine.

This work would not be possible without the dedicated field crews of the Forest Inventory and Analysis (FIA) program in Alaska, who for decades have been swimming through salmonberry thickets, wading through wetlands, and clinging to mossy slopes in order to describe the state's forests. My colleagues at the USFS Pacific Northwest Research Station (PNWRS) have been encouraging and patient as I focused on this project that sometimes distracted me from other work. I also thank the PNWRS Civil Rights Action Group (CRAG, now Employee Voice and Action, EVA) for their financial support of this project. My amazing family and friends kept me positive even when things got tough! I owe so much to my wife and partner, Hannah Kurtz, for her unending support of my focus to accomplish this work in the face of a global pandemic and so much uncertainty in the world. Finally, I couldn't have done it without my trusty pal Doc who made sure I got outside for exercise each day and then kept me company while sleeping next to the woodstove during data analysis and writing.

Contents

Introduction

Spatially comprehensive data describing structural and compositional characteristics of forests are useful for a variety of management and monitoring objectives. Regional vegetation maps are used to assess changes in land use and land cover (e.g. Moisen et al. 2020), predict fire behavior (e.g. Pierce et al. 2009), estimate timber volume (e.g. Lister et al. 2005), predict suitable wildlife habitat (e.g. Lorenz et al. 2021), and estimate total and net carbon or biomass storage (e.g. Wilson et al. 2013, Kennedy et al. 2018a, Bell et al. *In Press*). Monitoring change over time can enable assessment of the impacts of or resilience to changes in climate (e.g. Schleeweis et al. 2020), assessment of impacts from specific land management policies or legislation (e.g. Davis et al. 2015), or assessment of trends in natural disturbances (e.g. Zhao et al. 2018, Cohen et al. 2018).

Boreal and temperate forests represent substantial components (30.6%, and 17.1%, respectively) of Earth's forests (Keenan et al. 2015) and comprise some of the largest tracts of intact forest land remaining (Wells et al. 2020, Dellasala et al. 2011). Alaska's 52.2 mil ha of forests comprise an estimated 17% of total US forestland (Andersen 2019), with over 6.1 mil ha of forest in the southeast and southcentral region of the state (Cahoon et al. 2020). Much of this region is strongly influenced by a maritime climate and includes the perhumid and subpolar temperate rainforests of Alaska (~4.5 mil ha) as well as a portion of the boreal forest biome (~1.6 mil ha) in the transition zone of the western Kenai Peninsula along Cook Inlet (Cahoon et al. 2020). The forests of southcentral and southeast Alaska are subject to a complex administrative framework and host a more intensive history of management than much of the northern boreal forests in the state (Alaska Forest Association 2021, Marcille et al. 2021). The coastal temperate rainforests contribute substantially to the regional economy (e.g. Johnson et al. 2019), are regionally and locally valued for their cultural significance (e.g. Johnson et al. 2021) and may represent an important contribution to global carbon cycling (e.g. Buma and Barret 2015, McGuire et al.

20178, Genet et al 2017). They are described as being among the most intact tracts of coastal temperate rainforests in the world (Alaback 1991, Dellasala et al. 2011); yet despite their global and regional significance, a relative lack of consistent spatial data exists to help inform management decisions affecting forests across the region.

In southeast and southcentral Alaska, a variety of techniques have been employed in attempts to create spatially complete maps of vegetation attributes. However, mapping efforts in the region face several challenges. The vast size and remote nature of the region contributes to the risk, difficulty, and expense of collecting field observations, resulting in relatively few observational forest structure and composition datasets that represent the range and distribution of vegetative conditions. The USDA Forest Service Forest Inventory and Analysis (FIA) program provides the most comprehensive observational dataset across the region, yet even this regional forest survey is restricted to lands outside USFS Wilderness and Glacier Bay National Park. Forest inventory across the remote boreal regions of Interior Alaska face similar challenges (e.g. Barrett and Gray 2011) and a systematic statewide forest inventory was not initiated until 2014 (USDA 2014).

Remote sensing instruments also face challenges imposed by Alaska's high latitudes, steep and complex topography, and unfavorable weather patterns. Persistent cloud cover, atmospheric mist, and cloud shadows can lead to missing and inaccurate spectral values in remote sensing scenes (e.g. Braaten et al. 2015, Zhu and Woodcock 2011, Zhu and Woodcock 2014). Steep topographic relief, particularly on northern aspects in northern latitudes, can contribute substantially to terrain shadowing due in part to low sun angle (e.g. Stow et al. 2004, Beamish et al. 2020) and can impact reflectance values, misrepresenting surface conditions (e.g. Giles 2001, Gu and Gillespie 1998, Hantson and Chuvieco 2011). Finally, structurally complex forests with multilayer canopies cast shadows which can be useful to defining such forest characteristics (e.g. Cohen and Spies 1992), but also complicates the interpretation

of topographic shading (e.g. Kane et al. 2008) and can lead to pixel saturation and difficulty distinguishing characteristics between pixels (e.g. Lu et al. 2016). Heterogeneity within and between stands can also present a challenge when sensor pixel size is greater than the typical forest patch size (e.g. Ohmann et al. 2014).

Despite the challenges, many broad vegetation mapping initiatives have been undertaken in Alaska. The first spatially comprehensive mapping initiative in southeast Alaska began in the 1970s, with delineation of stereo-pair aerial photography into relatively homogenous polygonal timber volume classes across USFS managed lands (USDA 2012); these timber volume maps served to inform management decisions on federal lands in the region for decades. In 1997, the Tongass National Forest Land Management Plan (USFS 1997) required updates on the timber resources across the National Forest, so digitized timber volume maps were improved by integrating ground survey data along with topographic information to collapse stand data into statistically significant distinct classes (Julin and Caouette 1997).

Over the next decade, several other attempts to map forest and vegetation classes in the region were attempted. In 2004, Corne et al. used artificial neural networks to predict forest characteristics using a classification algorithm based on coarse digital elevation model (DEM) derivatives and the southeast Alaska FIA database. Caouette and DeGayner (2005) conducted multivariate analyses of forest volume class and ancillary datasets to refine earlier methods of classifying USFS managed forests in southeast Alaska using metrics of density (SDI) and size (QMD). Caouette and DeGayner in 2008 further refined their multivariate technique to improve classification accuracy and prediction of tree size and density but focused specifically on the productive old growth forests of southeast Alaska. Meanwhile, a consortium of US federal agencies collaborating to develop tools and techniques for classifying land cover, vegetation, and land use patterns (the Multi-Resource Land Characteristics, MRLC) employed

classification and regression tree algorithms to classify 30-m Landsat pixels and create National Land Cover Database (NLCD) and Landscape Fire and Resource Management Planning Tools (LANDFIRE) layers across Alaska representing model years of 2001, 2011, and most recently, 2016. These land cover maps rely on large databases of both field collected and remotely sensed training data from a variety of federal agencies to produce land cover and fuels characteristics maps for broad-scale planning applications (Jin et al. 2019). Given the potential importance of Alaskan forests in contributing to global carbon cycles, Blackard et al. (2008) used regression tree algorithms to predict aboveground live tree forest biomass at a nominal pixel size of 250-m across Alaska, based on composites from the Moderate Resolution Imaging Spectrometer (MODIS) along with several remotely sensed environmental datasets and classified vegetation datasets from NLCD.

More recently, Buma and Thompson (2019) employed a machine-learning decision tree classifier, Random Forests (Breiman 2001), to map aboveground forest C in unmanaged forests across southeast Alaska, leveraging field data from the FIA program in the region with a remotely sensed DEM and tree cover data from a MODIS and Landsat model known as Vegetation Continuous Fields (VCF, Sexton et al. 2013). Wang et al. (2019) also employed Random Forests and machine learning, with clustering and interpretation of field photography, to classify annual vegetation cover between 1984 and 2014 using 30-m Landsat pixels across Alaska and Canada as part of the Arctic Boreal Vulnerability Experiment (ABoVE). Landcover change assessment mapping work has also been undertaken in southeast and southcentral Alaska as part of the Landscape Change Monitoring System (Cohen et al. 2018, Healey et al. 2018). In each case, efforts have either focused on predicting specific forest attributes across specific land ownership or administrative units, on areas representing specific management or disturbance histories, or on predicting general landcover or vegetation classifications.

Objective

A gap in the existing body of work is a spatially continuous dataset representing the nature and arrangement of forest structural and compositional attributes available to inform land management and policy decisions in coastal southeast and southcentral Alaska. Furthermore, spatially complete models representing detailed forest attributes can contribute to regional efforts to research and monitor the status of land use and land cover change, and the effects of policy decisions, natural disturbances, and changes in climate on forests. This study aims to build upon previous mapping efforts in Alaska by addressing several of the challenges to effective forest modeling in the region: 1) leveraging a robust set of field observations from the USDA Forest Service Forest Inventory and Analysis (FIA) program in coastal Alaska collected across three decades, 2) applying a combination of cloud-filtering techniques to screen pixel values attributable to persistently unfavorable atmospheric conditions, and 3) incorporating 26-years (1995-2020) of harmonized LTS imagery corresponding to field observation years, temporally smoothed using the LandTrendr algorithm scripted in Google Earth Engine (LT-GEE). I employ a nearest neighbor imputation technique to map a suite of forest structural and compositional attributes across a broad geographic area in southeast and southcentral Alaska.

The Gradient Nearest Neighbor (GNN) imputation technique (Ohmann and Gregory 2002) provides a framework for mapping a wide array of forest attributes across a landscape by modeling forest structure and composition using a direct gradient analysis, specifically Canonical Correspondence Analysis (CCA; ter Braak 1986). Models are constructed relating species-size forest characteristics based on discrete field measurements to spatially comprehensive environmental predictor covariates, and results are imputed across the landscape using nearest neighbor imputation based on weighted Euclidean distance from the gradient analysis (Bell et al. 2015a). Cloud-based automated Landsat time series image processing (Kennedy et al. 2018b) presents an opportunity to dramatically improve the

speed of standardizing and extracting spectral data used as predictors in model development. The advantage of nearest neighbor imputation is that any forest attribute which can be calculated from observations at discrete field locations used in model development can then be imputed to similar pixels across the landscape.

In this study, I map a detailed set of structural and compositional attributes across all forested areas of southeast and southcentral Alaska, including the coastal temperate rainforest and the boreal transition area of the western Kenai Peninsula, inclusive of all management histories and across ownership and jurisdictional boundaries (Figure 1). I present model outputs at a pixel size of 30-m, in spatially consistent raster grids representing a modeling year of 2019, the most recent year in which spatially unbiased field survey data exist across the entire study area. In addition, I provide a detailed multi-scale accuracy assessment of maps within each modeling region to help potential users understand best practices for interpretation. I assess the location, magnitude, frequency, and type or nature of errors present in the modeled data and offer insights regarding opportunities for further research based on the strengths and limitations I observed with the GNN modeling approach as applied in the temperate and boreal regions of southeast and southcentral Alaska.

Specifically, my objectives for this study were two-fold:

1) To implement the LandTrendr-GNN approach to modeling and mapping a detailed set of forest attributes in high-latitude forests and to evaluate the effectiveness and accuracy of this approach, and

2) To illustrate one potential application of the mapping products in a management context, with an example in the perhumid temperate rainforests of the Tongass National Forest.

Land Acknowledgement

The region of interest in this study encompasses lands traditionally inhabited by a broad and diverse group of Alaska Native cultures and communities. In the southeast, the area encompasses traditional lands of the Haida, Tlingit, and Tsimshian. Farther north, along the Gulf of Alaska Coast, traditional stewards of the land included the Eyak; in Prince William Sound, down the southern coast of the Kenai Peninsula and across Kodiak Island, the Chugach Alutiiq / Sugpiaq, and across the boreal region of the Kenai peninsula north beyond Anchorage and into the Matanuska Valley lie the traditional lands of the Dena'ina (Krauss et al. 2011). For thousands of years, these Alaska Native cultures have been the traditional stewards of these lands and have relied upon an abundant provision of natural resources to subsist and thrive. The Alaska Native people who inhabited these lands long before Russian or Euro-American occupation were forcibly assimilated to western cultures and economic systems through a variety of government sponsored programs and legislation, particularly during the 20th century (University of Alaska Fairbanks 2022). It is my hope that this research will provide useful information for Alaska Native Tribal governments, communities, and corporations to make informed decisions as they navigate land management challenges in the face of changing climatic, socio-economic, and cultural conditions.

Motivation: Socio-Economic Context and a Brief History

Today, the forests of coastal southeast and southcentral Alaska are managed by a variety of federal, state, and local government agencies, Alaska Native Corporations, Tribal governments, and private individuals (Cahoon et al. 2020). The forests of this region and the communities who rely upon them have been subject to a variety of federal legislative actions over the past century which have contributed to dramatic swings in management approach, responsibility, and objectives. Understanding

the political, legislative, economic, and social history surrounding forest management in the region helps contextualize the motivation for undertaking this work. This study was motivated largely by a view that land management and policy decisions in general are better informed by more complete information regarding the resources they seek to govern.

The coastal temperate rainforests of Alaska have a relatively brief but expansive history of commercial forest management across jurisdictions (e.g. Brackley et al. 2009). Economic factors (e.g. Marcille et al. 2021), along with political influence (e.g. Dunleavy 2021) and a history of complex legislative actions transferring administrative jurisdiction and fiduciary responsibility among stakeholders have largely shaped management regimes across the region. Several legislative actions in the last half of the 20th century (i.e. the Alaska Statehood Act, the Alaska Native Claims Settlement Act [ANSCA] and the Alaska National Interest Lands Conservation Act [ANILCA]) transferred large tracts of high value timber from federal management to the state of Alaska and to Alaska Native Corporations in efforts to compensate Alaska Native populations for federal appropriation of their traditional homelands. Alaska Native communities were faced with complex decisions regarding their relationship to their lands and resources, the economic futures of their communities, and how they should be recognized by the federal government (Herz 2021). The organization of Alaska Native Corporations under ANSCA promoted the commercialization of Native lands to support economic development.

To further encourage economic development in the region during the 20th century, the US federal government offered long-term timber contracts to private corporations on large swaths of federal land (Alaska Forest Association 2021). The government was motivated to provide economic stability to a nascent industry in the region in order to support economic and population growth of communities in the region. Commercial logging in southeast Alaska peaked in the 1970s when nearly 500 million board feet (MMBF) of old growth timber were harvested per year, primarily from the most

densely populated stands of large trees (Fennel 2016). By the 1990s, the adoption of a multitude of regional and national land management policies drastically changed the industry in Alaska. Policies including the National Forest Management Act (NFMA, 1976), the National Environmental Protection Act (NEPA, 1970), and the Tongass Timber Reform Act (TTRA, 1990) were designed to balance the economic benefits of timber production more appropriately with the other social and ecological benefits that forests provide. Under the TTRA, the cancellation of long-term timber contracts in southeast Alaska ultimately shrunk annual timber harvest to less than 10% of their peak in the 1970's (Alexander et al. 2010), and commercial timber production now comprises less than 1% of the region's economy (Southeast 2019).

The development and subsequent shrinking of the timber economy in southeast Alaska, in combination with the creation of Alaska Native Corporations and the transfer of much productive forest land from federal to corporate management has contributed to a complex socio-economic landscape for forest management. Land transfers among USFS, the state of Alaska, Alaska Native Corporations, and private individuals continue under a number of federal legislative programs (e.g. ANSCA, ANILCA, ASA, MHTEA, Dunleavy 2022). These transfers contribute to the difficulty of projecting future forest conditions in the region and the complexity of understanding trends in regional forest conditions, as management objectives and management statutory requirements differ among landowners and land designations.

The 2001 Roadless Area Conservation Rule restricted development and management on some 3.7 mil ha (~55%) of the Tongass National Forest, designating these lands as Inventoried Roadless Areas. Several attempts have since been made to alter or reduce the restrictions imposed by this legislation (USDA 2021a). Most recently, the state of Alaska in 2018 petitioned USDA for a state-specific exemption to the 2001 Roadless Rule (Alaska Roadless Rulemaking 2020). In 2020, the exemption was granted in

full, following the exit of all six cooperating Alaska Native Tribal governments from the process (USDA 2021a). In turn, nine southeast Alaska Tribal governments petitioned USDA to undertake a new effort to protect their traditional homelands, arguing that USDA had inappropriately disregarded cooperator and public input during the review process. On November 23, 2021, USDA filed a new proposed rule in the Federal Register, seeking to undo its 2020 exemption for the Tongass National Forest and to re-instate the 2001 Roadless Rule protections (USDA 2021a).

Dramatic shifts in management objectives over large areas of federal land are not unusual in the US (e.g., Federal Register 2021), but they add to the uncertainty of future conditions on these landscapes and erode confidence in government commitments to protecting the heritage and cultural values of Native communities. Acknowledging the value of Alaska Native input in regional planning, recent research (e.g. Vynne et al. 2021) and some US government programs to promote economic and community vitality in southeast Alaska today explicitly call for the inclusion and involvement of Alaska Native communities (USDA 2021b). The Tongass National Forest comprises approximately 80% of the land area in the coastal temperate rainforest zone of southeast Alaska (Cahoon et al. 2020). While the Tongass has indicated since 2010 an intent to shift priorities from old-growth harvest towards young-growth management (Pendleton et al. 2013) as an acknowledgement of the many values these forests provide, part of the difficulty in making the transition lies in an incomplete understanding of the quantity, quality, and location of young growth stands across the Forest (Fenster 2022). It is in the context of this complex history of management and policy that I am motivated to contribute to our understanding of the condition and arrangement of forests across southeast and southcentral Alaska.

Methods

Study Area

The study area for this project encompasses the regions of southeast and southcentral Alaska, spanning 7 degrees of latitude (54°N to 61°N) and 24 degrees of longitude (130°W to 154°W), from the Canadian border in the southeast to the Kodiak Archipelago in the southwest, including the Kenai Peninsula and the Anchorage Bowl (Figure 1). Though comprising just under 13% of the state of Alaska, the area is immense (22.0 mil ha), characterized by dramatic topographic and climatic gradients and encompassing a host of diverse ecosystems including more than 6.1 mil ha of forest (Cahoon et al. 2020). Broadly, two ecological provinces are represented in the study area, with the Alaska Range Transition ecoprovince represented on the western Kenai Peninsula and north, but with most of the study area comprised by portions of the temperate Coastal Rainforest ecoprovince (Nowacki et al. 2002).

These two ecological provinces are further comprised of six ecosections, broad characterizations of geologic and ecological conditions, climate, and disturbance regimes across the landscapes of southeast and southcentral Alaska (Figure 1). The western Kenai Peninsula and the Anchorage Bowl comprise portions of the Cook Inlet Basin ecosection within the Alaska Range Transition Province and represent a transition to the boreal forest biome, characterized by cooler winters, warmer summers, and far less annual precipitation than the temperate maritime region (Nowacki et al. 2002). In contrast, ecosections within the Coastal Rainforest ecological province are characterized generally by warmer winters and cooler summers, with substantial annual precipitation (Figure 2).

Ecosections in the Coastal Rainforest province encompass the perhumid and subpolar rainforest zones (Alaback 1996), the northernmost temperate rainforests in North America. In the southeast portion of this ecoprovince, the Alexander Archipelago is comprised of thousands of islands along the

Pacific coast. Unique island biogeography and climatic conditions moderated by the hyper-maritime environment contribute to the region's mild temperatures (-3°C - 8°C annual average) and extreme precipitation (1212 -8604 mm annually; Daly et al. 2018). Just inland of the Alexander Archipelago along the Pacific Coast mountains in southeast Alaska, the Boundary Ranges ecosection comprises the zone between the hyper-maritime environment of the Archipelago and the continental climate influence of northern British Columbia and the Yukon Territory.

North and west, the Gulf of Alaska Coast ecosection is comprised by a relatively narrow band of post-glacial ecosystems sandwiched between the Pacific Ocean and the Chugach and St Elias ranges, stretching from Icy Strait in the east to Kachemak Bay in the west and characterized by temperatures moderated by its proximity to the ocean and high precipitation. The Chugach-St Elias Mountains comprise a rugged and expansive ecosection just inland of the Gulf of Alaska Coast, with dramatic topographic relief contributing to the more extreme temperature and precipitation gradients. Finally, the Kodiak Archipelago at the western boundary of the study area is characterized by its own ecosection (Kodiak Island) where topographic gradients are less extreme, the maritime influence moderates temperatures, and precipitation declines dramatically from east to west. More dramatic topographic gradients across these broad regions accompany steeper temperature (-26°C - 7°C annual average) and precipitation (299 – 9897 mm annually) gradients as well (Daly et al. 2018).

Broad forest community characteristics and associated disturbance regimes in the study area are largely driven by the climatic and environmental gradients. Across the temperate ecoprovince, co-dominance by *Picea sitchensis* is ubiquitous, with primary associates including *Tsuga heterophylla, Thuja plicata, and Callitropsis nootkatensis* in the south, and with *Pinus contorta* present particularly near wet forest openings, and *Tsuga mertensiana* increasing in prevalence at higher elevations. To the north and west along the Gulf of Alaska Coast, through Prince William Sound and the eastern Kenai Peninsula, *Tsuga mertensiana* co-dominates the forests all the way to sea level, with *Picea sitchensis* dominating

the coniferous maritime forests exclusively in the Kodiak Archipelago. Hardwood associates are less common in the maritime ecoprovince, particularly in the Alexander Archipelago in the southeast, and include *Alnus rubra* and *Populous balsamifera-trichocarpa* primarily occupying disturbed areas and riparian corridors, respectively. Widespread natural fire is essentially absent from the landscape in the maritime ecoprovince, and natural disturbance regimes are characterized by frequent small scale wind events, as well as larger mass movement and wind events, particularly in landscape positions predisposed to exposure. Among the most widespread disturbances characterizing forests of the southern portion of this region today is Alaska yellow-cedar decline, a condition driven by decreases in consistent winter snowpack associated with climate change (Buma et al. 2017, Beier et al. 2008), though some effects of yellow-cedar decline on population dynamics of *Callitropsis nootkatensis* are debated (e.g. Bidlack et al. 2017).

In contrast, forests of the western Kenai Peninsula in the Cook Inlet Basin are characterized by deciduous boreal tree species including assemblages of *Betula neoalaskana, Populous tremuloides,* and *Populus balsamifera,* and conifers including *Picea mariana,* and *Picea glauca.* This region is characterized as a transition zone to the Interior Alaska boreal forest biome, as permafrost is nearly absent and temperatures in the region are still somewhat moderated by the maritime influence of Cook Inlet. Community composition in this region is largely driven by complex interactions among edaphic factors (e.g. soil texture, drainage, temperature), microclimate, and disturbance history (ADFG 2022). *Populus tremuloides* and *Picea glauca* occur primarily on well drained sites, and *Populus tremuloides* tends to occupy warmer upland, south facing slopes, while *Picea mariana* tolerates poor drainage and lowland areas. *Betula neoalaskana* and *Populus balsamifera* can be found across a range of site conditions and tend to quickly colonize disturbed sites following stand replacing disturbance events. Disturbance regimes characterizing the forests of the western Kenai Peninsula are distinct from the temperate ecoprovince, shaped by widespread insect outbreaks and landscape-scale fires, often resulting in

widespread mortality and stand replacing events, more typical of boreal Interior Alaska forests (e.g. Baughman et al. 2020).

Field Reference Data

In this study, field survey records were used as training data for model development and to compute forest attributes for mapping. A robust sample of ground conditions representing the entire range and distribution of systems being modeled is necessary when vegetation models are constructed across broad geographic regions or covering diverse ecological conditions. The FIA dataset provides an unbiased sample of ground conditions with known measures of accuracy and precision accomplished using standardized quality assurance protocols (Bechtold and Patterson 2005). The landscape is sampled systematically, with the entire land base tessellated into equal area hexagons (2428 ha) each containing one randomly located sample plot. Plots are screened in the office utilizing aerial or satellite imagery for classification, and only plots classified as forest (>10% tree cover [1995-2003, 2014-2020] or >10% tree stocking [2004-2013]) or potential forested (not subject to a land use preventing tree establishment and growth and meeting a minimum area criteria) are measured on the ground (USDA 2021c). Each plot consists of a cluster of four 168.11 m^2 subplots within which trees ≥12.7cm DBH are measured, and each subplot contains a nested microplot (13.496 m^2) on which small trees (≥2.54cm, <12.7cm DBH) are measured. Subplots are spaced 36.576 m on center, over approximately a 0.64 ha area, and together comprise a ground sample of approximately 672.44 m^2 (0.067 ha) including all four subplots.

On each forested plot, and during non-forest surveys of vegetated USFS-managed lands in Alaska (2011-2020), field crews characterize general land conditions including evidence of present land use and past disturbance and collect a suite of basic mensuration attributes on qualified trees within each sampling unit. Trees are identified by species, their status is determined (live vs. dead), and

individual tree measurements include diameter at breast height (DBH), tree actual (unbroken) and total bole length (height measured along the stem), compacted crown proportion, crown class, and any qualifying evidence of damage is recorded. In addition, data were collected to characterize the understory vegetation, downed woody material, and the forest floor but were not used in this study. In Interior Alaska, additional FIA measurements include an expanded microplot to capture more small tree measurements, soils cores to characterize carbon and nutrient ratios, and a survey of the macrophytic lichen community comprising the forest floor.

In southeast and southcentral coastal Alaska, widespread surveys targeting productive timberlands took place initially during the 1950s, with surveys across the rest of the state beginning in the early the 1960s (LaBau 2013). However, a systematic inventory of all forested lands in the region of southeast and southcentral Alaska, regardless of productivity or ownership, was not initiated until 1995. ln 2004, the survey converted to an annualized inventory in which a more spatially balanced portion of plots across the entire region was measured each year (Figure 3). In a nod to the logistic complexity of traveling throughout this remote region each year, the 'panelization' of plots scheduled for annual field measurement in the coastal Alaska FIA unit was produced randomly rather than systematically, to promote geographic clumping across the unit (A. Gray, personal communication, November 2021). Importantly, the survey excludes the land managed by Glacier Bay National Park (~1.3 mil ha), and only included USFS designated Wilderness areas on the Tongass National Forest and recommended Wilderness areas on the Chugach National Forest during a single survey year in 2005. Together, these lands excluded from the inventory account for some 25% of the study area (Cahoon et al. 2020).

Image Processing

Landsat sensors (TM, ETM+, and OLI) provide a spatially complete and temporally continuous spectral dataset at a nominal 30-m pixel size which allows for landscape- to global-scale analyses of earth systems. With multiple operational sensors in orbit, Landsat provides approximately 8- to 9- day observation intervals across most of the archive (Young et al. 2017, Masek et al 2020). Given the broad extent (22.0 mil ha) and temporal span (1995-2020) of the study area and period, significant processing of the Landsat imagery was necessary to build effective annual composites prior to use.

Image pre-processing steps included alignment and harmonization of the Landsat sensors across generations (Roy et al. 2016, Young et al. 2017), masking of snow, clouds, and shadow (Zhu and Woodcock 2011, Google 2022), combining the Landsat collections from different sensors, reducing each annual collection to a single day, and finally calculating an appropriate spectral index for use in the segmentation algorithm. A focal year of 2019 was selected in which to model forest attributes, as this was the most recent year with a "complete" spatially unbiased sample of FIA field data available at the time of initial model development. All pre-processing steps were completed using scripts in the LT-GEE guide (Kennedy et al. 2018b), parameterized to the study area and time horizon, and updated by M. Gregory for the inclusion of additional cloud masking (Appendix 1).

Following sensor harmonization, initial assessments of imagery composites in the study area indicated that persistent cloud cover would still pose problems in some areas despite the masking algorithm (Figure 4), so I included an additional cloud masking step using Google's Simple Cloud Score (threshold = 30, Google 2022). The Simple Cloud Score algorithm identifies top of atmosphere (TOA) reflectance values with a combination of relatively high brightness in the visible and infrared bands and relatively low temperature, but avoids confusion with snowy pixels by using the normalized difference snow index (NDSI) to assess the relative likelihood of cloud cover. I determined an appropriate threshold

for the Simple Cloud Score by comparing masked and unmasked imagery across the study area in locations known to harbor persistent cloud cover during the growing season. I balanced aggressive masking of cloudy pixels with a desire to achieve maximum spatial coverage of imagery over each year of field reference data and over the entire study area. The two-step cloud masking procedure struck the appropriate balance and appeared to be sufficient to continue with imagery composite development.

After masking clouds, shadow, and persistent snow, I reduced each annual collection to a single image using a medoid function to identify a representative sample for each year. For each pixel in an annual collection, the medoid is identified by minimizing the sum of squared differences (SSD) between a multi-band pixel's raw values and the median values for each band calculated for that pixel from the annual collection. The medoid preserves the relationships among bands in a multi-band pixel by selecting the image date in which the SSD is minimized across all bands (Flood 2013) . Finally, images across the annual collections were transformed for input to the segmentation and smoothing algorithm LandTrendr (Kennedy et al. 2010).

LandTrendr

LandTrendr (Landsat-based detection of Trends in Disturbance and Recovery) provides an algorithm for automated image processing which builds a Landsat time series (LTS) for each pixel within a designated area of interest where each image in a stack represents a single year (Kennedy et al. 2010). Fitted image stacks are created with user-defined bands or spectral indices. A model is constructed representing the spectral signature of each pixel, with each year representing a node. I used the Normalized Burn Ratio (NBR) for the segmentation algorithm to identify pixel trajectory, vertices, and outliers.

LandTrendr exploits the trajectory of the spectral signature through time, filtering statistical anomalies but flagging distinct and persistent changes in the trajectory of each pixel. Dramatic changes in the trajectory of image segments between years (disturbance) are represented by a vertex following which the pixel takes a new trajectory during subsequent years (Figure 5). In years where a suitable cloud-free pixel cannot be identified or where a spectral value is missing from the sensor, the constructed model fills the missing value based on 'good' data from surrounding years. Similarly, the model promotes smoothing by preventing identification of a vertex with subsequent recovery following just a single year (despiking), in order to limit the introduction of noise from anomalies misrepresenting the true spectral trajectory of the pixel. From fitted image stacks, annual composites can be mosaicked across the landscape to provide spatially and temporally complete LTS.

The LandTrendr algorithm scripted in Google Earth Engine (LT-GEE, Kennedy et al. 2018b) provides a user interface to define model parameters (Table 1) and to facilitate access to the massive archives of publicly available imagery databases. I used GEE for image pre-processing and for running the LandTrendr algorithm to facilitate efficient processing of large geospatial datasets without straining local computing resources. LandTrendr in GEE was used to produce annual composites of georeferenced raster grids (GEOTIFFs) across the study area for each year between 1995-2020. Characteristics of vegetation density and vigor across the study area were calculated from the annual Landsat composites using the Tasseled Cap indices.

The Tasseled Cap (TC) transformations (Kauth and Thomas 1976, Crist and Cicone 1984) provide a set of spectral indices effective at capturing changes in the density and vigor of vegetative foliage (Tasseled Cap Greenness, TCG), surface reflectance from the particles which make up the bare earth (Tasseled Cap Brightness, TCB), and surface moisture (Tasseled Cap Wetness, TCW). Tasseled Cap Brightness is a weighted sum of the visible, near infrared, and shortwave infrared bands, such that areas

of the landscape which actually appear to be brighter in the visible spectrum, in fact are associated with higher TCB values. Tasseled Cap Greenness on the other hand is a weighted contrast between the visible and infrared bands, owing to high absorption in the visible spectrum but high reflection in the near infrared (NIR) by live foliage. Finally, TCW contrasts the sum of the visible and NIR bands with the sum of the shortwave infrared (SWIR) bands as soil and plant moisture are correlated with greater reflectance in the SWIR portion of the spectrum. Taken together, the TC indices provide an illustration of portions of the visible and infrared spectrums sensitive to changes in vegetation cover and vigor, helpful for reducing the broad array of Landsat spectral data to three key indices (Cohen and Goward 2004).

Gradient Nearest Neighbor Model Development

Canonical Correspondence Analysis (CCA) is a direct gradient analysis of constrained ordination and is the modeling framework underlying the nearest neighbor imputation technique known as Gradient Nearest Neighbor (GNN; Ohmann and Gregory 2002). This approach is robust to the nonlinear responses expected of vegetation communities to environmental gradients, and to response matrices containing many null values and without normal distributions as is common in plant community ecology (Palmer 1993). Further, environmental gradients are often correlated (e.g. elevation and temperature) and seldom meet the assumption of predictor independence required of techniques such as multiple linear regression. Canonical Correspondence Analysis was used to construct models of tree basal area by species and size class across multiple environmental gradients. In CCA, the ordering of community characteristics (plots) in model space reflects linear combinations of the environmental gradients measured, allowing predictions of community composition based on coefficients derived from a number of axes representing weighted combinations of environmental gradients. Once models are developed representing the complex relationships between environmental predictors and community

characteristics, community traits can be predicted (imputed) across the landscape wherever a complete set of environmental data are available.

Forest attributes from the FIA plot measurements were used to compute both the modeling variables and the mapping variables in Python 3 (Van Rossum and Drake 2009). I constructed models using tree basal area (BA, m^2 ha^{-1}) by species in 25cm DBH size classes, computed at the plot level (sum of BA across all four subplots). Plots with no trees present were assigned a dummy species, NOTALLY, with a dummy BA computed from a single dummy tree record with DBH 2.5 cm. Summaries of plot species presence were reviewed to identify species with sparse support for inclusion in model development. The scarcity of data representing rare features across the landscape makes predicting their presence and abundance difficult (e.g. Engler et al. 2004). Previous evidence suggests that nearest neighbor imputation is relatively poor at predicting rare features, particularly where $k>1$ (*sensu* Ohmann et al. 2014). Thus, only species with presence on >5% of field plots within a modeling region were included in model development.

Modeling Regions

I stratified the study area into three modeling regions, roughly aligning with existing ecological sections, to help constrain the ordination so that only neighbors from roughly similar ecological conditions would be considered candidates (Figure 1, Nowacki et al. 2002). Modeling regions were broad enough to encompass sufficient field plot measurements (~>300) to inform model development (M. Gregory, personal communication, Table 2). In my study area, the Alexander Archipelago ecosection contains the greatest density of field plot measurements (2493) and represents modeling region 101 (MR101). The western Kenai Peninsula and Anchorage Bowl within the Cook Inlet Basin comprise modeling region 105 (MR105) and contains a moderate density of field plot measurements (744).

Finally, the four ecosections comprising the relatively narrow band of mountainous terrain along the mainland and spanning from the farthest southeast extent of the study area north and west along the gulf coast, and including the Kodiak Archipelago, were combined to create modeling region 110 (MR110). Although together the Boundary Ranges, Chugach-St Elias Mountains, Gulf of Alaska Coast, and Kodiak Island span the latitudinal and longitudinal extent of my study area, they each represent a relatively narrow band of forested area within the maritime ecoprovince and individually host relatively small populations of candidate field plots. The total number of field plots ultimately included in model development for MR110 was 1699 (Table 2). After delineation of each modeling region, a 10km buffer was applied to the region boundaries (Ohmann et al. 2012) so that any field plot measurements within the 10km buffer were included in model development to improve sampling near the edges of ecological and climatic gradients and to limit the introduction of artificial boundaries in my models. Seamless regional predictions were ultimately created by trimming the buffer and mosaicking modeling region raster grid predictions in ArcGIS.

Environmental Covariates

To represent environmental gradients that constrain forest composition and structure, I identified a series of spatially continuous environmental datasets for mapping forest attributes across landscapes. Spatially continuous environmental raster datasets (Table 3) were derived from publicly available sources but required several pre-processing steps to ensure consistency in projection, scale, and alignment for use in analysis. All environmental raster datasets were additionally converted to integers for space efficiency.

I used NASA's ASTER GDEM3 (NASA 2018), a 30-m Digital Elevation Model (DEM), to create 30-m raster grids representing topographic gradients including aspect, slope, topographic position index (TPI)

and heat load index. I transformed aspect measured in degrees to aspect in radians using a cosine transformation and rescaled these values by 100. I calculated percent slope from the DEM and rescaled values by 100 as well. I calculated TPI at three scales (300m, 450m, and 1000m) to represent landscape position in the context of nearby terrain features at multiple extents (Weiss 2001). Finally, I used McCune and Keon's (2002) Heat Load Index (HLI) to estimate potential direct solar radiation. Heat Load Index computes potential surface heat loading using aspect, slope, and latitude, but without regard to atmospheric conditions, nearby terrain features or daily solar insolation models. Furthermore, HLI is recommended for use only south of 60°N latitude, so I included it as a predictor in model development with caution.

Climate plays an important role in driving forest structure and composition, so several climatological datasets covering the region were explored (e.g. SNAP CRU (Leonawicz et al. 2015), USFS-RMRS (Taylor et al. 2012, Abatzoglou and Brown 2012)) for use in model development. Oregon State University's PRISM (Daly et al 2018) datasets for Alaska represent precipitation and temperature means between 1981-2010, coinciding best with the timeframe of field observations (1995-2020) and representing the most current climate data available for the region. From the PRISM climate data, I computed several specific metrics: minimum December temperature (DECMINT), maximum summer temperature (defined as the maximum temperature observed between June – August over the 30 year period, SUMMAXT), average annual temperature (ANNTMP), and average annual precipitation (ANNPRE; Table 3). Seasonal patterns of temperature and precipitation in particular may contribute to and constrain the capacity for species-specific tree growth and recruitment in the region (Alaback 1996, Dellasala et al. 2011), and were found to be significant predictors of community structure and composition in Pacific Northwest temperate rainforests (e.g. Ohmann and Gregory 2002). Together, I

expected these metrics to characterize important components of the aboveground abiotic environment which drive and constrain forest development.

Soils hydrology and drainage characteristics are also thought to play an important role in driving forest structure and composition across the coastal Alaska region (e.g. Buma et al. 2016, Bisbing et al. 2016). The National Resource Conservation Service (NRCS) provides spatially continuous soils hydrology, structure, and classification information across parts of Alaska at nominal resolutions of 10-m to 30-m (NRCS 2022). Three NRCS soils classifications layers from the Soil Survey Geographic Database (SSURGO) were explored as environmental covariates in the model to assess the role of hydric soils classes, drainage classes, and water availability classes on prediction of forest attributes. However, vector-based soils classification data in the region are based on sampling at various intensities, with lower resolution appearing particularly in Wilderness and other extremely remote areas (personal observation of SSURGO layers). Canonical Correspondence Analysis can be sensitive to binned data, sometimes leading to outsized influence on resulting imputation surfaces, predicting sharp contrasts in relatively uniform areas (D. Bell, personal communication). Soil characteristics were ultimately removed from model development upon close inspection of imputed map characteristics which revealed patterns of forest attribute predictions mirroring the soils layers even when forests appeared relatively uniform in high resolution imagery (Figure 6).

Predictor Variable Extraction & Plot Footprint

Spatially continuous environmental predictor datasets were re-projected to EPSG:3338 (NAD83 Alaska Albers) and snapped to a common grid to ensure alignment across the study area. The climatological datasets were resampled (downscaled) from 771m to 30m using bilinear interpolation and all raster grids were clipped to the study area boundary. A nine-pixel (3 x 3) area (0.81ha) around

each field plot coordinate location was sampled and the mean pixel value extracted to represent the environmental conditions associated with the plot (Figure 7). For environmental predictor variables with a time component (annual LTS composites of TC indices), the nine-pixel mean value was extracted only from spectral index surfaces coinciding with the field plot measurement year (1995 - 2020). All other predictor variables were assumed to be constant (topographic) or were averages representing mean values occurring during a timeframe approximately overlapping the study period (climatic). In this way, each field plot measurement included in model development was associated with a suite of environmental predictor variables.

Nearest Neighbor Imputation & Forest Attribute Mapping

Nearest neighbor imputation allows any number of attributes measured at discrete locations (plots) to be mapped across the landscape based upon a set of spatially comprehensive predictor variables. In this study, I tested the application of GNN (Ohmann and Gregory 2002) for forest vegetation mapping in southeast and southcentral Alaska by modeling and assessing prediction accuracy for six structural attributes (Table 4) as well as tree species presence. For both CCA and nearest neighbor imputation, I utilized pynnmap (Gregory and Roberts 2020), a robust python library and application built for creating vegetation maps using nearest neighbor methods. Pynnmap facilitates the integration of CCA with nearest neighbor imputation based on a set of user-defined predictor and response datasets and options for model parameterization. Neighbors were identified in CCA gradient space by minimizing weighted Euclidean distance where axis scores are weighted by their eigenvalues.

Forest structural attributes were imputed to 30-m pixels using a k=7 weighted imputation where the seven nearest neighbors (in gradient space) to each pixel contribute to the imputed value based on a weighted average. The selection of k=7 and neighbor weighting (Table 5) was based upon previous work

estimating model uncertainty from nonparametric bootstrap sampling (Bell et al. 2015a) and a desire to balance locally accurate (single pixel) model predictions with prediction accuracy over greater extents (e.g. Riemann et al. 2010) while creating a realistic map appearance (Eskelson et al. 2009, Ohmann et al. 2014). By comparison, species attributes (BA by species) were imputed using only the single nearest neighbor (k=1) in order to constrain commission errors occurring due to the likelihood of species presence in at least one of the nearest seven neighbors (e.g. Ohmann et al. 2014, Henderson et al. 2014).

Following imputation, maps of individual attributes were clipped to the extent of each modeling region to remove the buffer, mosaicked, and then masked. I applied a mask to the imputed maps to limit inference to forested areas. I built a composite mask using USFS tree canopy cover data (Megown 2016) to mask out all areas classified has having less than 10% tree canopy cover and a 2016 NLCD (Dewitz 2019) landcover layer to mask areas classified as anything other than naturally vegetated land. The tree canopy cover layer performed better at masking apparently non-forested areas near the treeline, but performed relatively poorly at masking developed areas (Figure 8). I found that only including lands classified as forest in the NLCD layer tended to exclude many recently disturbed but clearly forested areas (e.g. clearcuts). However, the NLCD landcover layer was more successful at masking developed land conditions. Ultimately, I found that combining the two criteria (NLCD classification of naturally vegetated and tree canopy cover ≥ 10%) resulted in the most reasonable mask which omitted most developed pixels and clearly non-forested natural areas (Figure 8).

Plot Screening

The FIA field observations comprising the reference dataset provide an unbiased representation of the range and distribution of forest land classes in the study area. Because the focus of this study was

to map forested lands, only plots comprised by at least 50% forest land (defined as >10% tree cover [1995-2003, 2014-2020] or 10% stocking [2004-2013], USDA 2021c) were included in modeling. Forest Inventory and Analysis plots may be sub-divided by field crews who classify forest and other lands based on condition classes. It would be possible to pre-screen plots more strictly based on field classification of conditions, but I balanced a desire to include heterogeneous plots to better represent mixed and fragmented areas (*sensu* Riemann et al. 2010) with a need to build models based upon plots representing relatively uniform conditions over the 3x3 pixel area representing the plot footprint (e.g. Ohmann et al. 2014). Thus, I began model development including all plots passing the coarse filter (>50% forest), and applied subsequent screens based on individual review of the LTS spectral indices, high resolution digital imagery, and individual plot location records created during field visits. Plot screening was an iterative process in order to refine models by retaining as much field reference data as possible while weeding out those plots which may confound the model.

I used pynnmap to identify outliers by reviewing an intermediate imputation output which allows plots to identify as their own nearest neighbor. Specifically, I used three steps to review potential outliers. First, I identified all plots with a mismatch between the predicted and observed Vegetation Class (VEGCLASS) considered to be egregious (Table 6). Vegetation Class is a categorical variable representing 11 combinations of tree canopy cover, proportion of basal area occupied by hardwood tree species, and quadratic mean diameter (QMD). Independently, I used pynnmap to create an index to rank all neighbors for every plot in the model and noted the neighbor position at which a plot identified itself. Finally, plots which did not self-identify as one of their own 30 nearest neighbors *or* were identified as egregious mismatches between observed and predicted VEGCLASS values were reviewed individually by comparing high resolution satellite imagery and LTS TC indices, using several additional criteria to screen outliers (Table 7).

I selected a neighbor position index threshold of 30 based on time limitations restricting the ability to evaluate all plots. Based on ad hoc evaluation of high resolution versus LTS imagery, I also determined that far fewer plots self-imputing at positions below 30 tended to screen out based on the additional criteria. By far the most common criterion used to identify outliers at this stage was plots straddling a distinct boundary (e.g. mature forest adjacent to recent clear-cut or wet opening). Plots that straddled distinct boundaries and demonstrated strongly mixed values in the TC indices across the 3x3 pixel area of the plot footprint were removed. Similarly, plots which experienced a major disturbance between the date of measurement and the date of imagery acquisition (rare due to the alignment between imagery and measurement years) would introduce a mismatch between the spectral values and the measured forest attributes (e.g. McRoberts et al. 2016) and were screened out. After each application of the screening criteria, the direct gradient analysis and neighbor selection steps were repeated. This screening process was repeated until all egregious VEGCLASS mismatches were either tossed or explained, and the only plots remaining in the model which self-imputed at positions beyond 30 had been reviewed and did not appear to fail any of the additional screening criteria (Table 7). Few plots were ultimately screened out using the VEGCLASS metric for outlier identification due to apparently poor performance of regression equations at representing actual tree canopy cover, based on my evaluation of high-resolution satellite imagery and plot location records compared with canopy cover calculations at individual plots (see Discussion: FIA Field Observations).

Accuracy Assessments

I evaluated the accuracy of imputed maps to determine how effective models were at estimating structural attributes and tree species distributions. For brevity and simplicity, I selected six structural attributes *a priori* (Table 4) on which to focus the accuracy assessment and subsequently to

illustrate a potential application of these data. Several assessments were conducted to evaluate the location, magnitude, frequency, and nature of errors present in model predictions. This evaluation does not include an estimation of the variance of imputed surfaces (e.g. McRoberts et al. 2007), but I discuss the value of understanding uncertainty of estimates generated using model predictions in order to facilitate appropriate use and interpretation of mapped attributes (e.g. Nelson et al. 2021).

The use of FIA field observations for model evaluation presents both strengths and limitations. The strengths of the FIA dataset lie in its ability to provide unbiased area estimates of a wide range of forest attributes. The sampling intensity of the FIA grid, however, does not enable a focused assessment of fine spatial patterning (ca. 10 ha - 100 ha) observed in mapped predictions. Thus, a combination of approaches was employed to measure the accuracy of estimates and to evaluate the spatial arrangement of predicted forest attributes.

Accuracy assessments were conducted by comparing model predictions to observations from field plots within each modeling region at a variety of aggregation areas (e.g. Riemann et al. 2010), and by comparing predictions with high-resolution satellite imagery to evaluate fine spatial patterning of predicted surfaces (e.g. Nelson et al. 2021). I conducted the assessments at multiple scales and across six structural forest attributes, reporting a number of statistics describing the range and distribution of estimates, as well as the relationship between predicted and observed datasets. I also compared predicted tree species distribution maps to their observed distribution on field plots to evaluate the effectiveness of model predictions of forest compositional attributes.

Local Accuracy

In both local and multi-scale accuracy assessments, predictions are calculated as an unweighted average of the nine (3x3) pixel area coinciding with the plot footprint, using a modified leave-one-out cross validation (Ohmann and Gregory 2002) which prevents pixels from self-imputing (i.e. the observation at a given plot location is not used to create predictions for the same location). Predictions are compared with estimates computed from observations at the coincident plot location. I report a number of statistics for assessing the goodness of model fit to the observed data at the local (plot-pixel) level, at three intermediate extents, and at the extent of each modeling region as a whole.

At the local level, the Pearson correlation coefficient (Pearson's r) is used to evaluate the closeness of the two datasets to a linear relationship, and to describe the strength and direction (positive or negative) of the correlation. I also report a normalized root mean squared error (NRMSE), which provides another measure of the disagreement between observed and predicted values at the plot-pixel level, to enable comparison among attributes, where larger values indicate poorer prediction accuracy. Percent bias provides an indication about whether predictions tend to over- or under-estimate observations by normalizing the difference between predicted and observed values. Where a percent bias is positive, models are overestimating compared to observations; negative values indicate underestimation, and a value of 0.0 is optimal, indicating no consistent tendency for over- or under-estimation of attribute predictions. Finally, I report a simple coefficient of determination (R^2) as another mechanism for evaluating the amount of variation in observed values explained by the model.

Multi-Scale Accuracy

Area-based assessments at multiple scales facilitate an evaluation of the influence of spatial extent on prediction accuracy. Based on the procedures of Riemann et al. (2010), I tessellated the

landscape into hexagons of three sizes representing a range of areas potentially useful for reporting design-based FIA estimates (8,660 ha, 78,100 ha, and 216,500 ha). At each extent, I estimate structural attributes using two methods: a sample of model predictions based on the *k*=7 surfaces from the nine-pixel area coinciding with actual plot locations, and a design-based estimate computed using field observations over the same extent. The predicted versus observed estimates over each extent were compared using a number of statistics to describe the relationships between the datasets.

Because the FIA field data are used both as reference data for validation (observations) and in model development (predictions), a linear regression line can be developed between the two datasets using the symmetric geometric mean functional relationship (GMFR, Ricker 1984) to account for error in both the observed and predicted values. I compared the GMFR to the 1:1 line representing a perfect relationship between each dataset for each of six structural attributes. Differences between the datasets can be characterized by both systematic and unsystematic errors. The systematic agreement coefficient (AC_{sys}) describes the slope of the GMFR line in relation to the 1:1 line, illustrating *systematic* biases in either dataset (e.g. an attribute that is routinely under- or over-predicted when compared with observations). The unsystematic agreement coefficient (AC_{uns}) reflects the amount of scatter around the 1:1 line or a lack of estimate precision. Together, the agreement coefficient (AC) describes the relationship between two datasets, accounting for both bias and precision, where a value of 1 indicates perfect agreement and values of ≤ 0 indicate no agreement. Finally, I reported the Kolmogorov-Smirnov (KS) statistic (Massey 1951) to describe differences between the distributions of predicted versus observed estimates. I reported the mean and maximum KS values, describing the distance between predicted and observed empirical cumulative distribution functions (ecdf), where KS_{max} values indicate the extent of the greatest divergence between the two dataset distributions, while larger KS_{mean} values indicate greater overall divergence in distribution between the two datasets. I evaluated these metrics

for comparison of observed versus predicted datasets across a range of extents across the study area to assess trends in prediction accuracy with scale.

Regional Accuracy

To evaluate model prediction accuracy over the broader study area, I assessed structural attributes and species predictions at the extent of each modeling region and over the study area as a whole. For each of the six structural attributes, I compared the range and distribution of predicted versus observed estimates within each modeling region. Predicted total (or average [mean], as appropriate), of each of the six structural attributes were also compared with observed estimates (simple averages or expansions, not post-stratified), calculated by modeling region. For variables with published regional estimates available from other sources, I compared predicted model estimates with those published data covering the study area as well.

Species Accuracy

To identify the nature and frequency of species prediction errors within each modeling region, I constructed a matrix of species presence/absence at each field plot location for both predicted and observed values. For each species, I calculated the kappa coefficient (*k,* Cohen 1960) to describe the level of agreement between predictions and observations not attributable to random chance. I also assessed the proportion of correct predictions at each plot where an observation exists. Finally, I created maps of predicted versus observed species presence across the study area (Appendix 2) to evaluate and compare spatial patterns between the two datasets in relation to modeled environmental gradients.

Illustration of GNN

I used the Tongass National Forest (TNF) to illustrate a potential application of modeled forest attribute data in southeast Alaska. Based on the results of the multi-scale accuracy assessment, I summarized structural forest attributes by land category. Lands with surface ownership in the TNF were classified into three categories: congressionally designated Wilderness, inventoried roadless areas (IRA), and Other areas. Structural attributes were also binned to simplify comparisons for illustrative purposes. To assess the abundance of high biomass forested area, live aboveground tree biomass predictions were binned according to Krankina et al. (2014); Quadratic mean diameter (QMD) predictions were binned according to Caouette and DeGayner (2008), and stand height predictions were binned into equal interval 10m height classes (Table 8). Each metric was summarized by area across land categories on the TNF as a whole using Zonal Statistics and Tabulate Area tools in ArcGIS.

Additionally, I selected six focal regions across the study area to illustrate successes and challenges encountered with the GNN mapping approach in the region. Although I have not calculated uncertainty statistics in the imputed vegetation maps (e.g. McRoberts et al. 2007, Olofsson et al. 2013), I review the efficacy of capturing fine spatial patterns with a series of examples that span the geographic range, climatic and topographic gradients, and include a variety of management histories across forested landscapes in the study area. Maps were compared with high-resolution satellite imagery in each focal area to assess predictions and the 'look and feel' of GNN maps in southeast and southcentral Alaska.

Results

Accuracy Assessments

Local Accuracy

Models performed moderately well predicting structural attributes at the plot level across the study area. All live structural attributes were predicted moderately well in the maritime ecoprovince (MR101 and MR110), while metrics of volume and biomass, including snag biomass, were predicted more accurately in the boreal transition zone (MR105, Table 9). In the maritime ecoprovince, stand height predictions were particularly strong in MR101 (Pearson's correlation = 0.71) followed by other live structural attributes. Normalized RMSE also indicated lower prediction error in measures of size and density attributes compared to live volume and biomass, ranging from 0.35 (stand height) to 0.85 (live tree volume) in MR101 and MR110. In general, prediction error characterized by NRMSE at the plot-pixel level was slightly greater across attributes in the boreal transition zone as compared to the maritime ecoprovince (Table 9), but Pearson's correlation between predicted and observed values indicated stronger agreement for both live and dead biomass estimates in the boreal transition zone. Snag biomass prediction NRMSE values were >1 across all modeling regions, but Pearson's correlation indicated substantially better agreement between predictions and observations in the boreal transition zone than the maritime ecoprovince (Table 9). Similarly, with the exception of snag biomass (boreal R^2 = 0.35) and stand density (boreal R^2 = 0.49), correlation between predictions and observations were somewhat stronger across the maritime ecoprovinces compared with those in the boreal transition zone.

At the local (plot-pixel) level, models generally over-predicted structural attribute values when compared with observation estimates across the study area. The magnitude of bias was greater overall for structural attributes in the maritime ecoregion where predictions consistently overestimated

observed values (Table 9). In the boreal transition zone, prediction bias was mixed, with underestimates of QMD_DOM (-0.76%) and STNDHGT (-0.37%), but prediction overestimates of SDI_REINEKE as well as live and dead biomass. Across the maritime ecoprovince, directional bias was entirely positive, with the greatest magnitude of prediction bias occurring in overestimates of live biomass and volume (Table 9).

Multi-Scale Accuracy

In general, agreement between model predictions and estimates based upon FIA field observations improved with increasing extent, although the results were inconsistent among attributes and among modeling regions (Table 10). Agreement coefficients near and below zero (AC < 0.25) for all structural attributes indicated poor prediction accuracy at the smallest aggregation area (8,660 ha) across both ecoprovinces. However, prediction precision improved and bias decreased with increasing areas of aggregation. At the broadest area of aggregation (216,000ha), models of live structural attributes demonstrated relatively strong agreement with the observation datasets and little directional bias in all modeling regions (e.g. aboveground live tree biomass, Figure 9). Snag biomass showed poor agreement between predictions and observed estimates across all aggregation extents in the maritime ecoprovince (MR101 and MR110), but agreement improved with increasing area of aggregation in the boreal transition zone (MR105) and agreement was strong (AC = 0.96) at the largest area of aggregation in this region.

Unsystematic agreement (AC_{uns}) was greatest (closest to 1) at the largest area of aggregation (216,000 ha) across the study area, indicating improved precision of predictions across all structural attributes and modeling regions with increasing extent. Precision of predictions was highest in the boreal transition zone ($0.75 < AC_{uns} < 0.98$) and among live structural attributes in the maritime ecoprovince. Systematic agreement (AC_{sys}) was also greatest (nearest to 1) at the largest aggregation

area across modeling regions, indicating less directional bias in predictions with increasing sample size, though little difference was observed between the smaller two units of aggregation for most attributes (Table 10). Interestingly, aggregation at the intermediate 78,100 ha extent revealed a mixed response in AC_{sys} across attributes, in many cases indicating no improvement in prediction bias except at the broadest area of aggregation.

Some patterns of agreement between prediction and observation datasets also varied across structural attributes and modeling regions. In MR101, the agreement coefficient (AC) indicated no relationship ($AC < 0$) between predicted and observed estimates of volume or biomass at any except for the broadest (216,000 ha) extent. The size and density metrics (QMD_DOM and SDI_REINEKE) on the other hand improved dramatically with each increase in aggregation area. In the boreal transition zone (MR105), agreement of all attributes improved dramatically between the 8,660 ha and 78,100 ha extents, but only volume and live and snag biomass agreement continued to improve substantially between the 78,100 ha and 216,000 ha extents (Table 10). At the broadest extent, predictions of snag biomass in this region demonstrated little directional bias ($AC_{sys} = 0.98$) or scatter ($AC_{uns} = 0.98$). In contrast, snag biomass exhibited little agreement between predicted and observed estimates ($AC < 0.18$) at any extent across the maritime ecoprovince.

The distributions of structural attribute predictions were largely similar to those of observation datasets across the study area. In all modeling regions and across attributes, KS statistics remained nearly constant or increased slightly with increasing area of aggregation, indicating a consistent relationship between distribution patterns of predictions and observations across extents. This pattern may also be suggestive of heterogeneity in the observation dataset (wide distribution) which was curtailed in predictions at all extents of aggregation. Indeed, maximum differences between observed and predicted distributions across live attributes were somewhat large ($0.11 < KS_{max} < 0.23$) regardless of

aggregation extent. The mean difference, however, across the distributions of attributes and across extents, KS_{mean}, was much smaller ($0.02 < KS_{mean} < 0.10$), indicative of the overall similarity of prediction to observation distributions, and the likelihood that high KS_{max} values are attributable to the truncated ranges near distribution tails in most predictions.

Agreement between predicted and observed values was particularly strong in MR105, perhaps a reflection of the relatively dense sample size (84 plots) within each hexagon and the relatively small number of 216,000 ha hexagons present (9) within the modeling region (Table 10). By comparison, MR110 hosted a sparser sample of just 28 plots per hexagon across 57 hexagons at this extent, owing to its geographic expanse across broad non-forested areas. Sparse plot support in the regions of Glacier Bay National Park and USFS Wilderness contribute to the lack of estimates across these areas at the smallest aggregation extent (Figure 10). But viewed across the extent of the study area in its entirety, the aggregated estimates align with broad spatial patterns of biomass reported elsewhere (e.g. Blackard et al. 2008).

Regional Accuracy

I used Zonal Statistics in ArcGIS to summarize structural attribute predictions at the regional level and to assess similarities between modeled and observed dataset ranges and distributions. In general, the distributions of predicted values were similar to observation data as suggested by the KS_{mean} statistic, but ranges were somewhat truncated for most attributes where estimates approached lower and upper limits (Table 11), particularly in attributes with long distribution tails such as aboveground live biomass (Figure 11).

Across the study area, size and density attribute predictions tended to resemble the distribution of observation estimates most closely, with mean and median values for predictions of QMD_DOM, SDI_REINEKE, and STNDHGT all within 20% of the observed averages, and most within 10% (Table 11). Predicted minima and maxima of biomass and volume estimates were curtailed more substantially than were the ranges of the size and density attributes in all modeling regions. In the boreal transition zone, mean prediction estimates for structural attributes were nearly identical to observation means overall. However, predictions of live volume and live and snag biomass demonstrated an overall more pronounced shift in distributions towards the distribution center, reflected in median values (Table 11). In MR101, predicted mean snag biomass (36.5 Mg ha^{-1}) was very similar to the observed mean (34.3 Mg ha^{-1}), but the truncated tails resulted in substantially higher median predictions (31.7 Mg ha^{-1} predicted, 13.9 Mg ha^{-1} observed).

Species Accuracy

Models of species basal area by size class were created by constraining imputation to the *k*=1 nearest neighbor. I mapped predicted species presence across the study area and compared predicted presence with the mapped locations of observations from the FIA dataset (Appendix 2). Qualitative assessments of the geographic distribution of predictions of individual species abundance indicate relatively good alignment with reported species distributions (Little 1971). Similarly, comparisons between predicted and observed species presence maps indicate general agreement between estimates over broad geographic areas (Appendix 2). The spatial distributions of species along environmental gradients also appeared to align with published descriptions (Hulten 1968, Viereck and Little 1986, Alaback 1991), particularly where environmental gradients are dramatic and species distributions are distinct as seen across the Kenai mountains from Cook Inlet to Prince William Sound (Figure 12).

Still, errors of commission (predicted present, observed absent) were far more common than errors of omission (Table 12) and thus I recommend map users exercise caution when interpreting maps of species presence (Appendix 2), particularly when making interpretations near the edges of a known range. Errors of commission occurred nearly an order of magnitude more often than errors of omission across nearly all species and all modeling regions, findings consistent with GNN species predictions maps in the Pacific Northwest (M. Gregory personal communication). This finding is particularly evident in the predicted distributions of *Picea sitchensis* and *Tsuga mertensiana* in the Kodiak Archipelago, well beyond their observed ranges (Appendix 2). Predictions of species presence on the landscape reflect locations with similar combinations of the environmental predictor attributes to those occurring at sites where a species was observed. However, models are incomplete representations of reality, and many potential factors that were not included in the CCA (e.g. dispersal distance and mechanism, soils characteristics, hydrology, microenvironmental factors, etc.) also limit species distributions. Additionally, species presence predictions might be improved by inclusion of latitude and longitude as predictor variables to help constrain the selection of geographically distant neighbors.

In the maritime ecoprovince, comparisons of predicted versus observed presence at each FIA field plot location indicated the strongest prediction accuracy in MR101 of *Pinus contorta* (kappa = 0.41) and *Thuja plicata* (kappa = 0.40), whose ranges are fairly restricted in the region by topographic, competitive, edaphic factors, as well as latitude, respectively (e.g. Bisbing et al. 2016, Caouette et al. 2015, Neiland 1971). Although *Populus balamifera-trichocarpa* was accurately predicted 99% of the time, this species was so infrequently observed on the landscape in MR101 (10 instances observed present), the low kappa coefficient (0.09) reflects the likelihood that high prediction accuracy was largely a reflection of its low prevalence in the dataset. Prediction accuracy in MR110 was substantially higher overall as indicated by the kappa coefficients for *Picea glauca*, *Picea mariana*, *Tsuga heterophylla*,

and *Betula neoalaskana* (Table 12). Each of these species tends to occur in distinctive climatic zones across this region which may contribute to the strength of their differentiation in predictions. In contrast, *Picea sitchensis* occurs across much broader geographic ranges and elevational gradients within the forested areas of MR110 yet was still predicted accurately 76% of the time (kappa = 0.40).

Species prediction accuracy in the boreal transition zone (MR105) was generally lower than in the maritime ecoprovince, with strongest prediction accuracy for *Picea mariana* (kappa = 0.40), followed by *Tsuga mertensiana*, *Populus tremuloides*, and *Picea sitchensis* (Table 12). Among the most common conifer species of this region, *Picea glauca* presence was predicted surprisingly poorly (kappa = 0.03). It is possible that prediction accuracy in this region could be improved with the inclusion of additional primary drivers of forest composition in the boreal transition zone such as aerial disturbance maps, soil hydrology, and drainage.

Regional Estimates of Biomass

I estimated live tree and snag biomass across the study area extent to evaluate GNN model predictions against published datasets. Since several other studies have excluded USFS Wilderness and Glacier Bay National Park (GLBA) in their estimates, I report model results both including and excluding these areas to enable comparison (Table 13). Importantly, these protected areas comprise approximately 23% of total forestland in the study area and are present only in the maritime ecoprovince (MR101 and MR110).

Total aboveground live tree biomass predictions were substantially greater across the study area when USFS Wilderness and GLBA were included (1,680 Tg) compared to regional predictions excluding these protected areas (1,225.4 Tg), with increases due to both greater forest area and to

greater mean aboveground live biomass in the protected areas of USFS Wilderness and GLBA (Table 13). Predictions of live tree volume, both on a per-hectare basis and total, were also greater when including USFS Wilderness and GLBA in regional estimates, but snag biomass on a per-area basis was very similar with and without inclusion of the protected areas (Table 13).

Aboveground live and dead biomass predictions were both lower than design-based estimates reported by Cahoon et al. (2020) on a per-area basis over the same region (excluding USFS Wilderness and GLBA but covering the period 2004-2013, Table 13). Yatskov et al. (2019) also estimated higher aboveground live and dead biomass over a somewhat smaller but overlapping region, covering the period 1995-2003 (Table 13). However, predictions of total regional aboveground live biomass were within one standard error of design-based estimates reported by Cahoon et al. (2020) and were similar to the aboveground live biomass estimate reported by Yatskov et al. (2019) after adjusting for area (Table 13). The pattern was inconsistent in the boreal transition zone, where total live biomass was somewhat over-predicted compared to design-based estimates, but where the model under-predicted snag biomass by roughly half. This could be attributable to the prevalence of small diameter trees in the region and the difference in snag DBH threshold used in the GNN model of 25cm vs that used by Yatskov et al. (12.5cm, 2019). Overall, broad patterns of biomass and volume predictions in the maritime vs. boreal transition zones aligned with expectations from design-based estimates at regional scales, though some predictions differed from published estimates.

Illustration of GNN on the Tongass National Forest

The largest National Forest in the US, the Tongass (TNF) spans some 6.7 mil ha of the perhumid temperate rainforest zone in southeast Alaska and along the Gulf of Alaska Coast. It hosts 2.3 mil ha of congressionally designated Wilderness and is managed across 10 Ranger Districts. In addition to

Wilderness, some 3.7 mil ha of the TNF are protected from most development as Inventoried Roadless Area (IRA) under the 2001 Roadless Conservation Rule (USDA 2001). Though there are a variety of other land use designations, for simplicity, here I refer to the area of the TNF outside of Wilderness and IRA as Other. In general, the area outside of Wilderness and IRA designations is proportionally more heavily comprised of forested lands (91%) than those areas within the protected areas (64% and 63%, respectively). The total land base outside of these protected areas, however, is comparatively small (717,000 ha, 11%) and the TNF encompasses vast icefields, alpine tundra and nonforest openings over approximately 33% of its total area (Tables 13). This patchwork of land designations and ecological communities spread across hundreds of islands in the Alexander Archipelago provides an opportunity to illustrate some potential applications of GNN maps and summary data for the region.

Based on results of the accuracy assessment, I selected three structural attributes to broadly summarize height, diameter, and live biomass characteristics on the TNF and to illustrate the distribution of these attributes across land designations (Figure 13). Modeled stand heights indicate a majority of the forested area (~2.3 mil ha, 51%) across the TNF is characterized by stands of short and moderate stature in height classes 1 and 2 (<20 m average height of dominant and codominant trees) while just 228,000 ha (5.0%) is comprised by forests >30m (height classes 4 and 5 combined, Figure 13). The distribution of modeled stand diameter classes across land designations followed similar patterns to that of stand height models, with the central diameter class comprising a majority of forest land across all designations (Figure 13).

Aboveground live tree biomass on the TNF was classified into three bins according to a study by Krankina et al. (2014) characterizing the distribution of high-biomass forests of the Pacific Northwest (Table 8). Medium biomass forest classes (<200 Mg ha^{-1}) comprise the greatest forested area across all land designations on the TNF, though the proportion of medium biomass forests is greatest in IRAs

(43%). The highest biomass forests (>400 Mg ha^{-1}) comprise the smallest proportion of forested area across the TNF (Figure 13), yet the proportion of these very high biomass forests is greatest and nearly equal between Wilderness areas (12.3%) and areas outside the protected designations (12.1%). On an area basis, aboveground live biomass was predicted to be highest in Wilderness areas and lowest in the IRA (Figure 14).

Discussion

Southeast and southcentral Alaska is described as hosting among the world's largest tracts of intact temperate rainforest (Alaback 1991, Dellasala et al. 2011), yet relatively few spatially comprehensive datasets exist to describe the nature and arrangement of forest structure and composition across the region. The terrain and weather patterns typical of coastal temperate rainforests in Alaska represent challenges to obtaining traditional field inventory data as well as remotely sensed datasets. Yet regional forests provide tremendous value to local and regional communities (e.g. Johnson et al. 2021), play an important role in regional carbon and nutrient cycling (e.g. Bidlack et al. 2021), and may represent significant contributions to the global carbon balance (e.g. Zhu and McGuire 2016). In this study, I produced regional vegetation maps at a consistent resolution of 30-m covering all forested areas of southeast and southcentral Alaska using Gradient Nearest Neighbor methods (GNN, Ohmann and Gregory 2002) supported by LT-GEE (Kennedy et al. 2018b). Such geospatial data representing a range of vegetation characteristics have been used widely for monitoring the status and trends of forest conditions across broad regions (e.g. Davis et al. 2015, Davis et al. 2016, Lorenz et al. 2021). However, interpretation of spatially explicit modeled datasets necessarily requires an understanding of the accuracy and limitations for each intended use (e.g. Nelson et al. 2021). Careful evaluation of map accuracy, discussion of the sources and implications of prediction uncertainty, and the impacts of

reference datasets and decisions in model development on resulting imputation surfaces are critical to appropriate map interpretation and use.

GNN Accuracy in SE & SC AK

Gradient Nearest Neighbor predictions of structural forest attributes and tree species distributions in southeast and southcentral Alaska generally aligned well with expected patterns from published estimates (e.g. Blackard et al. 2008, Little 1971) at broad spatial extents in both the maritime and boreal transition ecoprovinces. Modeled regional predictions of aboveground live tree biomass aligned particularly well with design-based estimates (Cahoon et al. 2020) across the study area as a whole (Table 13). However, across the study area, modeled biomass predictions were generally lower than published estimates on a per-hectare basis. These discrepancies may have arisen in part from the temporal mismatch between observation dates in Cahoon et al.'s results (2004-2013) and those of my model predictions (2019). These results could be suggestive of losses due to disturbance (e.g. Alaska yellow cedar decline) and/or harvest which may have outpaced regional biomass accumulations from growth over the same period. However, direct comparison would be improved by producing model predictions for a focal year within the same timeframe as the design-based estimates.

While general geographic patterns of biomass predictions across the study area (Figure 10) aligned with expected patterns (Blackard et al. 2008), mapped differences between model predictions and design-based estimates of aboveground live biomass (Figure 15) revealed spatial patterns of the location, magnitude, and direction of prediction bias observed in the accuracy assessment (Table 10). Prediction bias was mixed across the maritime ecoprovince; the rainshadow along Lynn Canal in southeast Alaska, for instance, tended to correlate with areas of underpredicted biomass. Conversely, the eastern Prince William Sound area consistently contributed among the greatest over-prediction

biases (Figure 15), possibly associated with abundant deeply dissected east-west ridgelines with steep elevational gradients (Figure 16) contributing to terrain shadowing and pixel saturation (e.g. Lu et al. 2016, Zhao et al. 2016). The same assessments across the boreal transition zone reflected a far less structurally heterogeneous and topographically complex landscape and revealed reduced prediction bias and improved model accuracy for most attributes even when summarized over smaller areas (Table 10, Figure 10, Figure 15).

Single species distribution maps produced from GNN predictions indicated relatively strong prediction accuracy at broad geographic extents when compared with the distribution of observations at FIA field plots (Appendix 2). Although the kappa coefficient (Cohen 1960) of individual species prediction accuracy at observation locations ranged from poor to good (Table 12) across species and modeling regions, species range and distributions tended to agree with published accounts (e.g. Little 1971). I did not explore predictions of specific community assemblages or multi-species abundance in this report, but previous work in the Pacific Northwest suggests that nearest neighbor imputation may be effective for these uses (Henderson et al. 2014). Interpretations of stacked single species maps to predict community richness should be approached with caution since community assemblages inherently arise from inter and intra-species interactions (Henderson et al. 2014).

Finally, methods for spatially explicit variance estimation (e.g. McRoberts et al. 2007) across predictions covering large areas would help users understand the potential uses and limitations of these datasets. My validation and assessment procedures relied upon a set of field reference data which are by nature sparsely distributed across the landscape. Cumulatively, the field reference data capture the range and distribution of forest attributes present on the landscape, but only offer spatially explicit opportunities for map validation at relatively few locations. Detailed sampling of certain forest characteristics using expert interpretation of high-resolution satellite imagery may provide an

opportunity for improved variance estimates and stronger support of map use at finer spatial scales (e.g. Lister et al. 2021).

Sources of Uncertainty

Atmospheric and Terrain Effects on Landsat Imagery

Many challenges remain to predictive forest models in Alaska relying on optical-infrared remote sensing platforms. Topographic shading can lead to misrepresentation of surface reflectance (e.g. Gu and Gillespie 1998, Lu et al. 2016), particularly in steep, complex topography, accentuated in northern latitudes and on north-facing slopes (e.g. Giles 2001). In addition, multi-layered forest canopy shading can be indicative of complex forest structure (e.g. Sabol et al. 2002) but further contributes to early pixel saturation and can deteriorate the accuracy of spectral data to informing models of forest characteristics (Lu et al. 2016, Zhao et al. 2016). Particularly in the maritime climate zone of the study area, persistent cloud cover and atmospheric mist also contribute substantially to missing or invalid pixel values (Zu and Woodcock 2011, Braaten et al. 2015); and in Alaska, data downlink issues from Landsat sensors in the 1990s also led to missing and inconsistent data for some years (B. Roberts Pierel, personal communication).

This study employed several methods for addressing the challenges to acquiring accurate surface reflectance values from Landsat scenes with particular attention to atmospheric noise and missing values. Because temporal alignment between field survey and spectral data acquisition plays an important role in prediction accuracy (e.g. McRoberts et al. 2016), CCA models relied upon annual imagery mosaics corresponding with field measurement years over the study period (1995-2020). A multi-pronged approach to cloud, snow, and shadow masking (Zu and Woodcock 2011, Google 2022) substantially improved coverage of Landsat pixel values across the landscape by identifying suspect

pixels and substituting values from nearby collection dates to fill gaps using the medoid (Flood 2013). Persistently cloudy pixels which were screened completely out of an annual mosaic were subsequently filled using the LandTrendr smoothing algorithm following segmentation. This combination of approaches appeared to substantially reduce missing pixels in the annual LTS mosaics (Figure 4) but did not explicitly address the impacts of terrain or complex canopy shading on surface reflectance.

Topographic corrections for Landsat imagery have been widely proposed to reduce the impacts of terrain shadowing on pixel saturation (e.g. Hantson and Chuvieco 2011). In addition, active remote sensing techniques offer several promising opportunities for direct measurement of vertical elements of canopy structure to inform models where natural illumination and atmospheric interference pose problems. Light Detection and Ranging (LiDAR) is extremely effective at canopy height modeling (Kane et al. 2010) and has demonstrated great improvement to model predictions of forest attributes in other studies (e.g. Zald et al. 2014, Babcock et al. 2018). Vertical canopy structure data might also be derived from surface height and terrain models developed from Interferometric Synthetic Aperture Radar (InSAR) to inform models where optical-infrared sensor data is missing or suspect. Airborne platforms, however, are plagued by similar difficulties of other data collection efforts in the coastal temperate rainforests of Alaska: steep topographic relief, vast geographic extent, and poor weather lead to difficulty of accurate and consistent data acquisition (e.g. Gatziolis and Andersen 2008). Satellite-based sensors offer a solution to the challenges with aviation in coastal Alaska but are also subject to poor atmospheric conditions impacting measurement accuracy and offer limited spatial and temporal coverage (Dubayah et al. 2020) compared to the expansive Landsat library and global coverage (Masek et al. 2020).

FIA Field Observations

The application of GNN in coastal Alaska offers an opportunity to improve assessments of forest conditions in areas with relatively sparse field observations. The GNN method relies upon an unbiased set of field data representing the range and distribution of vegetation types being modeled (Ohmann and Gregory 2002, Duane et al. 2010, Bell et al. 2015). As the national forest inventory in the USA, the FIA dataset is critical to providing a consistent sample of all forest conditions with known estimates of measurement error (Bechtold and Patterson 2005) and has been widely used to support remote sensing research (Lister et al. 2020). Yet substantial gaps in the dataset exist in Alaska owing to the difficulty of access (Barret and Gray 2011). Strategic sampling in Interior Alaska began in 2014 (USDA 2014) and only limited sampling of Wilderness has ever occurred in the coastal southeast and southcentral region of the state (Smith and Gray 2021). Indeed, one critique of evaluating regional trends in forest condition is the exclusion of Wilderness in most design-based estimates (e.g. Bidlack et al. 2017). GNN models in this study were informed by 26 years of forest inventory data across coastal Alaska (excluding Glacier Bay National Park), but sampling in USFS Wilderness in the region was limited to a single year in 2005, offering just a snapshot, but nonetheless providing an unbiased sample, of forest conditions in USFS Wilderness areas of the region. Not surprisingly, neighbor distance appeared to be greatest in areas with sparse plot support (Figure 17), contributing to prediction uncertainty in these areas. Still, GNN maps provides an opportunity to enhance forest monitoring across all lands in the region.

In an effort to better inform models of forest attributes where the FIA data are sparse or in areas where neighbor distance is large (Figure 17), one avenue for future work focuses on gathering and harmonizing forest data from adjacent inventories. This would both facilitate model improvement over sparsely sampled areas within the existing modeling regions in the current study area (e.g. USFS Wilderness and GLBA) and would facilitate development and harmonization of forest modeling to

encompass the entire North American coastal temperate rainforest biome beyond national jurisdictional boundaries (e.g. McNicol et al. 2019, Bidlack et al. 2021).

Notably, I did not include modeled estimates of canopy cover or canopy cover derivatives (e.g. Vegetation Class) in attribute maps due to irregularities I observed in tree-level and plot-level canopy cover calculations from the FIA data. Canopy cover was calculated for individual trees based upon measures of tree diameter, height, and crown length as described in the FIA to FVS guide (Keyser 2008). Individual tree canopy widths were first computed using species specific regression equations as described, and plot-based percent cover estimates accounting for overlapping crowns were subsequently computed. However, inspection of individual tree canopy cover calculations revealed overt overestimates, particularly for very small trees, and apparent underestimates for some very large trees, which cumulatively led to suspicious plot-based canopy cover estimates in a variety of forest settings. Expert evaluation of these tree cover estimates, along with ad-hoc comparison to field crew observations (available from field plots measured between 1995-2003 and 2012-2020) ultimately led to their exclusion from mapped forest attributes in this study. As tree canopy cover can be an important indicator of many landscape characteristics, future mapping efforts could be improved by incorporating tree cover estimates at the plot level from field observations rather than from estimates derived from regression equations. Limitations in the availability and consistency of FIA canopy cover data collected by field crews hindered my ability to include cover-related attributes in the current maps.

Nonforest Mask

Estimates made by summarizing the GNN dataset over a given geographic extent are subject to a certain level of bias associated with the selection of a nonforest mask. For particular research questions, an un-masked version of the GNN data may be preferable to elucidate information about

areas considered to be near the forest edge or transition areas. I elected to create a custom mask for the GNN forest maps in southeast and southcentral Alaska based on a desire to a) limit general user inference to forested lands in the study area, and b) align areas of inference with those reported by the FIA program to facilitate comparisons with design-based estimates. The custom mask excluded 30-m pixels estimated to contain less than 10% tree canopy cover (Megown 2016), and areas classified as any kind of developed land use condition (Dewitz 2019). Comparisons to high resolution satellite imagery indicate the resulting mask successfully captured most obviously forested areas and excluded many obviously nonforest areas (Figure 8). The resulting estimated forestland across the study area was 6% greater than the design-based forestland estimates by Cahoon et al. (2020, Table 13). As compared with structural attribute predictions which may be of concern to informing management questions at watershed or landscape scales, the areal extent of GNN maps contributes substantially to regional predictions, for instance, of total biomass or carbon.

Scale and the Effects of Averaging

My selections of the value of *k* (7 for structural attributes, 1 for species composition predictions), the model grain size (0.81ha), imputation grain size (0.09ha), the spatial extents analyzed for accuracy assessment, and the criteria used to screen plots for model development were based primarily upon previous research and recommended practices (e.g. Ohmann et al. 2014, Bell et al. 2015a, Riemann et al. 2010, Gregory et al. 2011). Each decision regarding model parameterization impacts the resulting imputation surfaces, and the choice of extents over which to evaluate model accuracy has direct impacts on the assessment results. Additional sources of error and averaging come from the environmental predictor covariates; climate data were downscaled from data modeled at larger pixel sizes using bilinear interpolation, and Landsat timeseries were constructed using a variety of

masking and pixel substitution algorithms to produce a spatially and temporally comprehensive dataset. In each case, decisions were made to balance the availability and accuracy of input data sources with a desire to construct effective models and generate predictions across a variety of spatial extents.

Selection of a 30-m pixel size takes advantage of a spatially and temporally rich Landsat dataset, but potentially misses biologically important variation in topographic or climatic environmental predictors occurring at finer spatial scales (e.g. Zald et al. 2014). Additionally, some ecologically important components of forest structure, such as standing dead trees and down wood, may be difficult to detect at the 30-m pixel size due to their relatively limited contribution to spectral reflectance compared with live vegetation (although see Bell et al. 2021). The spatial mismatch between the scale of the FIA plot footprint (0.067 ha) and the 3x3 average pixel value used in model development (0.81ha) also leaves uncertainty in whether forest attributes estimated in the field at the plot level are consistent representations of the conditions present across the entire 3x3 pixel footprint (e.g. Ohmann et al. 2014). Plot screening criteria were implemented to help identify and exclude outliers from model development, but screening was restrained to avoid bias towards homogenous forest conditions (*sensu* Riemann et al. 2010), and I did not explore in this study whether heterogeneity in forest patterns may be better described at a finer resolution, though research suggests that gap dynamics in the region may occur across finer spatial scales (e.g. Ott and Juday 2002).

An abundance of forest-nonforest ecotones in the region near the altitudinal tree-line and alpine tundra, and among forested wetlands and wet openings (muskegs) (e.g. Alaback 1991, Neiland 1971) make these important transition zones to capture in forest models. Neighbor distance was particularly large in high elevation areas (Figure 17), but modeled conditions near or across such transition zones may have benefitted from a robust set of field reference data collected in naturally vegetated non-forested areas on USFS managed lands throughout the region between 2011-2020.

Indeed, fine spatial patterning observed in the GNN models appears in most cases to mirror observations from high resolution satellite imagery along such natural gradients, though patterns are less distinct on the Kenai Peninsula (Appendix 3).

The selection and weighting of *k* in nearest neighbor imputation have been the subject of much research (e.g. Stage and Crookston 2007, Bell et al. 2015). Values of $k>1$ better represent characteristics of more common types but tend to truncate distributions (Table 11) by producing averaged estimates at the expense of rarer attributes (e.g. Ohmann et al. 2014). My selection of $k=7$ to build GNN maps in this study balances a desire to mirror the range of conditions observed in the field reference data (as in $k=1$), with a desire to constrain the absolute influence of a single nearest neighbor by incorporating elements of multiple neighbors to imputation surfaces. Similarly, the selection of multiple extents over which to conduct accuracy assessment was based in part on expected uses of mapped datasets and reasonable areas over which inferences should be made from mapped predictions (Riemann et al. 2010). However, the relative scarcity of field observation data in some geographic areas of the region imposes limitations to the multi-scale accuracy assessment technique, which relies on direct comparisons between model generated predictions and field observations across each extent.

Finally, the effects of masking and temporal smoothing of spectral data in creation of the Landsat timeseries could lead to inadvertent loss of detail in areas of persistent cloud cover or where transient surface conditions are interpreted as anomalies and replaced. Cloud, snow, and shadow masking is intended to reduce noise in the annual composites, and the temporal smoothing in LandTrendr is intended to fill missing data. LandTrendr additionally reduces noise arising from variation in plant phenology, sun angle, and atmospheric effects, but could mask important but short-lived ecological impacts (e.g. pathogens that impact community dynamics but do not kill trees). However, I

expect such impacts to be limited in stable forested ecosystems where intra-annual variability is relatively low (e.g. Kennedy et al. 2018b).

Selection of Predictor Variables

Canonical correspondence analysis is robust to many of the limitations of multiple linear regression (e.g. data which contain many null values and are not normally distributed) and does not require iterative successional runs to elucidate the effects of many predictors on many response variables. However, selection of appropriate predictor variables is still critical to effective model development, and to prevent unintended consequences of overly complex models (e.g. Palmer 1993, Bell and Schlaepfer 2016). Selection of appropriate environmental predictors is critical in model development as it is not unusual for community assemblages or structural conditions to be associated with similar sets of environmental conditions across the landscape. Future modeling efforts in Alaska may consider inclusion of cumulative Potential Relative Radiation (Pierce et al. 2005), a more robust measure of solar insolation than the Heat Load Index, accounting for sun angle and terrain interference; the effects of which can be particularly pronounced at higher latitudes (e.g. Beamish et al. 2020). Additional environmental predictor covariates which were not included in the current study but may play an important role in driving forest composition and structure in the region include geomorphologic, edaphic and hydrologic characteristics (e.g. Hoffman et al. 2021, Bisbing et al 2016, Neiland 1971), along with aerial survey disturbance history data (e.g. Brannoch and Moan 2020). In all cases, the accuracy and consistency of spatial resolution across predictor datasets may play important roles in model development.

Potential Applications

These new GNN data for southeast and southcentral Alaska may provide opportunities to inform research, management or policy decisions in a variety of applications due to their capacity for describing a range of forest attributes across the landscape. Regional vegetation maps have been used elsewhere to inform assessments of regional biomass and carbon storage (e.g. Kennedy et al. 2018a, Bell et al. *In Press*), to monitor spatial patterns of disturbance (e.g. Cohen et al. 2018) or land cover change through time (e.g. Moisen et al. 2020), and to assess patterns of vegetation response to climatic changes (e.g. Schleeweis et al. 2020). In the hypermaritime forests of southeast and southcentral Alaska, these data may support research on carbon and nutrient fluxes between terrestrial and aquatic ecosystems (e.g. Bidlack et al. 2021), or on the spatial arrangement and continuity of forest structural classes characterizing critical wildlife habitats (e.g. Lorenz et al. 2021).

Alaskan ecosystems may store as much as 53% of the nation's total terrestrial carbon (Zhu and McGuire 2016). Projections indicate that the boreal and temperate ecosystems of the state may reveal complex responses to climate change (Wolken et al. 2011, Shanley et al. 2015, Hayward et al. 2017, Fellman et al. 2017), with increasing temperatures possibly increasing emissions in the boreal region but increasing sequestration rates in the coastal temperate zone (McGuire et al. 2018). Though a majority of the carbon in Alaskan ecosystems is stored below-ground (Zhu and McGuire 2016, McNicol et al. 2019, Cahoon et al. *In Review*), forests play an important role in contributing biomass inputs to belowground carbon pools (e.g. Adams et al. 2019), moderating soil temperatures (e.g. Li 1926, Bonan 1991), and cycling water and nutrients (e.g. Bisbing and D'Amore 2018) which drive rates of respiration and decomposition (e.g. Fellman et al. 2017). In addition, above-ground biomass pools in the temperate forests of Alaska are substantial (Blackard et al. 2008, Buma et al. 2016, Table 13) and may constitute a relatively stable carbon reservoir in national reporting (USEPA 2021).

Forest management plays an important role in affecting carbon storage as well as the nature and arrangement of forest characteristics as they relate to other management objectives and ecosystem services. Timber harvest in southeast Alaska has fallen dramatically in recent years, but still 56% of timber volume harvested in the state originates from this region. The proportion of timber volume harvested from National Forest lands in the region has fallen from greater than 90% in the 1970s to just 22% in 2015 (Marcille et al. 2021), yet the Tongass National Forest (TNF) represents ~30% of earth's remaining old-growth temperate rainforest (Alaback 2015). The majority of TNF forestlands are designated either as Inventoried Roadless Area (IRA, 52%, 2.4 mil ha) or Wilderness (33%, 1.5 mil ha) and reserved from active management operations (Table 13). The remaining 14% of forestland on the TNF outside the IRA and Wilderness boundaries is comprised of several other conservation designations, and an even smaller proportion has been the primary source of commercial timber supply in the region for the past decades. Still, independent reviews have demonstrated a disproportionate impact of timber harvest to stands of the largest trees (e.g. Albert and Shoen 2007, Fennel et al. 2016). Recent efforts to allow development in the IRA (USDA 2021b) warrant more explicit information regarding the nature and condition of forests in these areas specifically. Further, the public image of the TNF largely relies on its 'wilderness character,' yet systematic sampling by the FIA program is prohibited in Wilderness areas (USDA 2008), leading to a relative scarcity of field data describing forests in USFS Wilderness across the region.

While broad categories of biomass, tree size, or density are useful indicators of some forest characteristics, GNN might be used to estimate any number of forest attributes across the landscape based on measurements collected in the observation dataset. Of interest on the TNF may be investigations exploring forest characteristics associated with suitable wildlife habitat, patch size and distribution of merchantable young-growth stands, or assessments of the status and spatial distribution

of culturally, ecologically, and economically important tree species such as *Callitropsis nootkatensis*. Summaries of modeled attribute data are possible across a range of extents by aggregating data to meet monitoring objectives, exploring connectivity and fragmentation patterns, and by enabling comparisons across smaller areas, such as ranger districts or watersheds, for example. Fine scale spatial patterning across land use designations (e.g. Figure 14) may also be of interest for some applications. Accuracy assessments help inform decisions about potential uses of GNN data for a variety of purposes by indicating the precision and bias of predictions of each attribute and by reporting on the magnitude, frequency, and location of prediction errors. My goal with this study was to provide managers and policymakers with a new dataset to support informed decision making, and to facilitate future research initiatives with a baseline dataset describing status of forest conditions across southeast and southcentral Alaska.

Conclusion

Alaska's boreal and coastal temperate forests comprise an estimated 17% of all US forestland (Andersen et al. 2019) and are described as being among the world's most intact terrestrial ecosystems (Dellasala et al. 2011, Wells et al. 2020). Vynne et al. (2021) argue that Alaska ought to be "considered as a key element of a climate stabilization and biodiversity conservation strategy for the United States" based upon the extent of intact ecosystems and species assemblages across the state. Alaska's perhumid and subpolar coastal temperate rainforests are characterized by complex structural heterogeneity, developed in the absence of fire over centuries of gap-phase dynamic disturbance regimes (e.g. Alaback 1996, Hastings 1997, Ott and Juday 2002, Schneider and Larson 2017). Their influence over a productive terrestrial-marine ecotone contributes substantially to regional carbon and nutrient transport (Bidlack et al. 2021), and their relative stability (e.g. Dellasala et al. 2011, Wolken et

al. 2011) and high biomass (e.g. Cahoon et al. 2020, McNicol et al. 2019) makes them ideal candidates for conservation efforts aimed at preserving natural terrestrial carbon stocks (e.g. Vynne et al. 2021, Griscom et al. 2017).

Coastal temperate rainforests of this region are naturally fragmented owing to their unique island biogeography and to a mix of areas of glacial refugia (Carrara 2007) and of relatively recent deglaciation (Alaback 1991, Dellasala et al. 2011). A jurisdictional framework including many land managers (e.g. Cahoon et al. 2020), land-use designations (e.g. US Forest Service 2016), ongoing land conveyances (e.g. Dunleavy 2022), and shifting management objectives (e.g. Sealaska 2021) add to the complexity of understanding historic trends and projecting future conditions across the landscape. Uncertainty surrounding potential impacts of future climate scenarios to Alaska's forests (e.g. Wolken et al. 2011, Kelly 2013, Hayward et al. 2017) add urgency to the need for spatially comprehensive and consistent data facilitating local- to region-wide analyses of forest conditions and trends (e.g. Schleeweis et al. 2020).

This study contributes to a body of work aimed at characterizing and mapping forests of the temperate and boreal biomes across broad geographic extents. To my knowledge, the application and assessment of Gradient Nearest Neighbor (GNN) methods (Ohmann and Gregory 2002) parameterized to southeast and southcentral Alaska are previously untested. A multi-step cloud masking procedure along with LandTrendr implemented in Google Earth Engine (LT-GEE, Kennedy et al. 2018b) facilitated annual alignment between imagery and the inventory plot data used for GNN modeling (e.g. Kennedy et al. 2018a). These methods enabled the development of a new set of maps representing a suite of forest attributes at a consistent resolution of 30-m across ~8.5 mil ha of forestland in Alaska, including Wilderness and other areas with relatively lean observational datasets.

The spatial complexity of forests and forested wetlands mosaicked across the region offered an opportunity to test GNN predictions in a heterogeneous, high-latitude landscape. Challenges remain in addressing the impacts of terrain shadows and canopy shading on pixel saturation which can be particularly pronounced at high latitudes and in high-biomass forests were canopy structure tends to be complex and shading is substantial. In the coastal temperate rainforests, rugged terrain and horizontal and vertical heterogeneity in forest structure contributed to reduced model accuracy when results were aggregated at intermediate extents (Table 10, Figure 9), but fine-scale spatial patterning in predicted forest attributes appeared to align relatively well with high resolution satellite imagery (Appendix 3), and some region-wide predictions aligned closely with design-based estimates (Table 13). Accuracy assessments suggest that GNN may offer a particularly promising option for mapping forest conditions in Alaska's boreal forests (Tables 10-13, Figures 15, 17) and support calls for spatially unbiased field surveys by the national Forest Inventory and Analysis (FIA) program across the state (e.g. Barrett and Gray 2011, Andersen et al. 2019).

I established in this study a framework for integrating existing tools for compilation of annual imagery mosaics (LT-GEE), for ingesting regional observational datasets, and for implementing GNN modeling and imputation methods (pynnmap) in Alaska. Future directions for building upon this work include the creation of annual timeseries of forest attribute predictions for forecasting and back-casting, geographic expansion to adjacent areas with different or only recently acquired survey information, and the exploration of active, higher resolution, and newly acquired remotely sensed datasets to help inform model predictions. The availability of these new GNN data and regionally parameterized models now present an opportunity to implement widespread and consistent monitoring to inform research direction and policy decisions across some of the most culturally significant, carbon rich, and biologically intact ecosystems in the world.

Tables

Table 1. LandTrendr parameters implemented in this study

Parameter	Value	Description
Start and End year	1995 - 2020	Defines the start and end years of the timeseries
Imagery Dates	06/20 – 09/20	Annual Image Date Range
Segmentation Index	NBR	Segmentation Index
Pixel Selection	Medoid	See Flood (2013)
Max Segments	8	Maximum # Image Segments
Spike Threshold	0.9	Threshold for Dampening Spikes
Vertex Count Overshoot	3	Initial Model can overshoot vertices by this number
Prevent One Year Recovery	TRUE	Prevents Segments that represent recovery in a single year
Recovery Threshold	0.75	If a segment has a recovery rate faster than 1/threshold, segment disallowed
p-Value Threshold	0.05	If the p-value of a fitted model exceeds this threshold, the model is discarded and a new model fitted.
Best Model Proportion	0.5	Allows models with more vertices to be chosen if their p-value is less than 2 minus this value times the p-value of the best model
Min Observations Needed	8	Minimum number of observations needed to perform output fitting

Table 2. Number of field plots in each modeling region, before and after plot screening

	Field Plots in Final Model			
Year	MR101	MR105	MR110	Total
1995	198	0	22	220
1996	234	0	29	263
1997	273	0	64	337
1998	192	0	45	237
1999	0	27	196	223
2000	0	0	30	30
2001	0	211	83	294
2002	0	31	88	119
2003	0	5	39	44
2004	94	63	84	241
2005	137	10	82	229
2006	130	52	86	268
2007	117	15	66	198
2008	103	49	86	238
2009	104	21	90	215
2010	116	45	75	236
2011	104	9	63	176
2012	120	40	78	238
2013	111	16	60	187
2014	0	35	23	58
2015	86	27	57	170
2016	81	11	42	134
2017	73	40	70	183
2018	112	8	71	191
2019	78	27	62	167
2020	30	2	8	40
Field Plots Screened Out	562	19	36	617
TOTAL	2493	744	1699	4936

Table 3. Environmental covariates, data sources, ranges, and scaling

Variable Subset	Source	Code	Units	Transformation	Range	Description
Annual Landsat timeseries, expressed using tasseled cap transformations, processed using LandTrendr algorithms	Kennedy et al. 2010, Crist and Cicone 1984	TCB		none	(-15) - 17491	Brightness (axis 1) from tasseled cap transformation
		TCG		none	(-4516) - 4726	Greenness (axis 2) from tasseled cap transformation
		TCW		none	(-3950) - 6704	Wetness (axis 3) from tasseled cap transformation
Climate, from 771-m 30-year normal PRISM rasters, downscaled using bilinear interpolation	Daly et al. 2018	ANNTMP	°C	* 100	(-1615) - 830	Mean annual temperature
		SUMMAXT	°C	* 100	(-500) - 1933	Mean maximum temperature between June-August
		DECMINT	°C	* 100	(-2439) - 248	Mean minimum temperature in December
		ANNPRE	mm	ln * 1000	0 - 922	Mean annual precipitation
Topography, from 30-m ASTER digital elevation model (DEM)	NASA 2018	ELEV	m	none	0 - 3750	Elevation
		ASP	degrees	cosine * 100	0 - 200	Aspect
		SLOPE	%	* 10	0 - 2243	Slope
	Weiss 2001	TPI300		none	(-130) - 180	Topographic position index; the difference between a cell's elevation and the mean elevation of cells within a 300-m radius neighborhood
		TPI450		none	(-192) - 283	Topographic position index; the difference between a cell's elevation and the mean elevation of cells within a 450-m radius neighborhood
		TPI1000		none	(-455) - 529	Topographic position index; the difference between a cell's elevation and the mean elevation of cells within a 1000-m radius neighborhood
	McCune and Keon 2002	HLI	unitless	none	0-989	Potential annual direct incident radiation

Table 4. Forest attributes computed at each field plot location used for illustration of potential *mapping* variables

Variable	Range	Units	Description
BPH_GE_3_REG	0-1416	Mg/ha	Aboveground total biomass of live trees >2.5cm DBH calculated using regional FIA biomass equations
QMD_DOM	0-110	cm	Quadratic mean diameter of all live dominant and codominant trees
SBPH_GE_25	0-787	Mg/ha	Aboveground total biomass of dead trees >25cm DBH calculated using regional FIA biomass equations
SDI_REINEKE	2-976	unitless	Reineke's Stand Density Index
STNDHGT	0-52	m	Average height of all dominant and codominant live trees
VPH_GE_3	0-1631	m3/ha	Aboveground net volume of live trees >12.5cm DBH between a 1-foot stump and a 4-inch top

Table 5. Neighbor weighting based on bootstrap sampling approximation (Bell et al. 2015a)

Neighbor Position	Weighting
1	0.6321
2	0.2325
3	0.0855
4	0.0315
5	0.0116
6	0.0043
7	0.0016

Table 6. Vegetation Class (VEGCLASS) categories and errors considered to be egregious between predicted vs. observed values

Vegetation Class	VEGCLASS #	Definition	Egregious errors between Predicted and Observed VEGCLASS
Sparse	1	Canopy Cover < 10%	10, 11
Open	2	10% < Canopy Cover < 40%	11
Broadleaf, small	3	Canopy Cover >40%, BA Proportion Hardwood > 65%, QMD <25	
Broadleaf, medium/large	4	Canopy Cover >40%, BA Proportion Hardwood > 65%, QMD >25	
Mixed conifer-broadleaf, small	5	Canopy Cover >40%, 20% < BA Proportion Hardwood < 65%, QMD <25	11
Mixed conifer-broadleaf, medium	6	Canopy Cover >40%, 20% < BA Proportion Hardwood < 65%, 25 < QMD < 50	
Mixed conifer-broadleaf, large/very large	7	Canopy Cover >40%, 20% < BA Proportion Hardwood < 65%, QMD > 50	
Conifer, small	8	Canopy Cover >40%, BA Proportion Hardwood < 20%, QMD <25	11
Conifer, medium	9	Canopy Cover >40%, BA Proportion Hardwood < 20%, 25 < QMD < 50	
Conifer, large	10	Canopy Cover >40%, BA Proportion Hardwood < 20%, 50 < QMD < 75	1
Conifer, very large	11	Canopy Cover >40%, BA Proportion Hardwood < 20%, QMD > 75	1, 2, 5, 8

Table 7. Screening criteria used to remove plots from model

Criteria	Description
Boundary	Plots which straddle distinct ecological boundaries, e.g. at the edge of a densely forested area along an open, non-forested area.
Disturbance	Plots where a disturbance occurred (either natural or anthropogenic) between the date of field measurement date and the date of spectral data acquisition.
Imagery	Plots where the LTS spectral data covering the plot area and associated with the year of plot measurement does not reflect the conditions observed using alternative imagery sources or ancillary information; those errors often associated with shadow, snow, or clouds impacting imagery over part or all of the nine-pixel window covering the plot footprint.
Location	Plots where a clear error exists in the coordinates associated with the field plot measurement such that the conditions at the coordinate location do not match those of the field measurements.
Other	Any other reason for screening out a plot not covered by the other descriptions.

Table 8. Structural attribute classes used for illustration of potential GNN application

		QMD			Biomass		Stand Height
Reference		Caouette and DeGayner 2008			Krankina et al. 2014		
Units		percentile	cm		Mg/ha		m
Classes	1	<25th	<23.7	1	1-200	1	<10
	2	>25th, <75th	<44.3	2	201-400	2	<20
	3	>75th	>44.3	3	>400	3	<30
						4	<40
						5	>40

Table 9. Local accuracy: predicted (*k*=7) vs. observation estimates at the plot (3x3 pixel) level

			QMD_DOM	STNDHGT	SDI_REINEKE	VPH_GE_3	BPH_GE_3_REG	SBPH_GE_25
Maritime	MR101	R_SQUARE	0.35	0.5	0.34	0.34	0.34	-0.02
		PEARSON R	0.60	0.70	0.59	0.59	0.59	0.21
		NORMALIZED_RMSE	0.42	0.35	0.41	0.69	0.67	1.77
		BIAS_PERCENTAGE	1.14	1.61	0.23	2.2	2.24	3.69
	MR110	R_SQUARE	0.24	0.34	0.4	0.37	0.39	0.01
		PEARSON R	0.52	0.60	0.64	0.63	0.63	0.26
		NORMALIZED_RMSE	0.48	0.41	0.5	0.85	0.81	1.99
		BIAS_PERCENTAGE	2.54	3.7	2.97	7.19	6.57	1.92
Boreal	MR105	R_SQUARE	0.11	0.23	0.49	0.27	0.36	0.35
		PEARSON R	0.37	0.49	0.70	0.53	0.60	0.59
		NORMALIZED_RMSE	0.58	0.41	0.61	1.12	0.8	1.89
		BIAS_PERCENTAGE	-0.76	-0.37	1.34	0	0.16	1.02

Table 10. Multi-scale accuracy: agreement coefficients and the KS statistic for *k*=7 predictions vs observation estimates

10a. MR101

		QMD_DOM	STNDHT	SDI_REINEKE	VPH_GE_3	BPH_GE_3_REG	SBPH_GE_25
PLOT_PIXEL	AC	-0.20	0.20	-0.22	-0.15	-0.16	-3.18
	AC_SYS	0.81	0.91	0.78	0.83	0.83	-0.14
	AC_UNS	-0.01	0.29	0.01	0.02	0.02	-2.04
	KS_MAX	0.12	0.11	0.14	0.14	0.15	0.28
	KS_MEAN	0.04	0.03	0.05	0.04	0.03	0.02
HEX_10 8,660 ha scale # hexes = 550 Avg. # plots per hex = 5	AC	-0.16	0.15	-0.30	-0.43	-0.43	-1.62
	AC_SYS	0.79	0.88	0.67	0.63	0.62	0.43
	AC_UNS	0.05	0.27	0.02	-0.06	-0.05	-1.06
	KS_MAX	0.12	0.12	0.15	0.16	0.16	0.25
	KS_MEAN	0.03	0.04	0.05	0.04	0.04	0.03
HEX_30 78,100 ha scale # hexes = 99 Avg. # plots per hex = 30	AC	0.14	0.34	0.13	-0.25	-0.21	-0.37
	AC_SYS	0.78	0.85	0.68	0.62	0.64	0.72
	AC_UNS	0.36	0.49	0.45	0.13	0.15	-0.08
	KS_MAX	0.14	0.16	0.14	0.17	0.18	0.23
	KS_MEAN	0.05	0.05	0.05	0.04	0.04	0.08
HEX_50 216,000 ha scale # hexes = 44 Avg. # plots per hex = 69	AC	0.35	0.52	0.51	0.52	0.52	0.18
	AC_SYS	0.81	0.89	0.77	0.89	0.92	0.80
	AC_UNS	0.54	0.63	0.74	0.63	0.60	0.38
	KS_MAX	0.18	0.18	0.18	0.18	0.18	0.34
	KS_MEAN	0.04	0.06	0.08	0.04	0.05	0.12

10b. MR105

		QMD_DOM	STNDHT	SDI_REINEKE	VPH_GE_3	BPH_GE_3_REG	SBPH_GE_25
PLOT_PIXEL	AC	-0.87	-0.87	-0.87	-0.74	-0.27	-0.48
	AC_SYS	0.57	0.57	0.57	0.72	0.78	0.69
	AC_UNS	-0.44	-0.44	-0.44	-0.46	-0.04	-0.17
	KS_MAX	0.15	0.15	0.15	0.25	0.15	0.51
	KS_MEAN	0.07	0.07	0.07	0.04	0.05	0.02
HEX_10 8,660 ha scale # hexes = 118 Avg. # plots per hex = 6	AC	-0.33	-0.33	-0.33	-0.39	0.16	0.14
	AC_SYS	0.72	0.72	0.72	0.84	0.92	0.89
	AC_UNS	-0.05	-0.05	-0.05	-0.23	0.24	0.25
	KS_MAX	0.18	0.18	0.18	0.17	0.14	0.20
	KS_MEAN	0.06	0.06	0.06	0.06	0.05	0.03
HEX_30 78,100 ha scale # hexes = 22 Avg. # plots per hex = 34	AC	0.50	0.50	0.50	0.31	0.53	0.64
	AC_SYS	0.69	0.69	0.69	0.81	0.92	1.00
	AC_UNS	0.81	0.81	0.81	0.50	0.62	0.65
	KS_MAX	0.23	0.23	0.23	0.14	0.14	0.14
	KS_MEAN	0.09	0.09	0.09	0.06	0.07	0.03
HEX_50 216,000 ha scale # hexes = 9 Avg. # plots per hex = 84	AC	0.52	0.52	0.52	0.93	0.94	0.96
	AC_SYS	0.76	0.76	0.76	0.99	0.99	0.98
	AC_UNS	0.75	0.75	0.75	0.94	0.95	0.98
	KS_MAX	0.22	0.22	0.22	0.22	0.22	0.22
	KS_MEAN	0.10	0.10	0.10	0.04	0.05	0.05

10c. MR110

		QMD_DOM	STNDHT	SDI_REINEKE	VPH_GE_3	BPH_GE_3_REG	SBPH_GE_25
PLOT_PIXEL	AC	-0.40	-0.02	0.07	0.04	0.04	-2.56
	AC_SYS	0.80	0.89	0.89	0.90	0.90	0.11
	AC_UNS	-0.20	0.09	0.18	0.14	0.14	-1.67
	KS_MAX	0.11	0.13	0.13	0.15	0.15	0.41
	KS_MEAN	0.04	0.03	0.04	0.03	0.02	0.02
HEX_10 8,660 ha scale # hexes = 424 Avg. # plots per hex = 4	AC	-0.32	0.04	0.25	0.09	0.09	-2.05
	AC_SYS	0.80	0.88	0.90	0.87	0.87	0.31
	AC_UNS	-0.12	0.16	0.35	0.22	0.23	-1.36
	KS_MAX	0.15	0.14	0.12	0.15	0.14	0.27
	KS_MEAN	0.04	0.04	0.05	0.03	0.03	0.05
HEX_30 78,100 ha scale # hexes = 111 Avg. # plots per hex = 15	AC	0.23	0.37	0.54	0.61	0.62	-0.59
	AC_SYS	0.91	0.90	0.95	0.96	0.96	0.62
	AC_UNS	0.31	0.47	0.59	0.65	0.66	-0.21
	KS_MAX	0.17	0.15	0.13	0.17	0.19	0.26
	KS_MEAN	0.04	0.05	0.05	0.05	0.05	0.05
HEX_50 216,000 ha scale # hexes = 57 Avg. # plots per hex = 28	AC	0.57	0.48	0.73	0.65	0.69	-0.17
	AC_SYS	0.96	0.91	0.98	0.97	0.98	0.65
	AC_UNS	0.60	0.57	0.75	0.68	0.72	0.18
	KS_MAX	0.21	0.18	0.12	0.18	0.16	0.25
	KS_MEAN	0.06	0.08	0.04	0.05	0.05	0.07

Table 11. Distribution of prediction vs. observation estimates by modeling region

				Min	Lower Q	Median	Mean	Upper Q	Max
Maritime	MR101	QMD_DOM	obs	0.0	20.5	30.7	33.9	45.2	122.2
			k7	2.9	25.0	33.9	34.4	43.3	82.6
		SDI_REINEKE	obs	1.9	197.8	321.6	321.6	441.5	1081.1
			k7	4.1	267.6	351.7	328.0	404.8	627.8
		VPH_GE_3	obs	0.0	85.9	221.7	281.3	415.8	1807.3
			k7	0.3	149.7	291.5	293.5	412.4	1256.2
		BPH_GE_3_REG	obs	0.0	75.0	170.2	220.7	318.2	1547.4
			k7	0.7	120.5	226.9	230.1	319.8	949.5
		STNDHGT	obs	0.0	10.7	15.5	17.0	22.3	56.1
			k7	0.8	12.2	17.2	17.2	22.1	43.3
		SBPH_GE_25	obs	0.0	2.4	13.9	34.3	40.2	1089.2
			k7	0.0	15.6	31.7	36.5	50.5	394.5
	MR110	QMD_DOM	obs	0.0	18.6	28.7	30.9	40.4	112.5
			k7	6.2	22.5	31.9	31.8	39.9	76.5
		SDI_REINEKE	obs	1.9	112.2	241.6	252.3	373.8	906.0
			k7	23.5	157.1	265.9	261.1	354.3	602.7
		VPH_GE_3	obs	0.0	35.3	136.5	210.6	324.3	1807.3
			k7	5.9	75.0	208.7	228.1	344.4	1004.1
		BPH_GE_3_REG	obs	0.0	36.0	109.5	158.3	237.1	1547.4
			k7	7.6	63.3	153.1	170.4	252.3	762.1
		STNDHGT	obs	0.0	9.9	14.1	15.4	19.9	56.1
			k7	4.0	11.4	15.4	16.0	20.0	42.5
		SBPH_GE_25	obs	0.0	0.0	2.7	13.0	14.2	304.2
			k7	0.0	4.4	10.0	13.4	18.4	122.6
				Min	Lower Q	Median	Mean	Upper Q	Max
Boreal	MR105	QMD_DOM	obs	0.0	7.9	14.5	16.1	22.7	65.3
			k7	4.5	12.1	15.4	16.0	19.5	42.8
		SDI_REINEKE	obs	1.9	38.7	104.7	127.9	196.8	609.6
			k7	2.8	58.5	124.7	130.3	192.4	485.9
		VPH_GE_3	obs	0.0	2.6	18.8	38.2	55.1	307.4
			k7	0.4	15.6	31.6	38.7	54.1	165.3
		BPH_GE_3_REG	obs	0.0	10.2	28.2	42.4	63.4	244.3
			k7	0.4	19.1	40.3	42.9	62.7	142.3
		STNDHGT	obs	0.0	7.0	10.6	10.4	13.8	23.5
			k7	1.3	8.7	10.5	10.4	12.3	18.5
		SBPH_GE_25	obs	0.0	0.0	0.0	10.3	9.4	199.9
			k7	0.0	1.5	4.3	10.3	12.3	122.0

Table 12. Species accuracy

OP_PP: Observed present, predicted present (count)

OP_PA: Observed present, predicted absent (count)

OA_PP: Observed absent, predicted present (count)

OA_PA: Observed absent, predicted absent (count)

		SPECIES	OP_PP	OP_PA	OA_PP	OA_PA	FALSE NEGATIVE	FALSE POSITIVE	PERCENT CORRECT	KAPPA
Maritime	MR101	ALRU2	93	47	472	1880	0.34	0.20	0.79	0.19
		CHNO	1205	43	941	303	0.03	0.76	0.61	0.21
		NOTALLY	20	13	90	2369	0.39	0.04	0.96	0.26
		PICO	441	27	655	1369	0.06	0.32	0.73	0.41
		PISI	1690	14	686	102	0.01	0.87	0.72	0.16
		POBAT	2	8	29	2453	0.80	0.01	0.99	0.09
		THPL	598	32	751	1111	0.05	0.40	0.69	0.40
		TSHE	2147	6	293	46	0.00	0.86	0.88	0.21
		TSME	1441	28	819	204	0.02	0.80	0.66	0.20
	MR110	ALRU2	0	8	25	1648	1.00	0.01	0.98	-0.01
		BEPA	216	23	272	1170	0.10	0.19	0.82	0.50
		CHNO	70	29	192	1390	0.29	0.12	0.87	0.33
		NOTALLY	9	17	114	1541	0.65	0.07	0.92	0.10
		PICO	10	14	71	1586	0.58	0.04	0.95	0.17
		PIGL	249	15	164	1253	0.06	0.12	0.89	0.67
		PIMA	95	11	121	1454	0.10	0.08	0.92	0.55
		PISI	1061	33	363	224	0.03	0.62	0.76	0.40
		POBA2	0	0	0	1681	0.00	0.00	1.00	0.00
		POBAT	158	67	440	1016	0.30	0.30	0.70	0.24
		POTR5	32	22	150	1477	0.41	0.09	0.90	0.23
		THPL	0	1	2	1678	1.00	0.00	1.00	0.00
		TSHE	565	23	379	714	0.04	0.35	0.76	0.54
		TSME	666	40	479	496	0.06	0.49	0.69	0.42
Boreal	MR105	ALRU2	0	0	0	744	0.00	0.00	1.00	0.00
		BEPA	360	9	310	65	0.02	0.83	0.57	0.15
		NOTALLY	21	19	147	557	0.48	0.21	0.78	0.13
		PIGL	497	6	232	9	0.01	0.96	0.68	0.03
		PIMA	309	6	233	196	0.02	0.54	0.68	0.40
		PISI	24	14	129	577	0.37	0.18	0.81	0.18
		POBAT	36	23	193	492	0.39	0.28	0.71	0.14
		POTR5	88	21	277	358	0.19	0.44	0.60	0.19
		TSME	26	12	100	606	0.32	0.14	0.85	0.26

Table 13. Regional biomass and volume prediction estimates

			Area		Aboveground Live Tree (>2.5cm DBH) Biomass			Aboveground Snag (>25cm DBH) Biomass			Live Tree (>12.5cm DBH) Volume		
			(1000 ha)		(Mg ha^{-1})		(Tg)	(Mg ha^{-1})		(Tg)	(m^3 ha^{-1})		(mil m^3)
			Total	Forested	Mean	Median	Total	Mean	Median	Total	Mean	Median	Total
Study Area excluding USFS Wilderness and Glacier Bay National Park	GNN	Boreal	878.5	709.4	38.5	27.0	27.3	7.7	2.0	5.5	26.1	5.0	18.5
		Maritime	12,340.9	5,870.4	204.1	172.0	1,198.0	26.0	14.0	152.7	176.1	100.0	1,033.5
		COAK Unit	13,219.4	6,579.8	178.7	138.0	1,225.4	23.2	11.0	158.2	159.9	71.0	1,052.0
	Cahoon et al. 2020	COAK Unit	22,020.0	6,196.1 **(95.3)**	200.2 **(5.5)**		1241.5 **(34.0)**	31.9 **(1.2)**		197.5 **(7.5)**	137.1 **(5.4)**		1,610
	Yatskov et al. 2019	Boreal		595	41.6 **(2.5)**		24.6 **(1.7)**	23.5 **(2.4)**		13.9 **(1.6)**			
		Maritime		3,660	218.9 **(4.6)**		790.5 **(17.3)**	30.5 **(1.0)**		110.0 **(3.8)**			
		COAK Unit		4,255	194.0 **(4.1)**		815.1 **(17.3)**	29.5 **(1.0)**		123.9 **(4.0)**			
Study Area including USFS Wilderness and Glacier Bay National Park	GNN	Boreal	878.5	709.4	38.5	27.0	27.3	7.7	2.0	5.5	26.1	5.0	18.5
		Maritime	16,300.2	7,796.7	212.0	180.0	1,652.5	26.7	15.0	208.5	187.8	117.0	1,464.6
		COAK Unit	17,178.7	8,506.2	191.7	153.0	1,679.9	24.5	13.0	213.9	174.4	91.0	1,483.1
Tongass National Forest	GNN	Not Reserved	717.2	652.5	238.2	207.0	155.4	31.3	20.0	20.4	306.3	269.0	199.9
		Inventoried Roadless Area	3,726.4	2,362.9	218.8	186.0	516.9	31.2	20.0	73.6	281.0	241.0	664.0
		Wilderness	2,334.0	1,503.6	244.0	215.0	366.9	36.5	24.0	54.9	314.4	283.0	472.7
		Forest Total	6,777.6	4,518.9	229.8	199.0	1,039.2	32.0	20.0	148.9	295.5	259.0	1,336.6

Figures

Figure 1. Study area including modeling regions modified from Nowacki et al. (2002) Ecological Provinces of Alaska

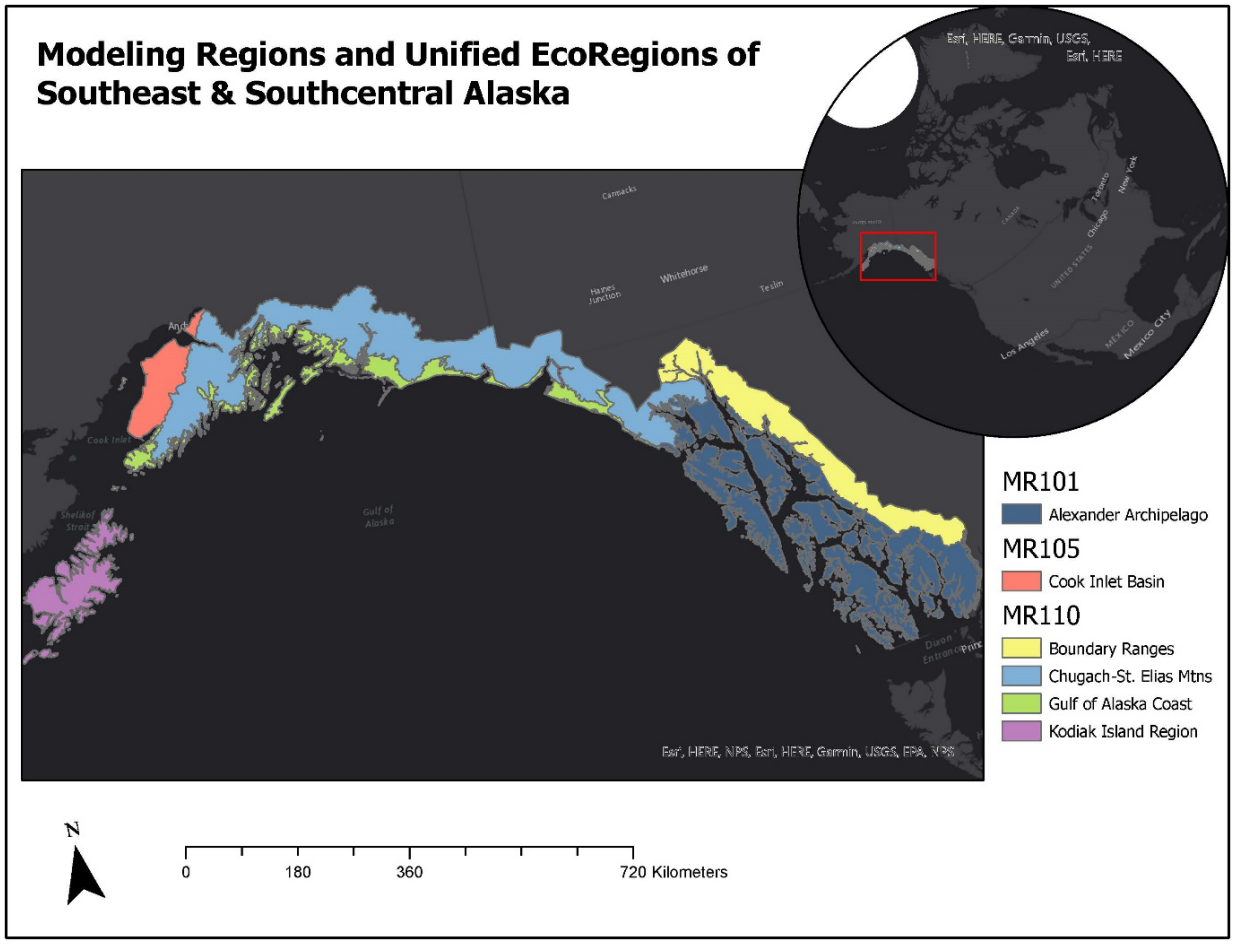

Figure 2. Environmental characteristics across the coastal Alaska region

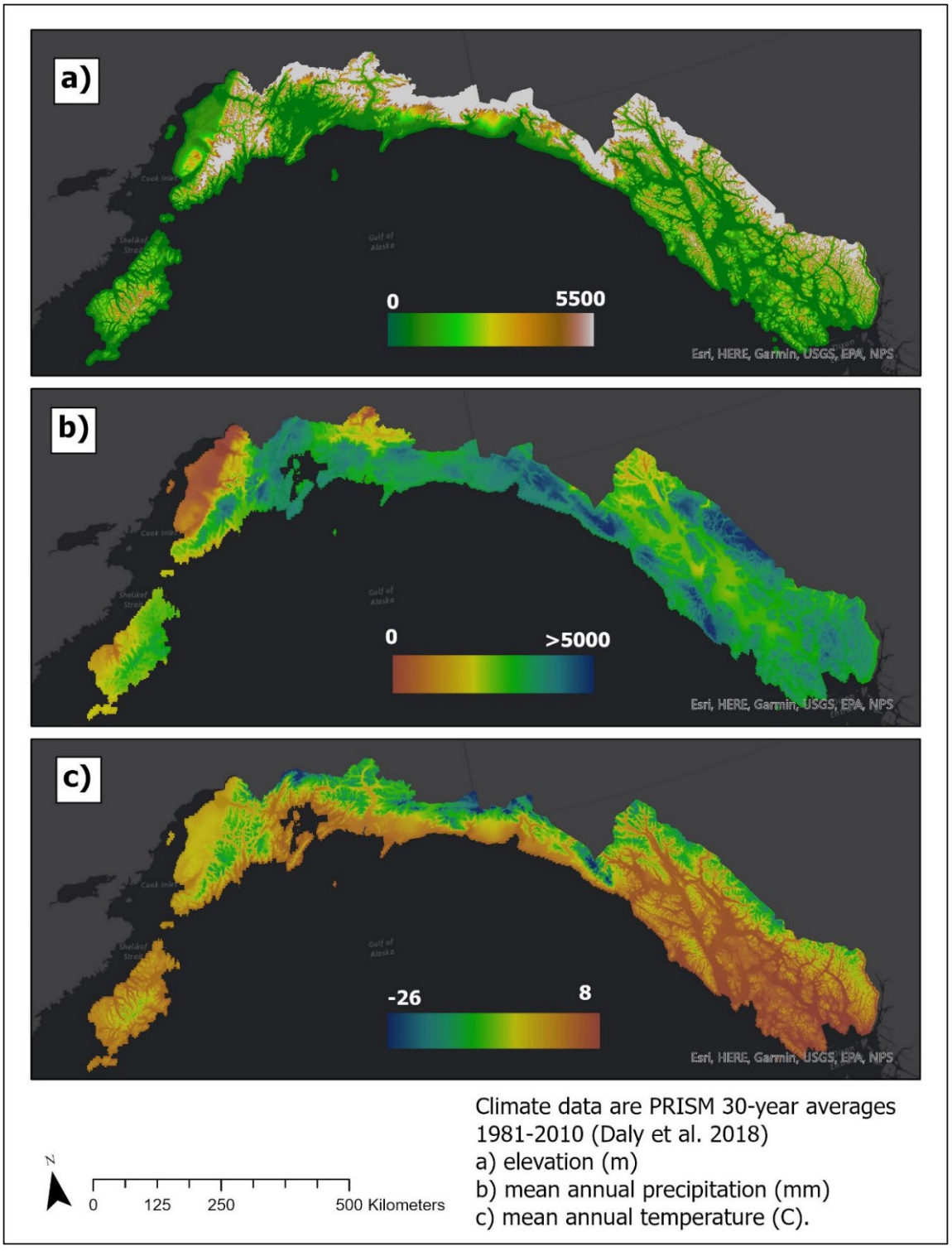

Figure 3. Approximate FIA field plot locations across the study area

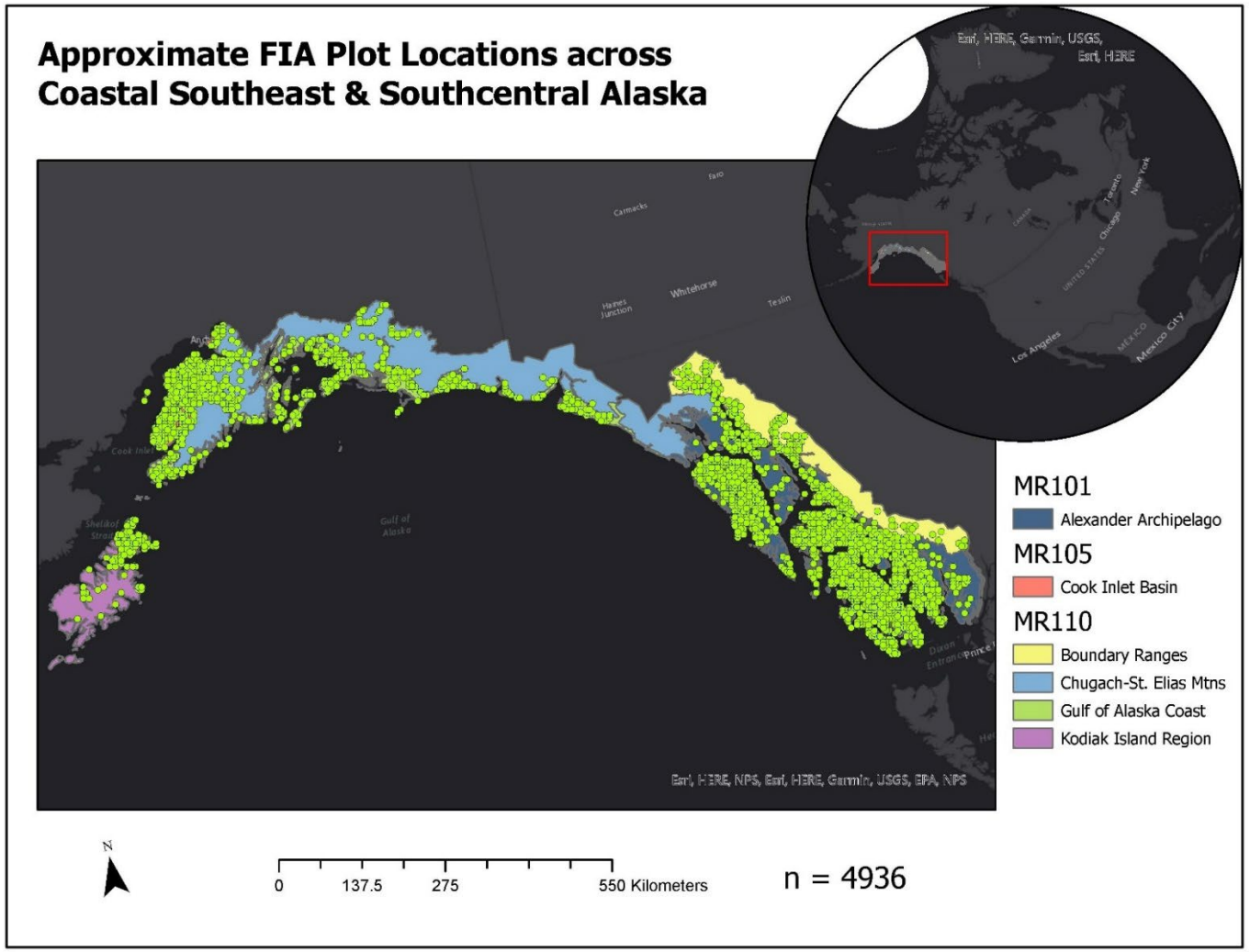

Figure 4. Effects of various cloud masking techniques on Landsat surface reflectance

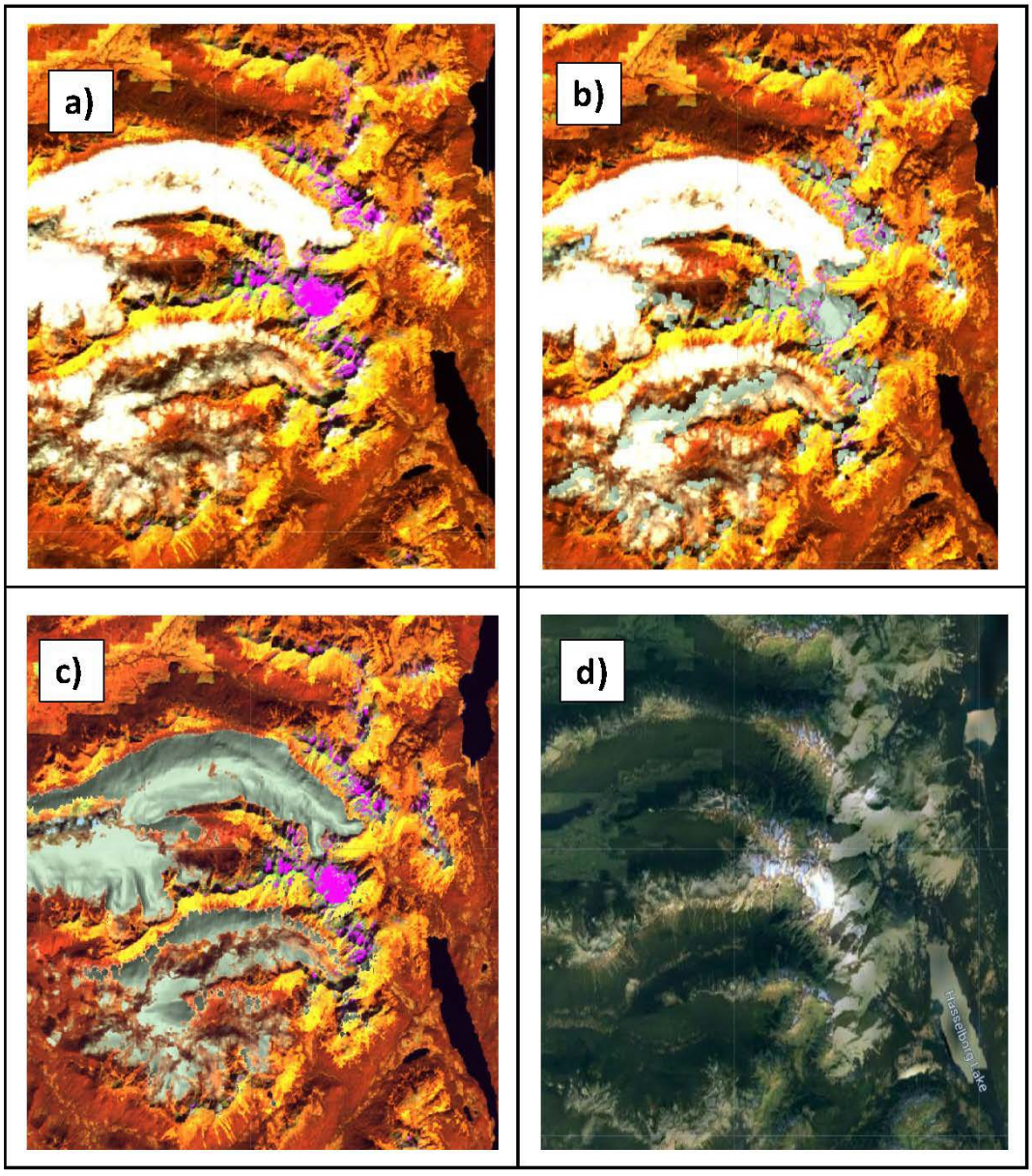

West Admiralty, Aug 15, 2001

Landsat mosaic before and after multi-step approach to cloud masking.

a) Original surface reflectance image
b) Cloud masking using Fmask (Zhu and Woodcock 2011)
c) Cloud masking with Google Cloud Score, threshold = 30 (Google 2022)
d) High resolution true color TerraMetrics satellite imagery

Figure 5. LandTrendr pixel timeseries

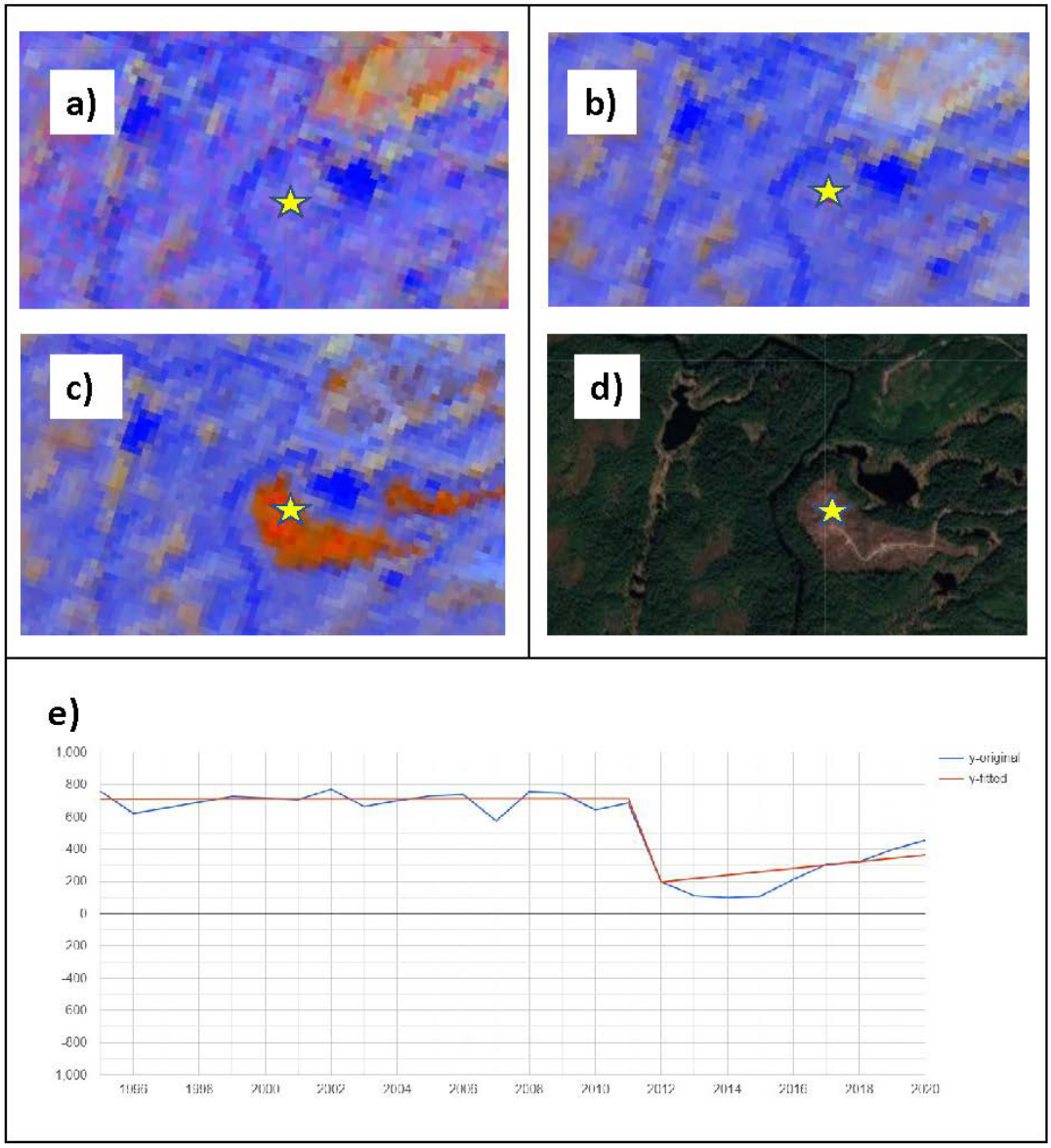

N. Prince of Wales Island

Tasseled cap brightness, greenness, wetness, rendered in RGB. From top left: Landsat timeseries a) 1995, b) 2005, c) 2015. d) 2018 high resolution satellite image. e) LandTrendr pixel timeseries fitting and segmentation algorithm based on the Normalized Burn Ratio (NBR) demonstrating original pixel spectral values, fitted trajectory, and segmentation.

Figure 6. Soil hydrologic characteristics influence on model output

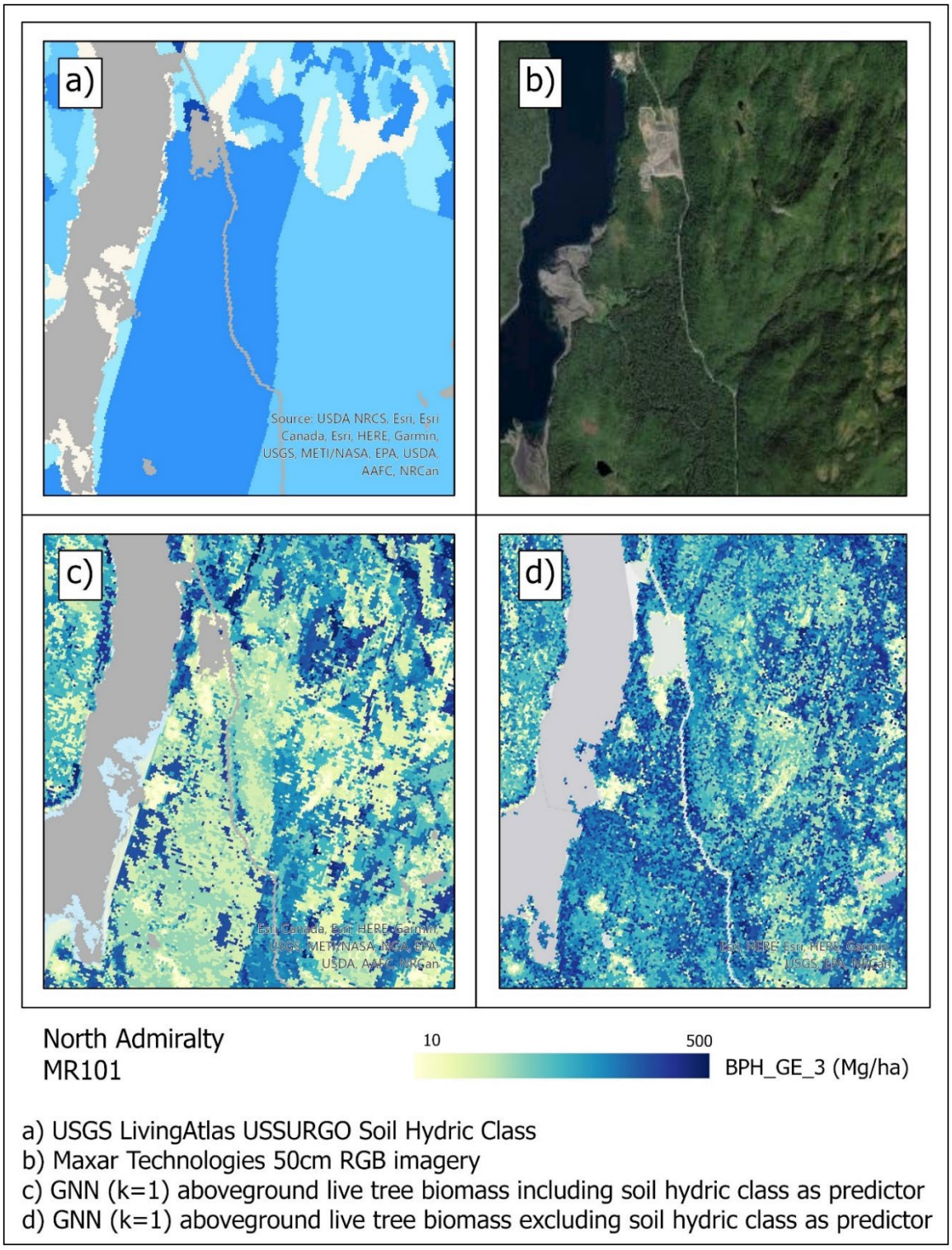

a) USGS LivingAtlas USSURGO Soil Hydric Class
b) Maxar Technologies 50cm RGB imagery
c) GNN (k=1) aboveground live tree biomass including soil hydric class as predictor
d) GNN (k=1) aboveground live tree biomass excluding soil hydric class as predictor

Figure 7. FIA field plot footprint overlaid by 3x3 30-m Landsat pixels.

Microplot was centered at subplot centers during periodic surveys in Alaska (1995-2003) but offset by 3.7m as shown during annual inventories (2004-2020). FIA crews in Alaska install plot footprints without adjusting for declination (USDA 2021c).

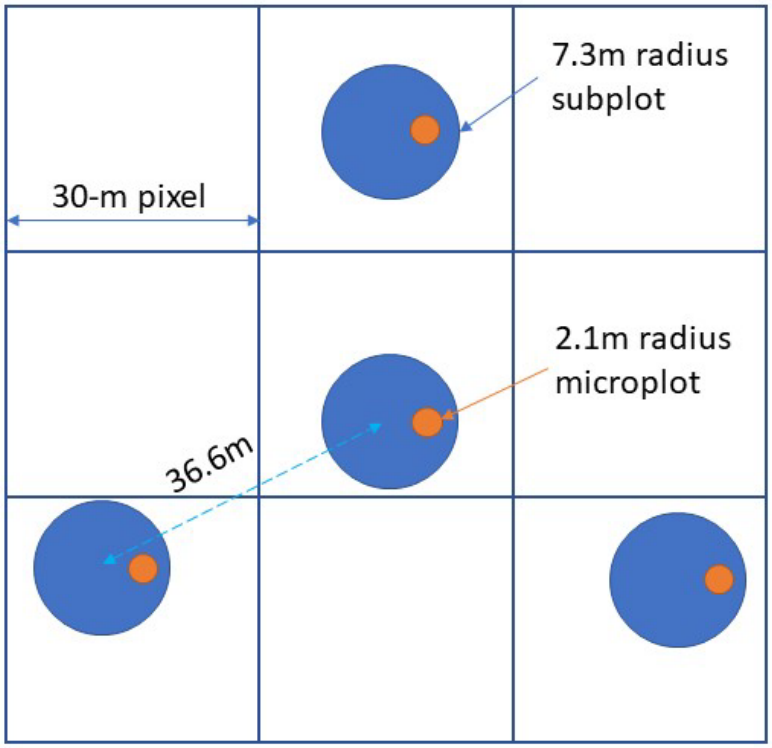

Figure 8. Nonforest mask options and development

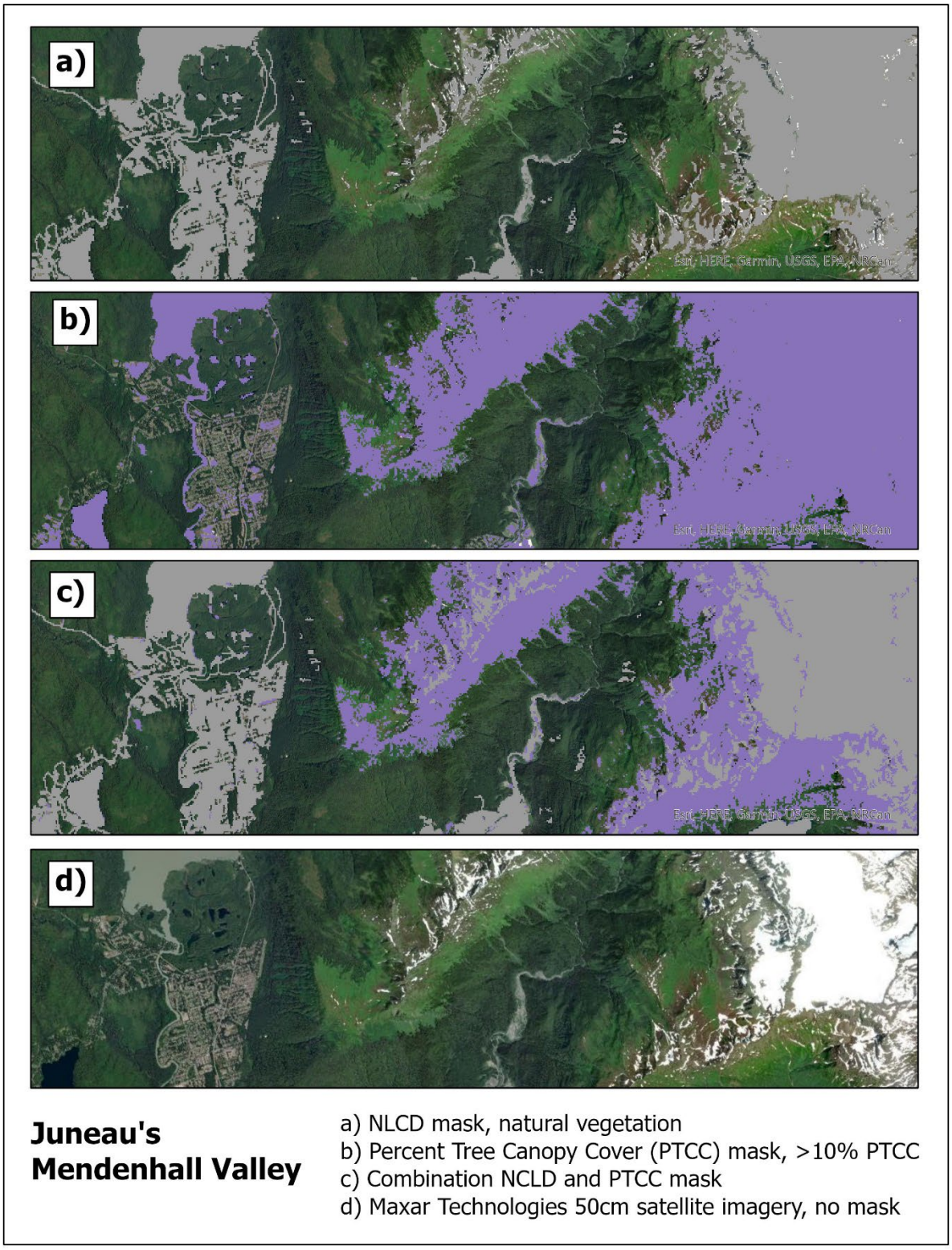

Figure 9. Multi-scale accuracy assessed using the Geometric Mean Functional Relationship (GMFR) for aboveground live tree biomass

9a. MR101

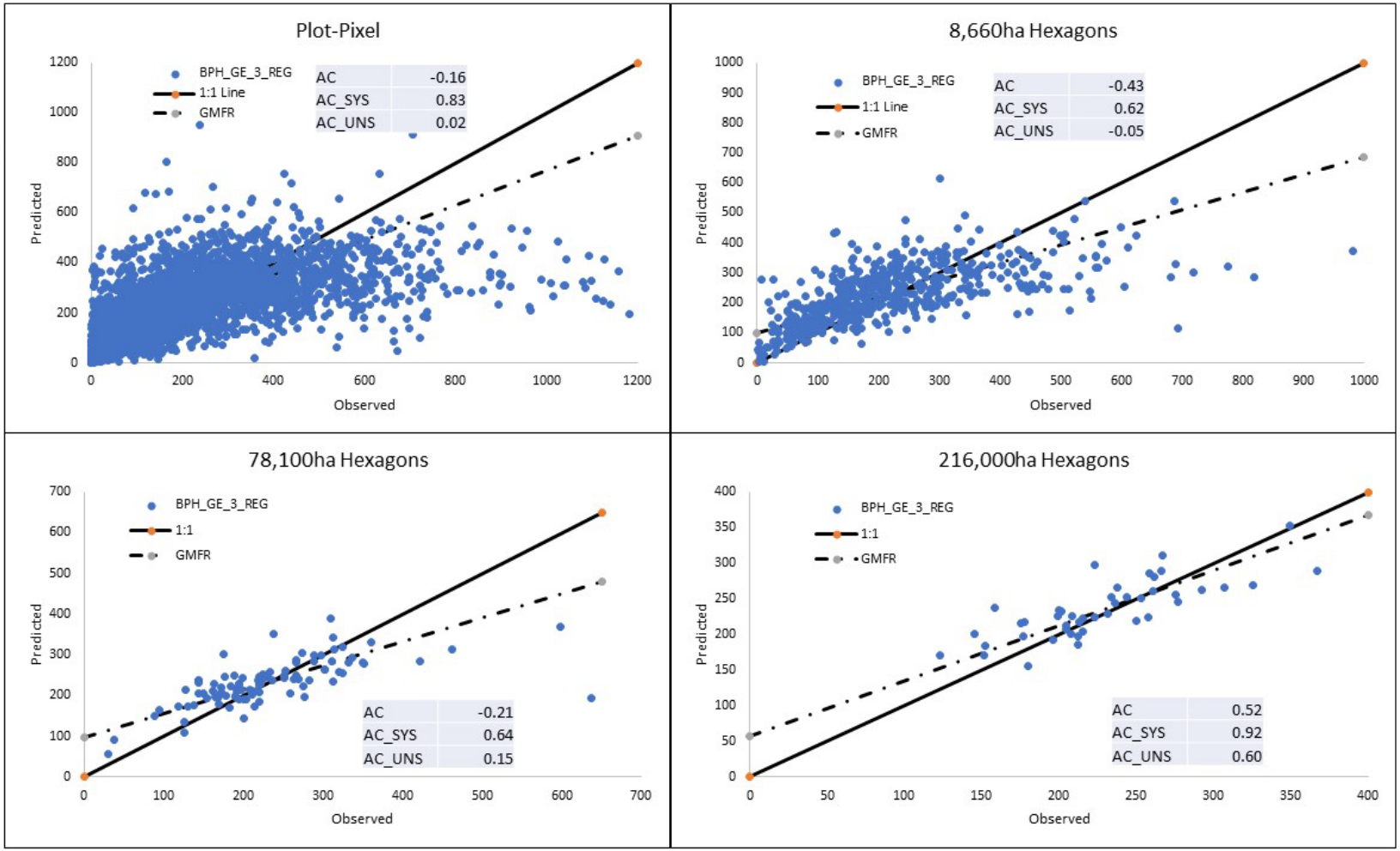

9b. MR105

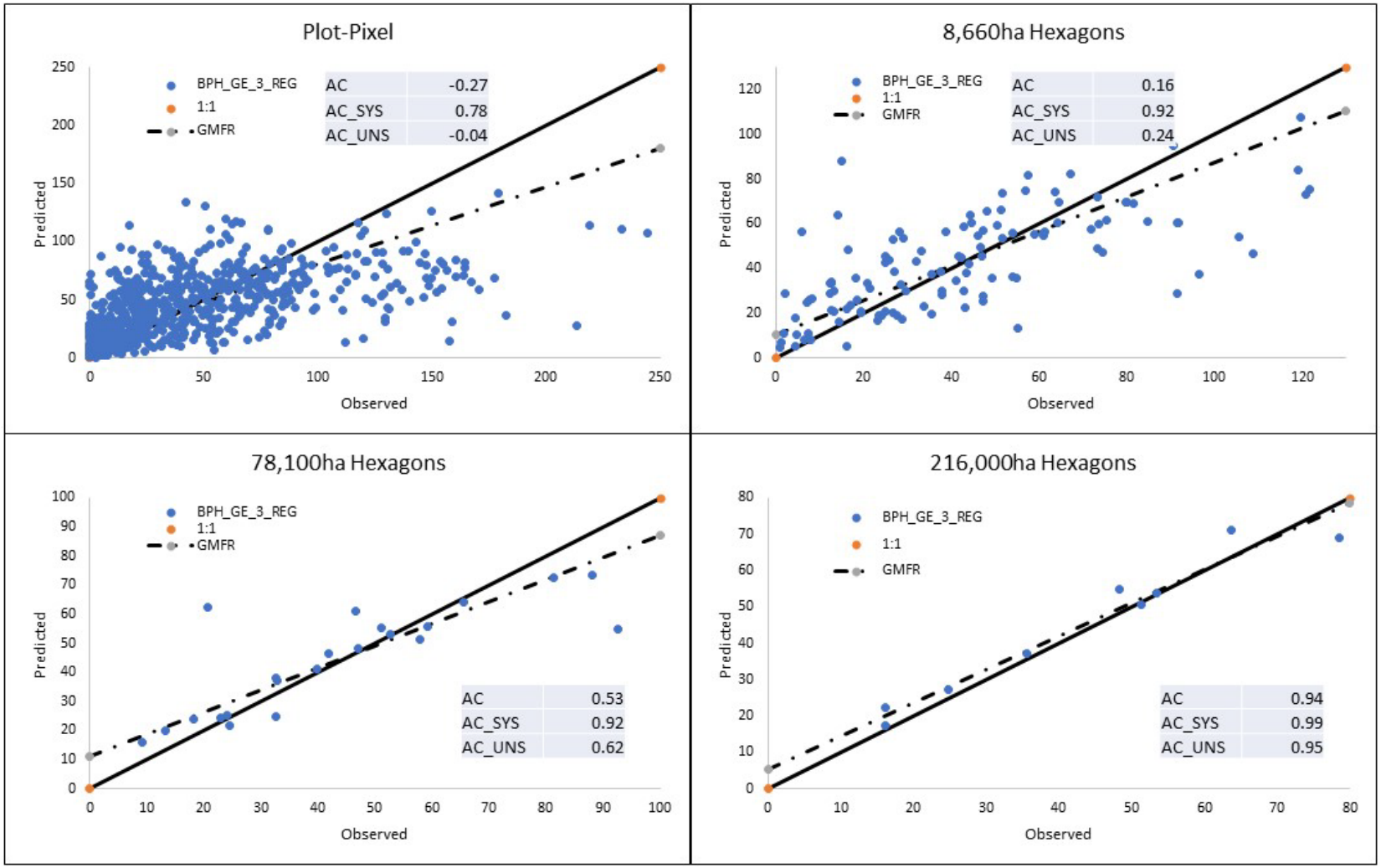
Plot-Pixel
BPH_GE_3_REG
1:1
GMFR
AC -0.27
AC_SYS 0.78
AC_UNS -0.04
Predicted
Observed
8,660ha Hexagons
BPH_GE_3_REG
1:1
GMFR
AC 0.16
AC_SYS 0.92
AC_UNS 0.24
Predicted
Observed
78,100ha Hexagons
BPH_GE_3_REG
1:1
GMFR
AC 0.53
AC_SYS 0.92
AC_UNS 0.62
Predicted
Observed
216,000ha Hexagons
BPH_GE_3_REG
1:1
GMFR
AC 0.94
AC_SYS 0.99
AC_UNS 0.95
Predicted
Observed

9c. MR110

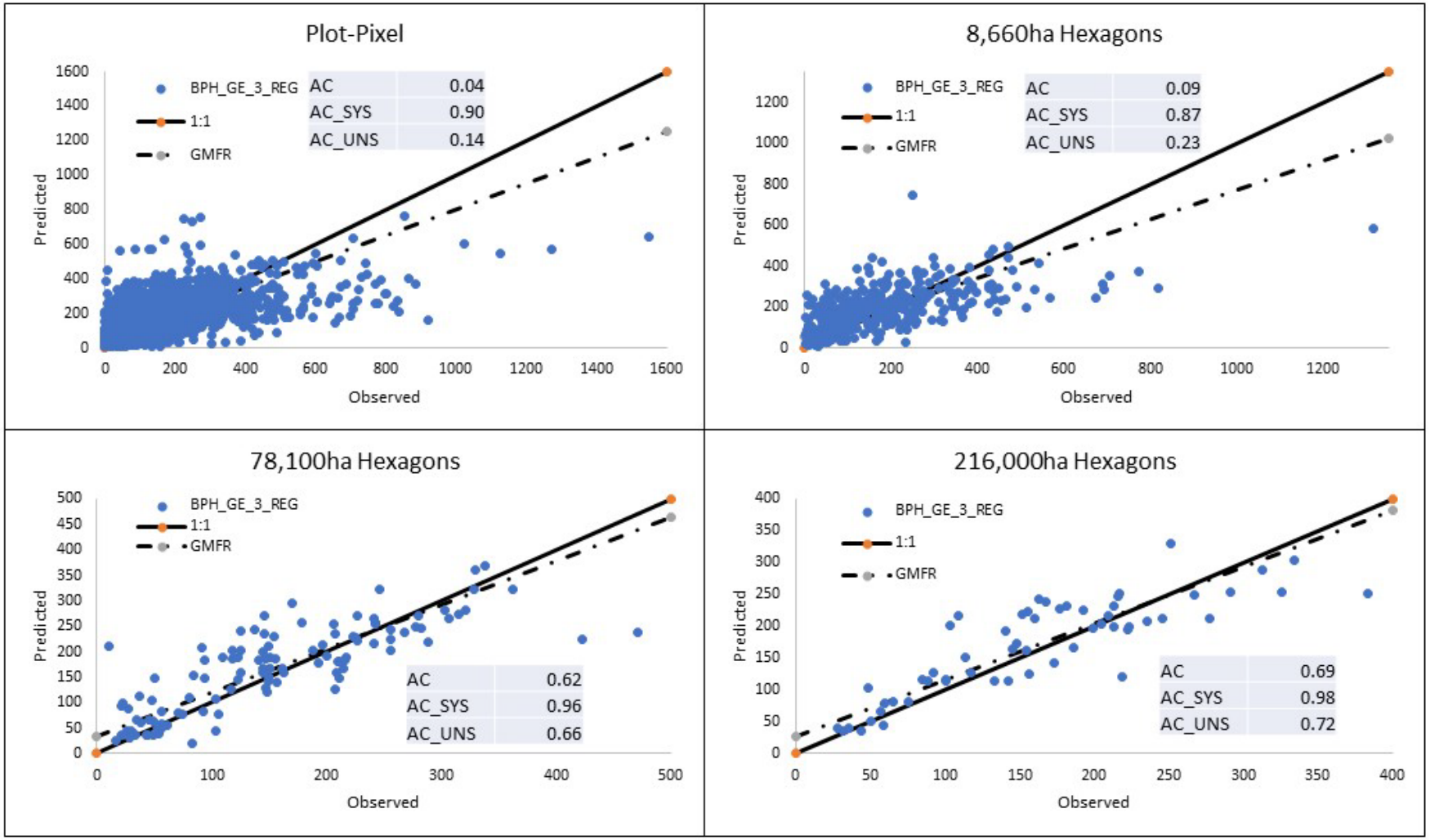
Plot-Pixel
BPH_GE_3_REG
1:1
GMFR
AC 0.04
AC_SYS 0.90
AC_UNS 0.14
Predicted
Observed
8,660ha Hexagons
BPH_GE_3_REG
1:1
GMFR
AC 0.09
AC_SYS 0.87
AC_UNS 0.23
Predicted
Observed
78,100ha Hexagons
BPH_GE_3_REG
1:1
GMFR
AC 0.62
AC_SYS 0.96
AC_UNS 0.66
Predicted
Observed
216,000ha Hexagons
BPH_GE_3_REG
1:1
GMFR
AC 0.69
AC_SYS 0.98
AC_UNS 0.72
Predicted
Observed

Figure 10. Mapped results of biomass predictions at multiple scales

10a. Hex-10km (8,660 ha)

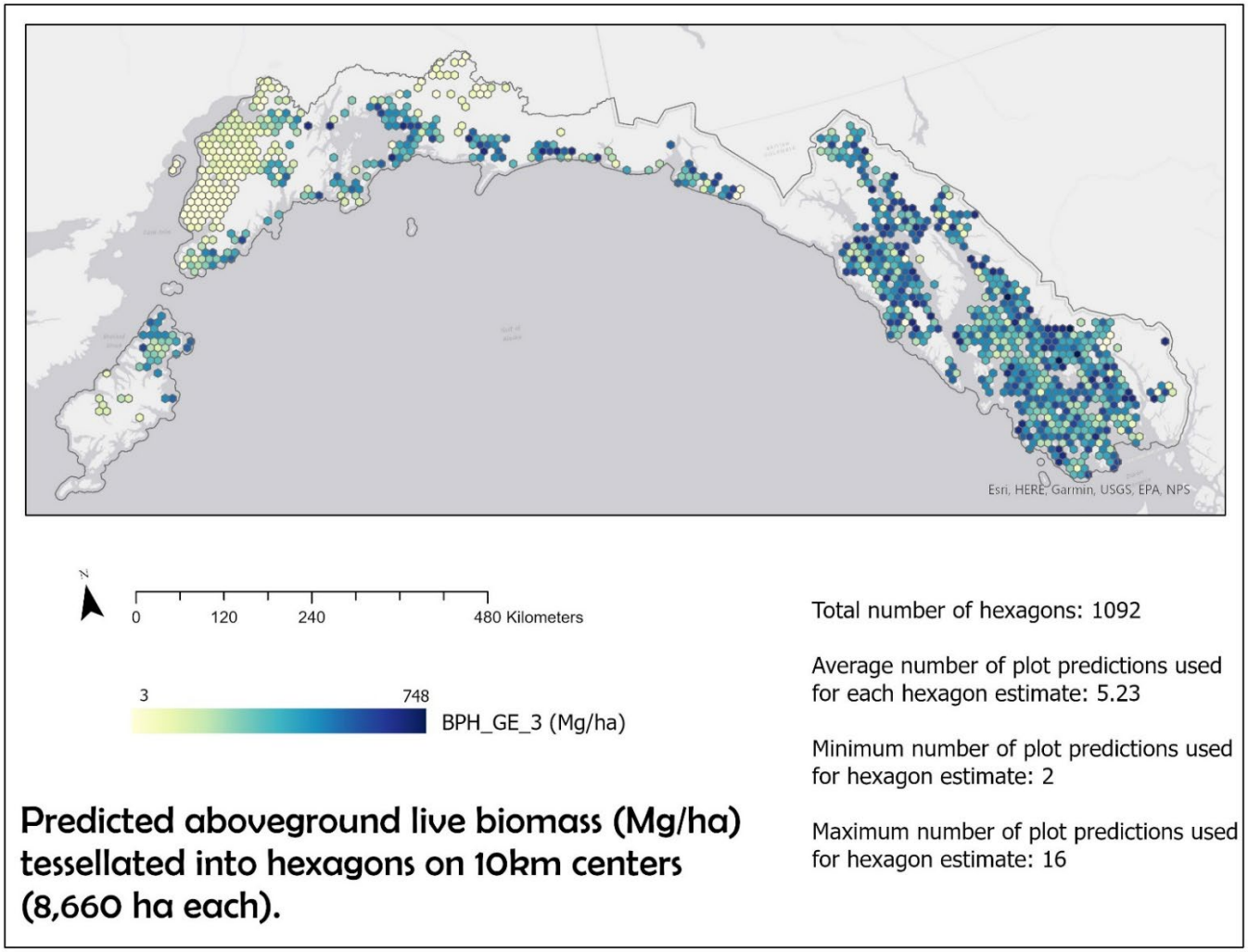

10b. Hex-30km (78,100 ha)

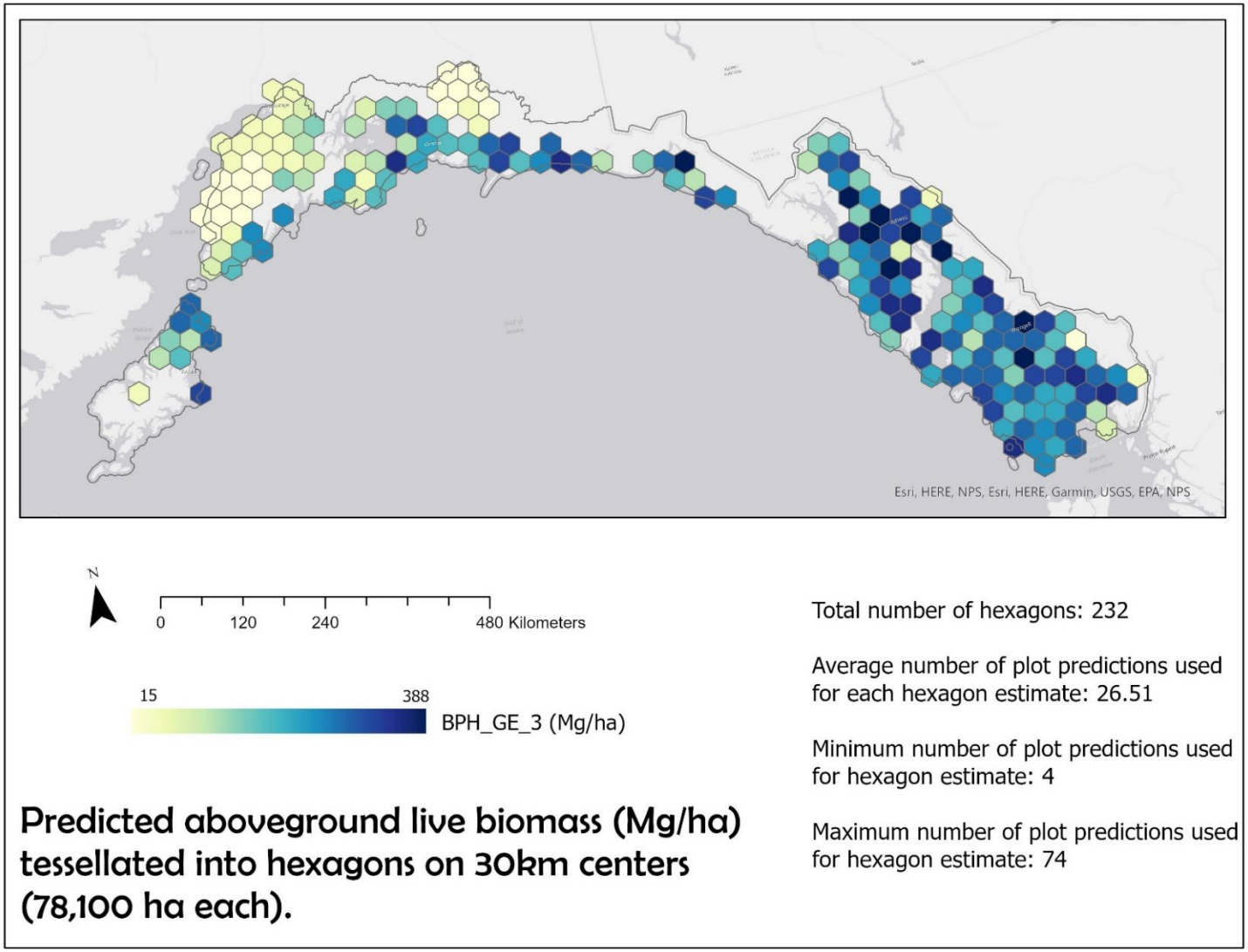

10c. Hex-50km (216,000 ha)

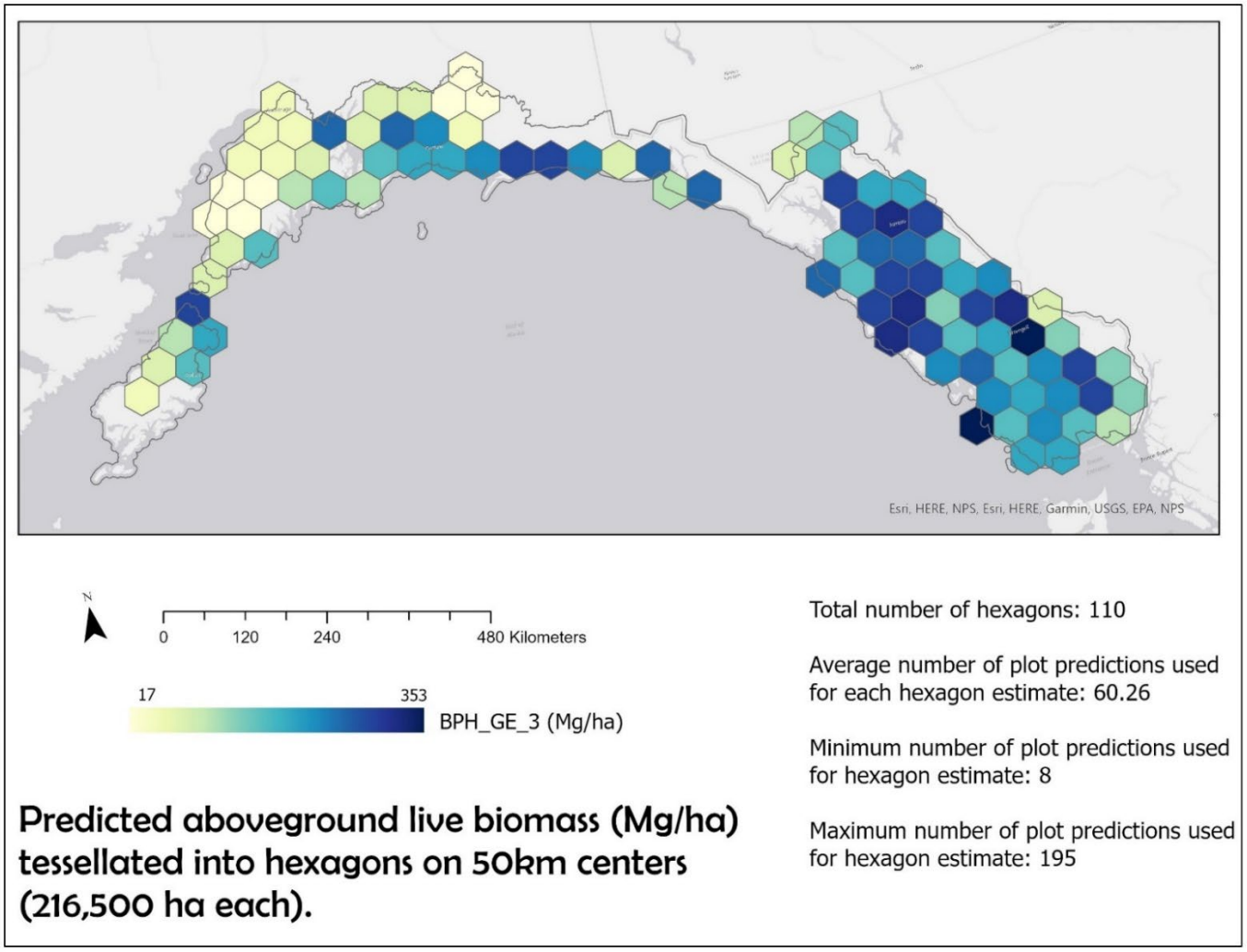

Figure 11. Distribution and frequency of aboveground live tree biomass by Modeling Region (plot-pixel)

11a. MR101 observed vs. predicted (*k*=7)

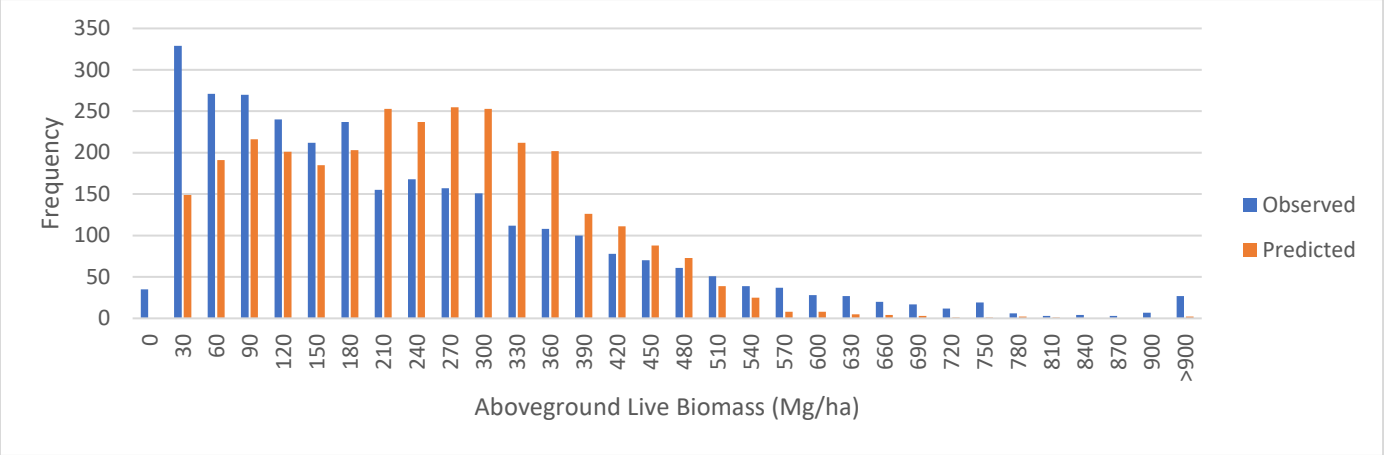

11b. MR105 observed vs. predicted (*k*=7)

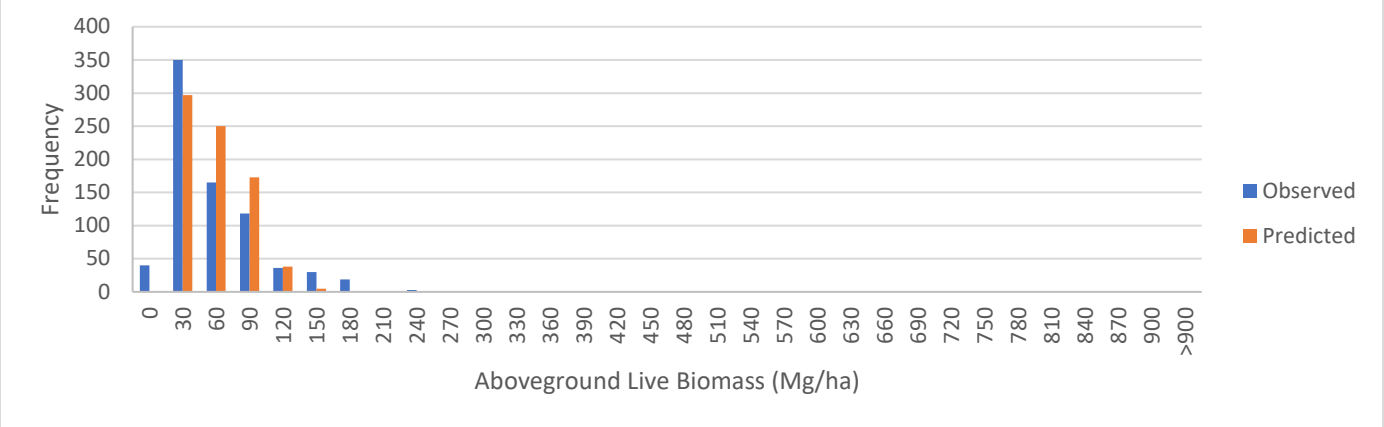

11c. MR110 observed vs. predicted (*k*=7)

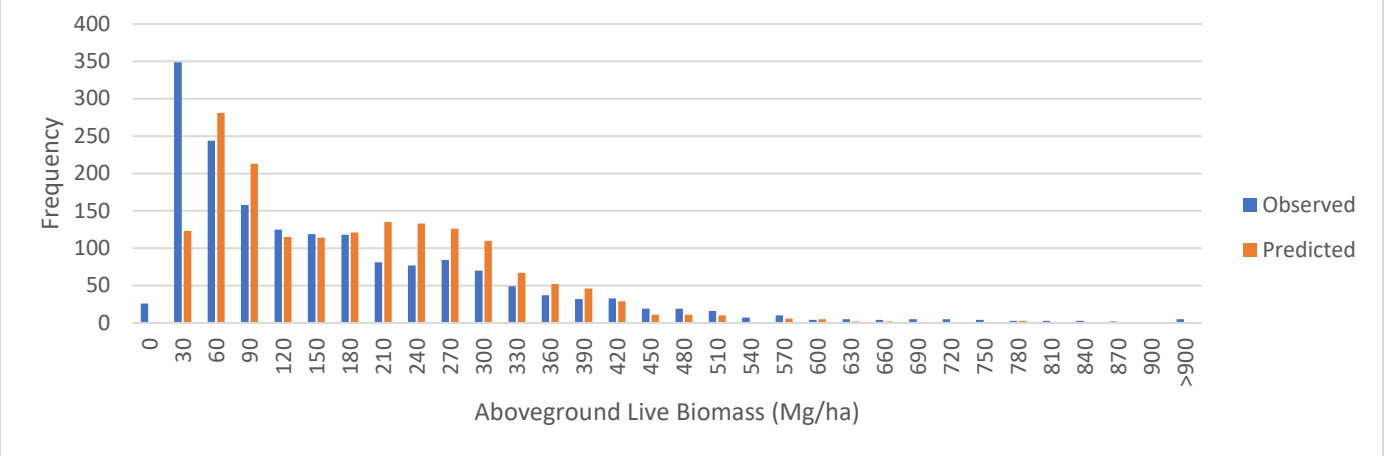

Figure 12. Environmental Predictors and Species Abundance

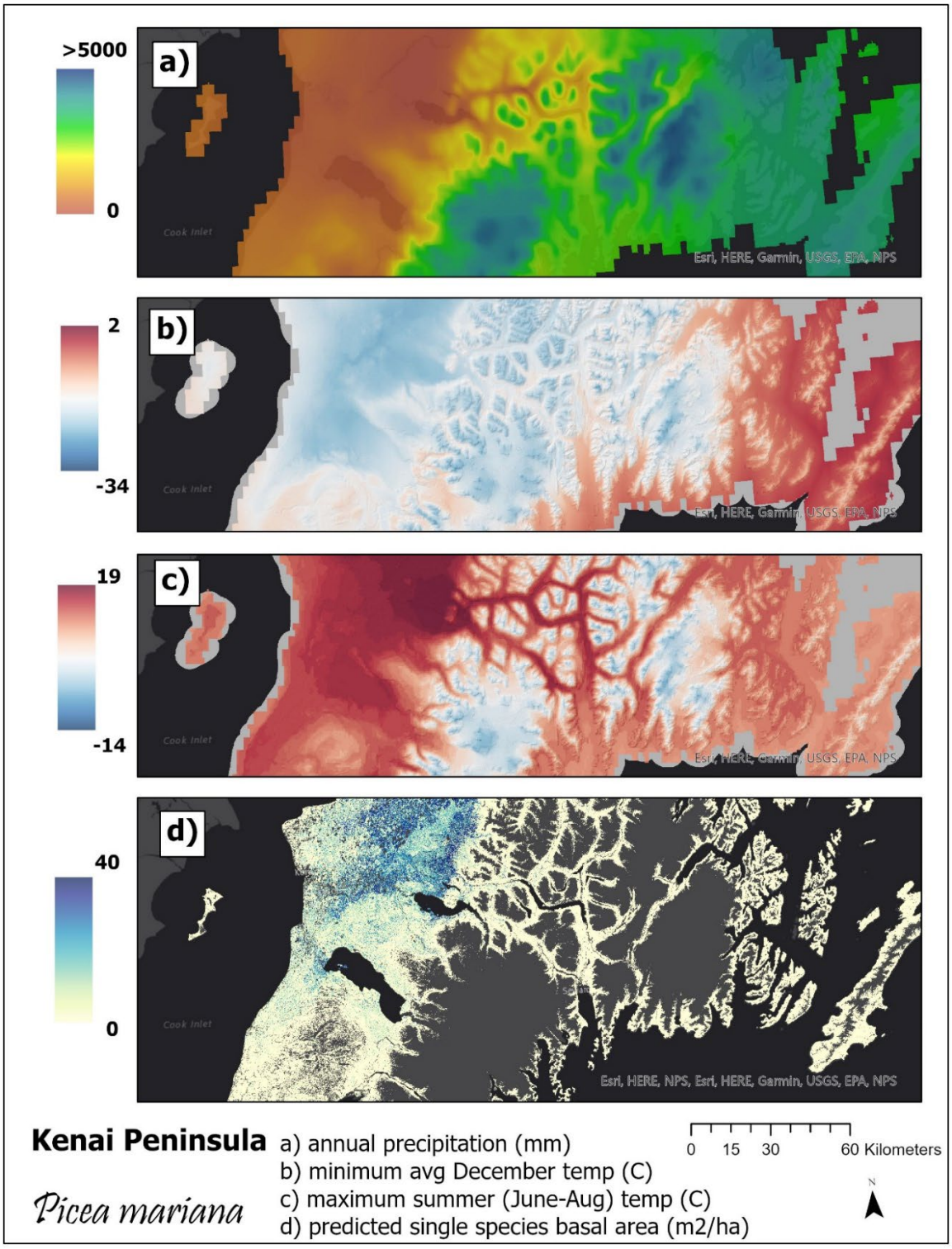

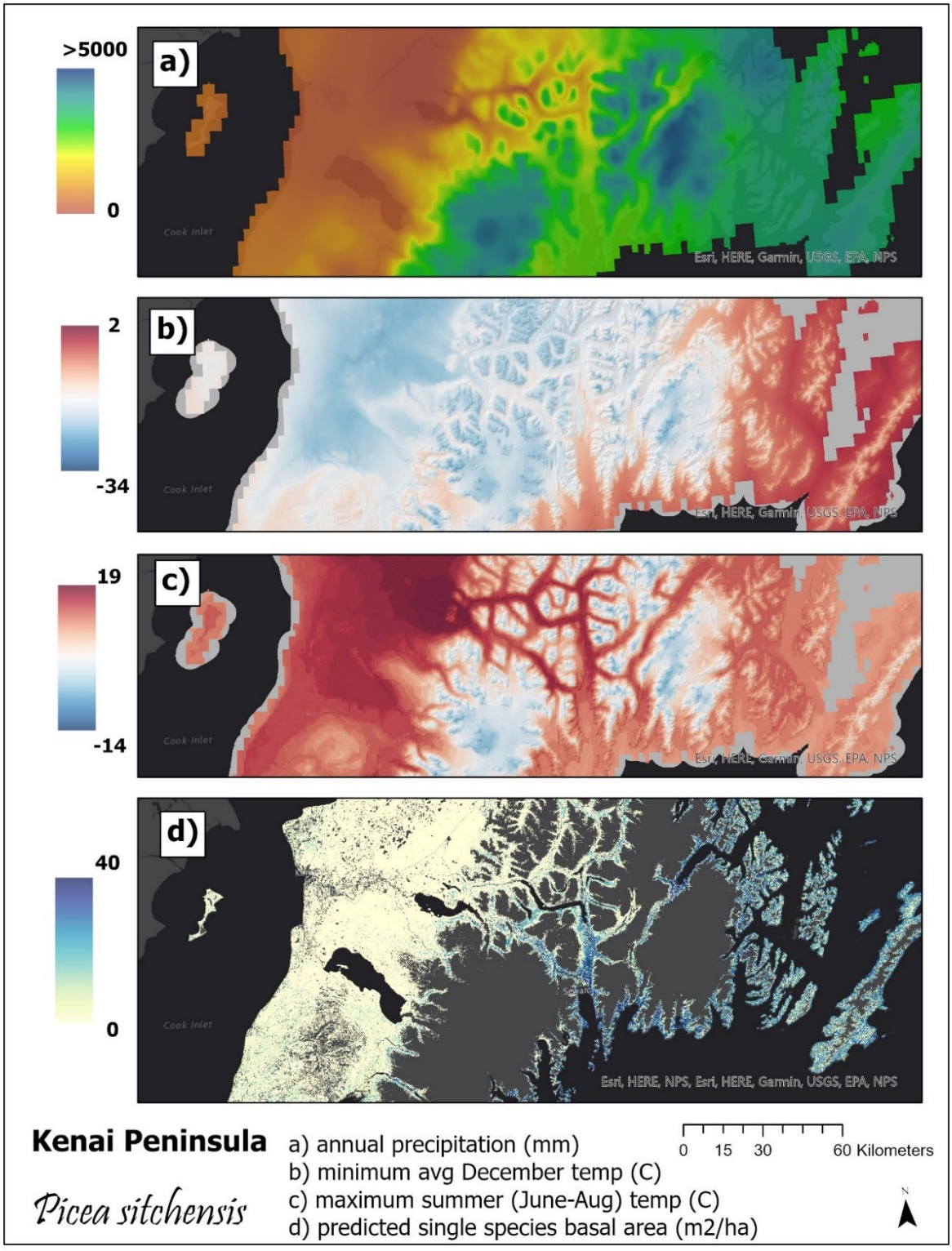
>5000
0
a)
Cook Inlet
Esri, HERE, Garmin, USGS, EPA, NPS
2
-34
b)
Cook Inlet
Esri, HERE, Garmin, USGS, EPA, NPS
19
-14
c)
Cook Inlet
Esri, HERE, Garmin, USGS, EPA, NPS
40
0
d)
Cook Inlet
Esri, HERE, NPS, Esri, HERE, Garmin, USGS, EPA, NPS
Kenai Peninsula
Picea sitchensis
a) annual precipitation (mm)
b) minimum avg December temp (C)
c) maximum summer (June-Aug) temp (C)
d) predicted single species basal area (m2/ha)
0 15 30 60 Kilometers
N

Figure 13. Tongass National Forest biomass, diameter, and height classes showed similar distributions across land designations

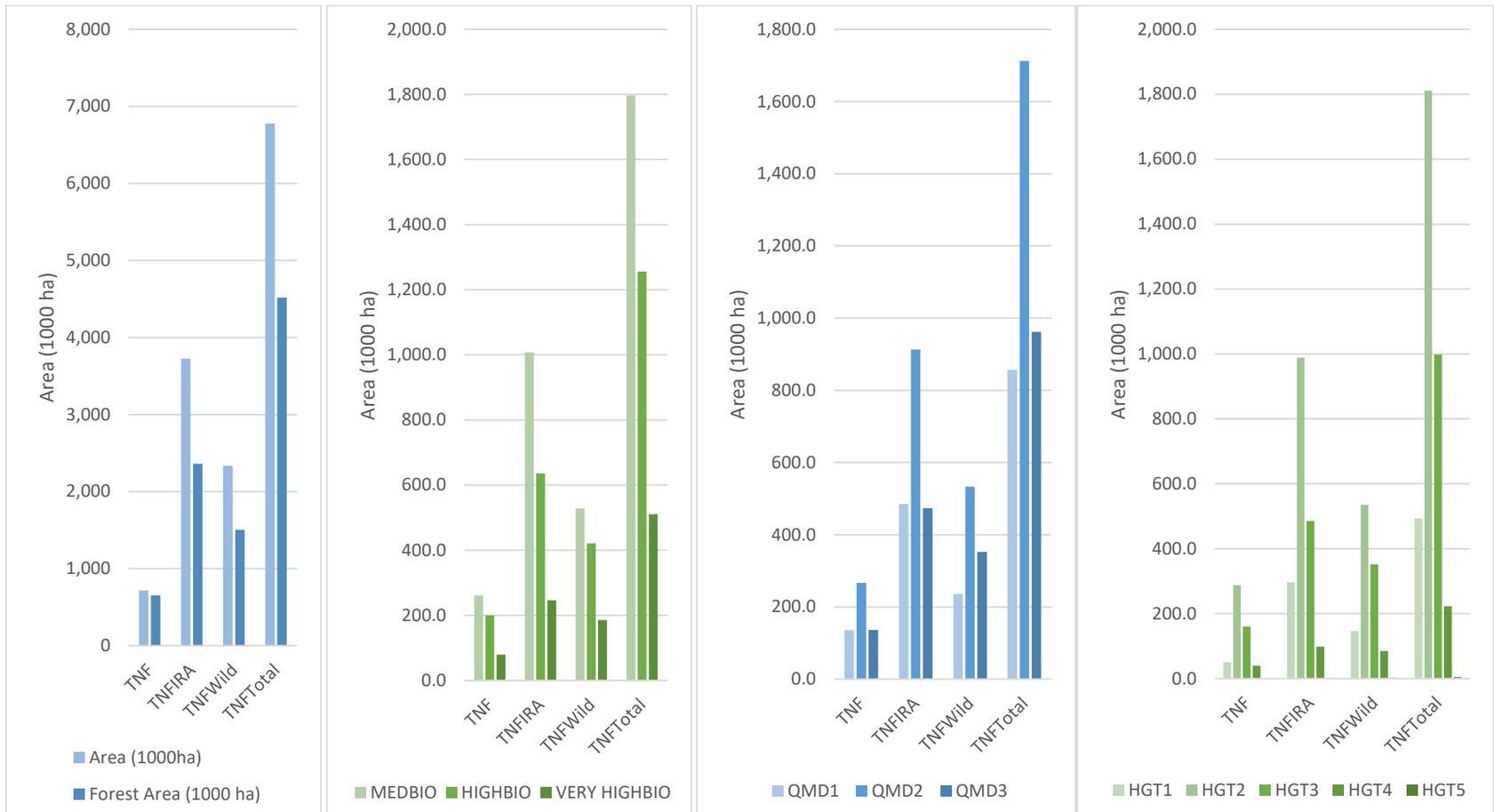

Figure 14. Aboveground live tree biomass on the Tongass National Forest

14a. Average aboveground live tree biomass per hectare by land designation

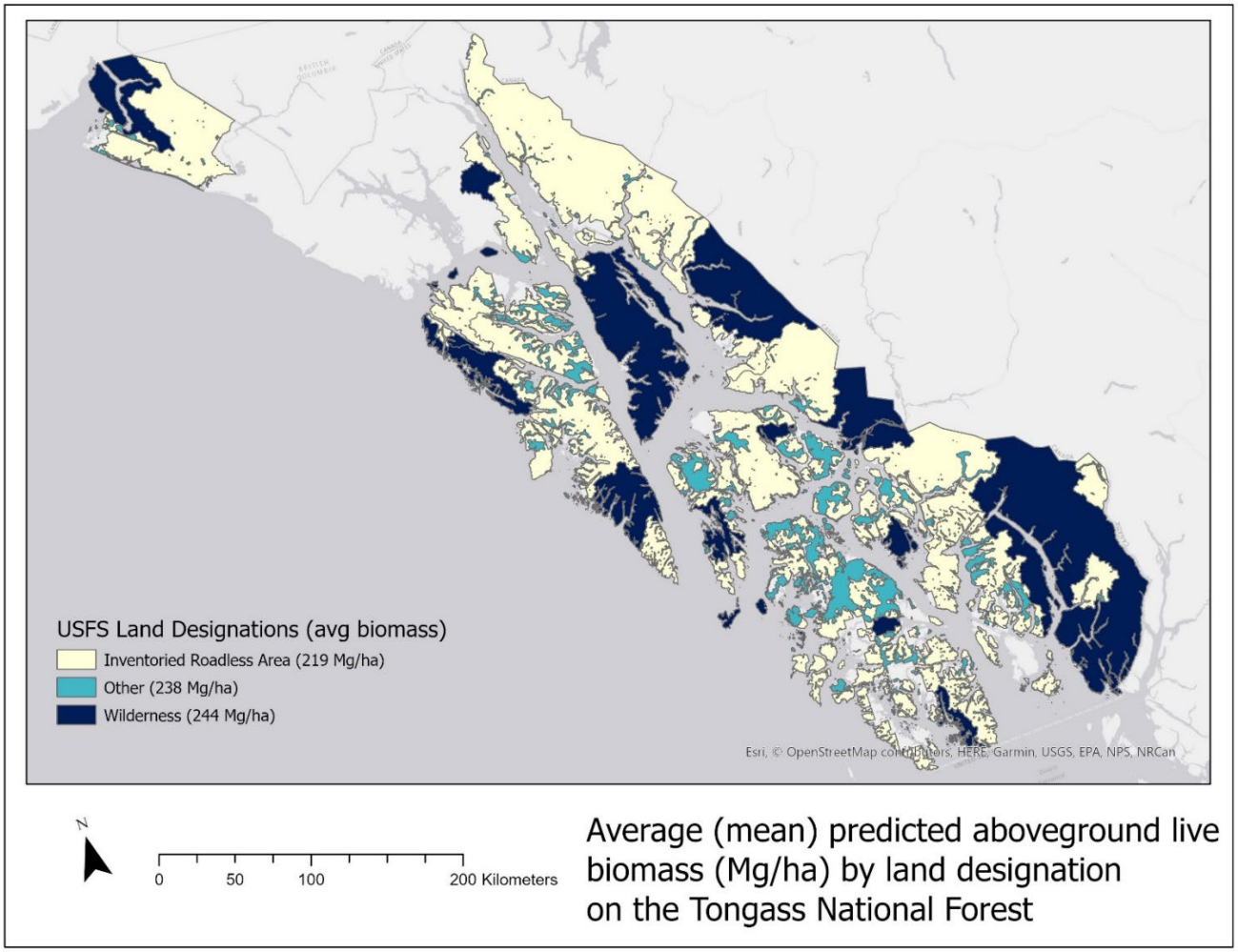

14b. Predicted biomass per hectare at 30-m pixel resolution

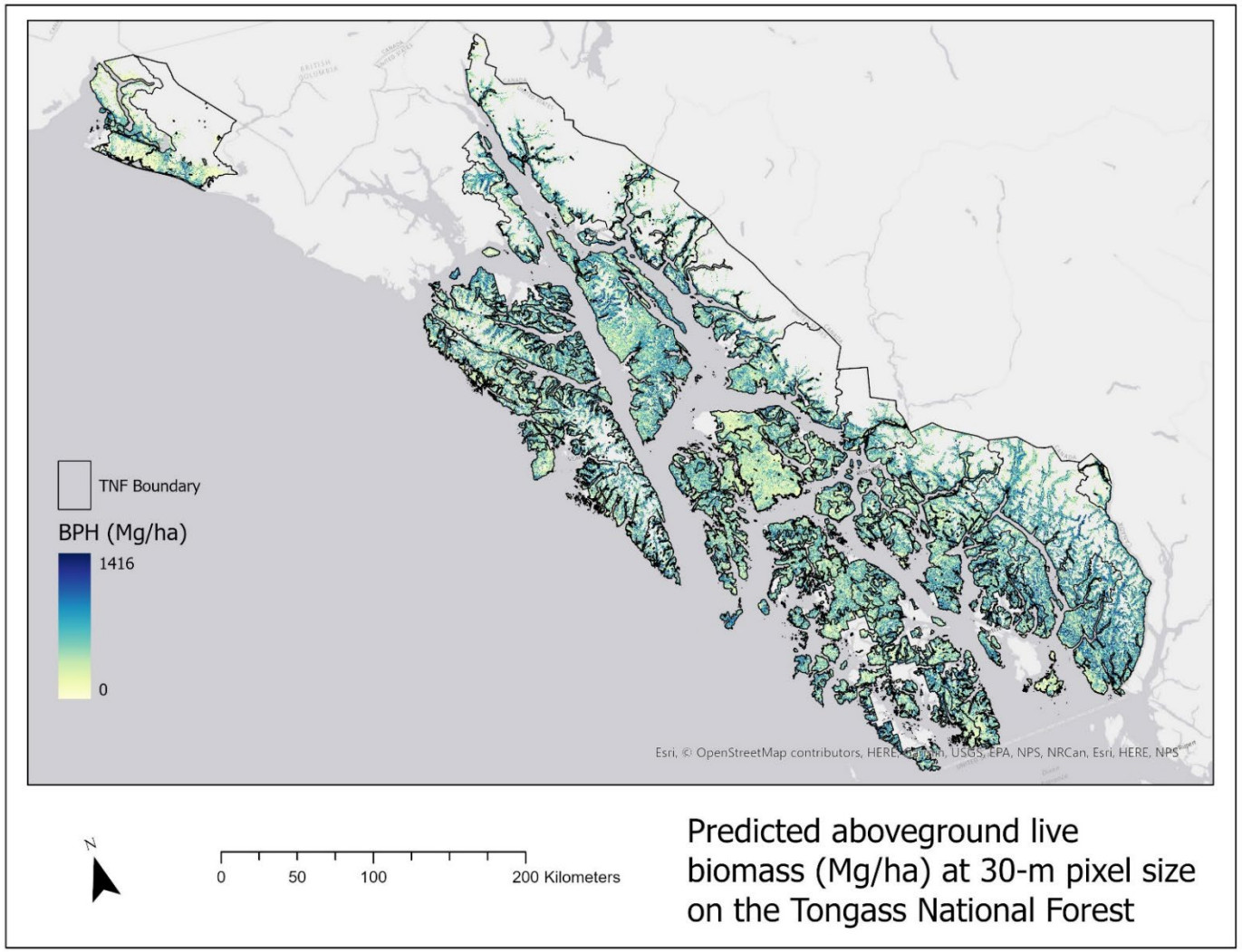

14c. Comparison of high resolution satellite imagery vs predicted biomass (Mg/ha) at 30-m pixel resolution on Prince of Wales Island

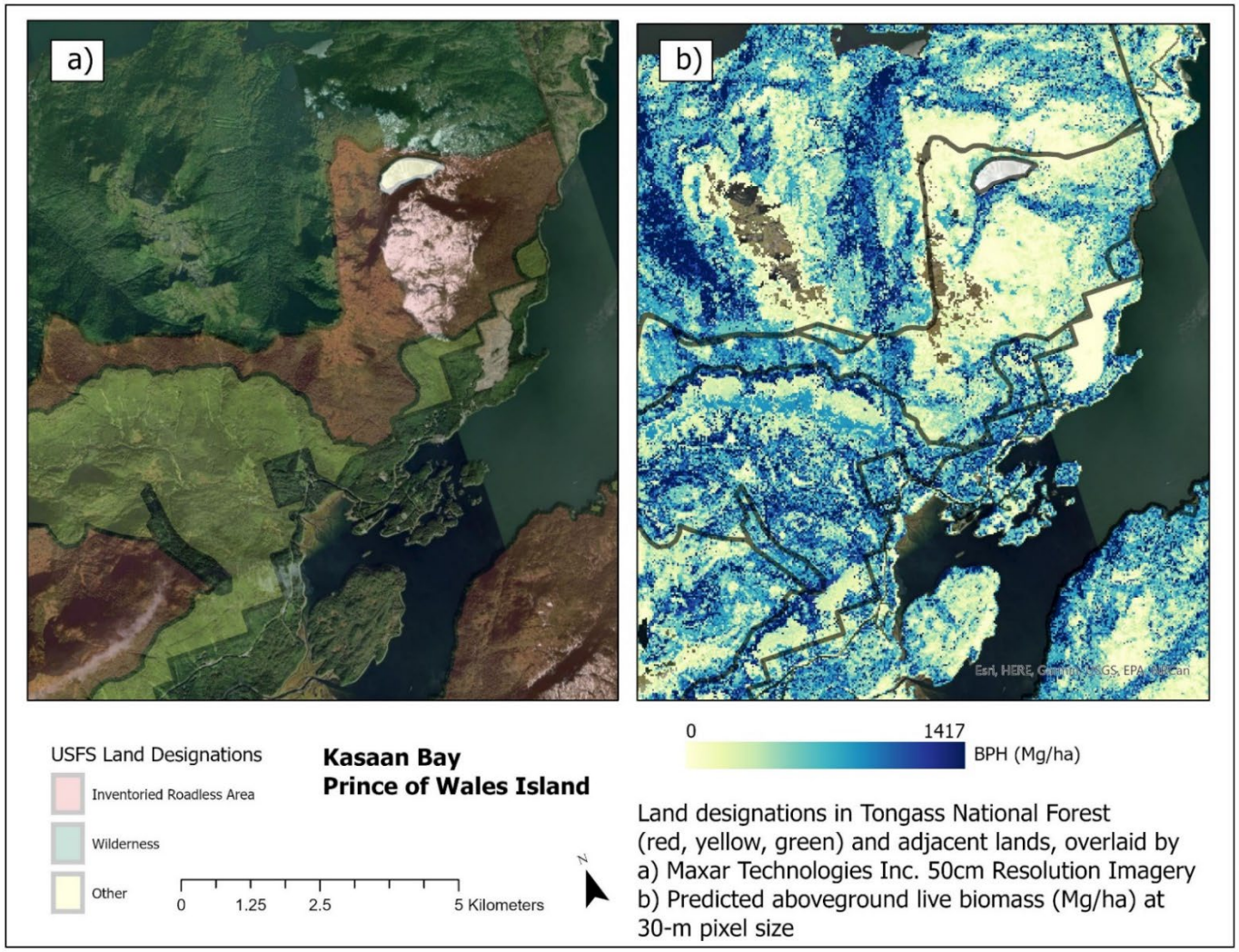

Land designations in Tongass National Forest (red, yellow, green) and adjacent lands, overlaid by a) Maxar Technologies Inc. 50cm Resolution Imagery b) Predicted aboveground live biomass (Mg/ha) at 30-m pixel size

Figure 15. Biomass estimate difference (predicted - observed) across aggregation extents

15a. Hex-10km (8,660 ha)

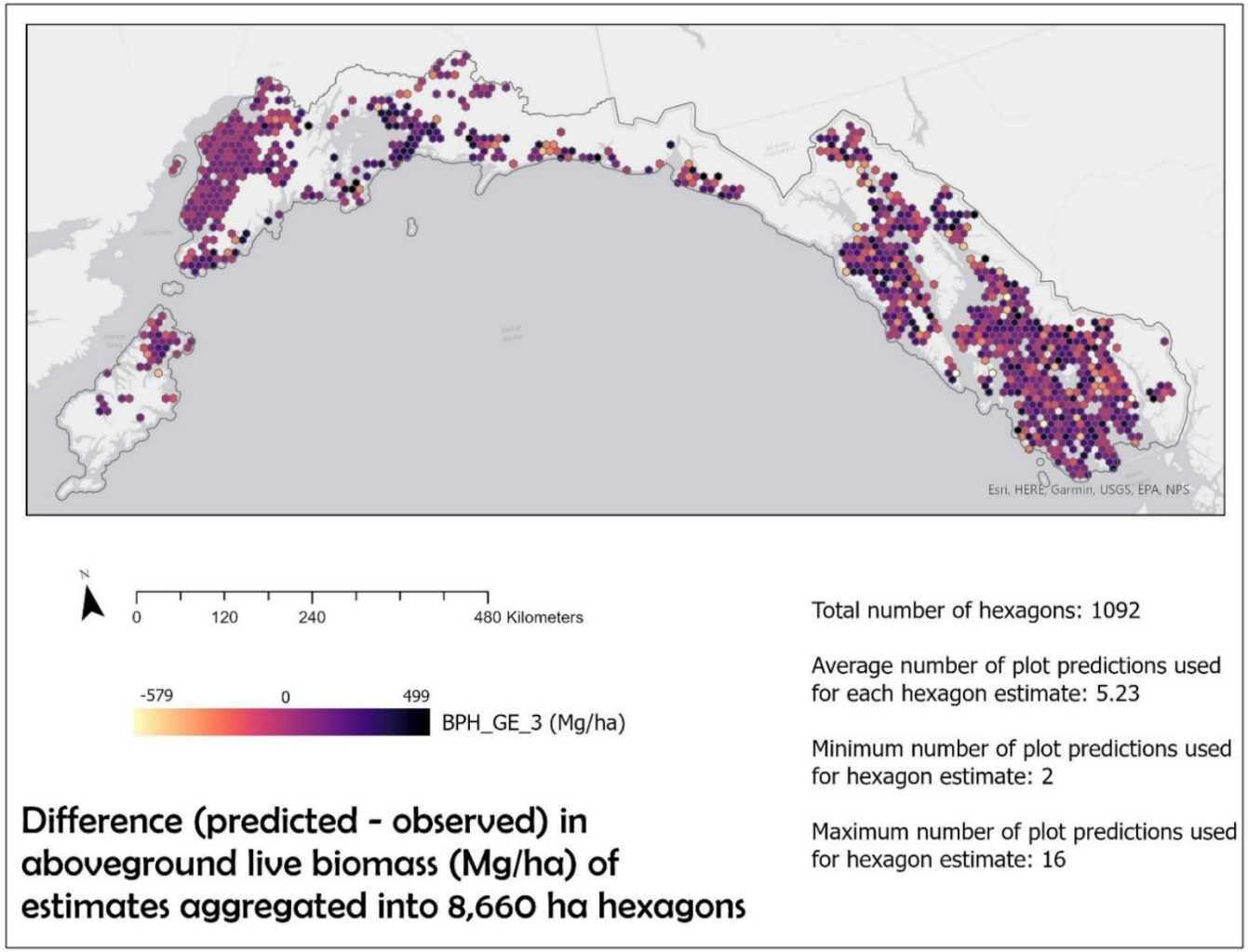

15b. Hex-30km (78,100 ha)

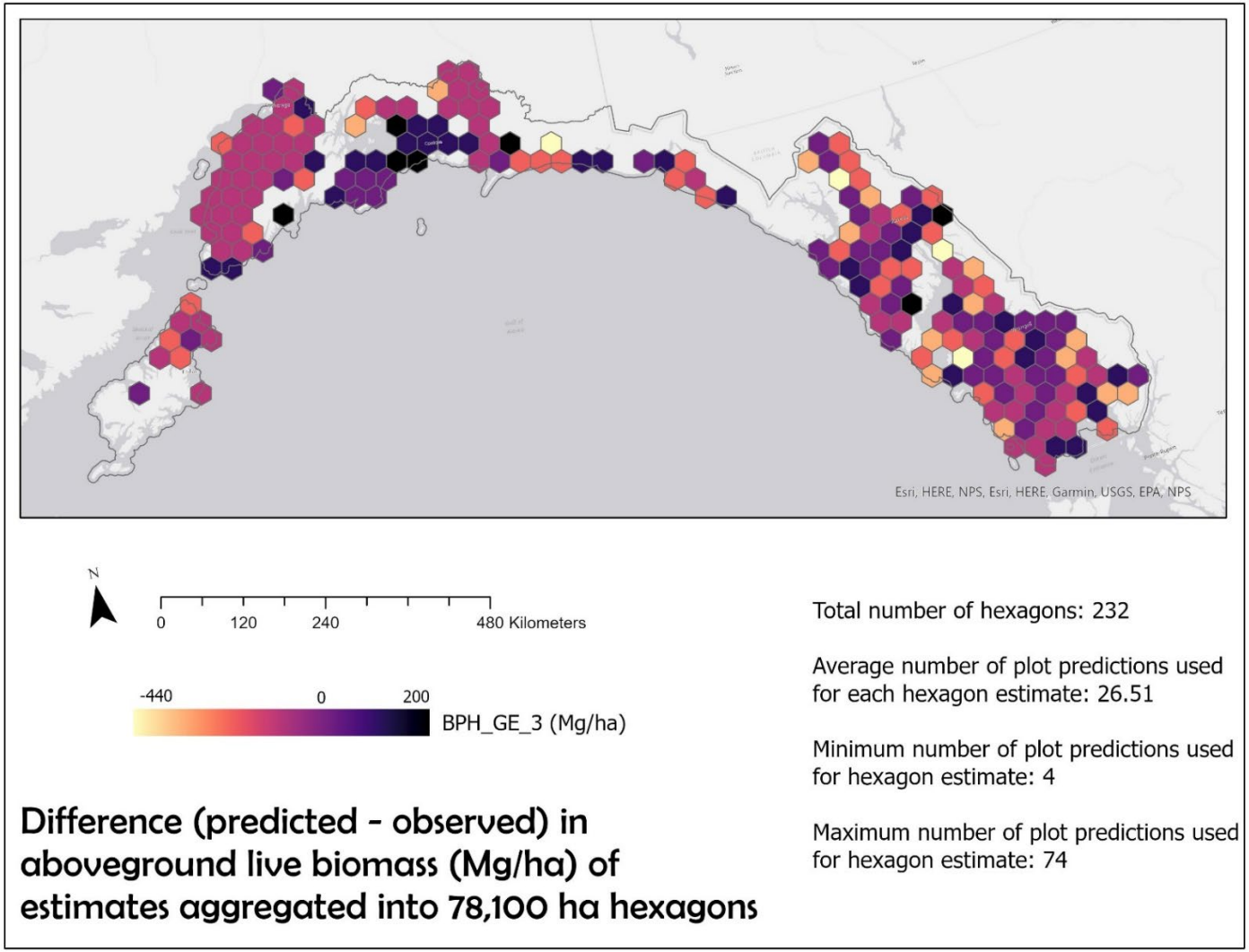

15c. Hex-50km (216,000 ha)

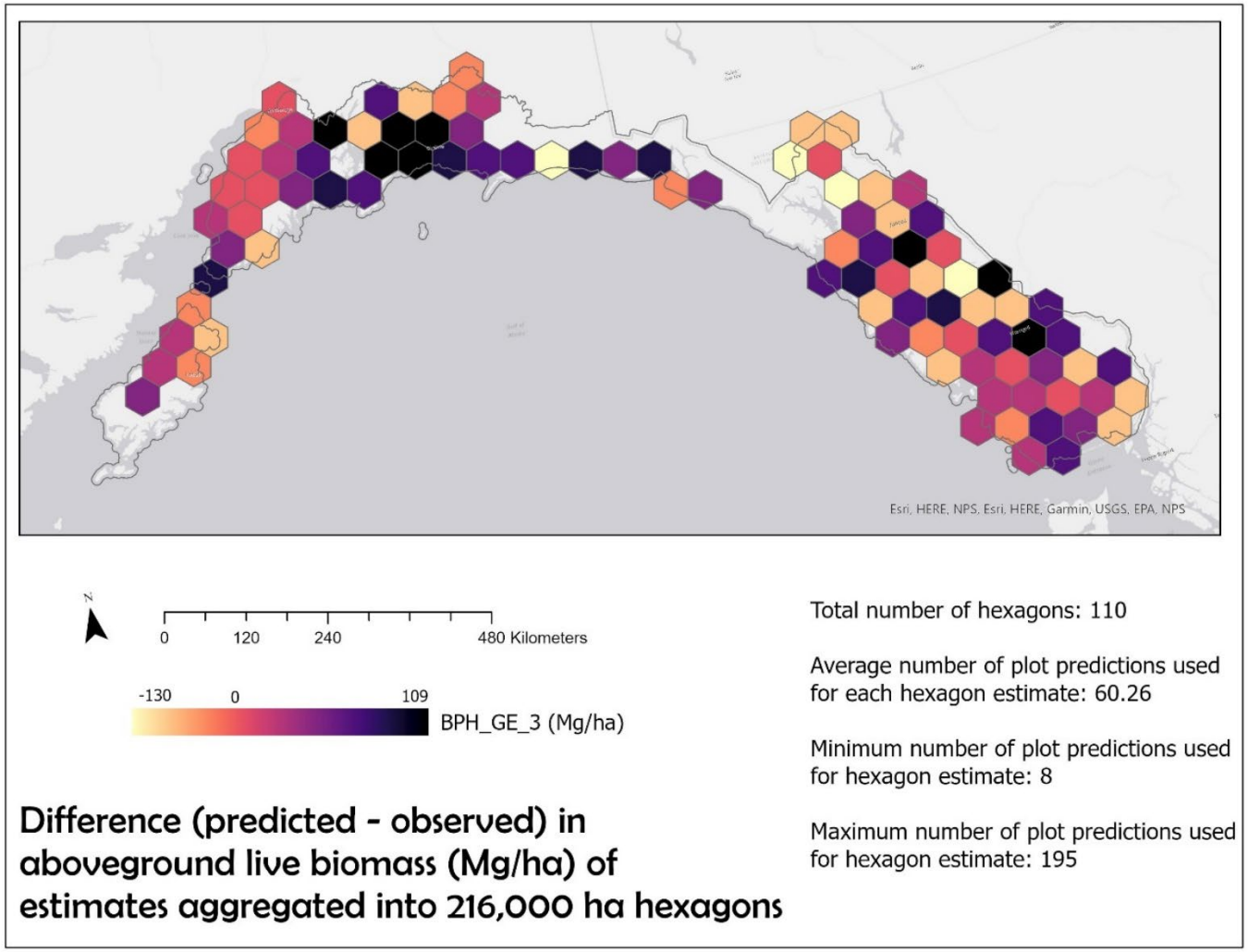

Figure 16. Terrain shadowing: high resolution satellite imagery vs. aboveground live biomass predictions (30-m) in Prince William Sound

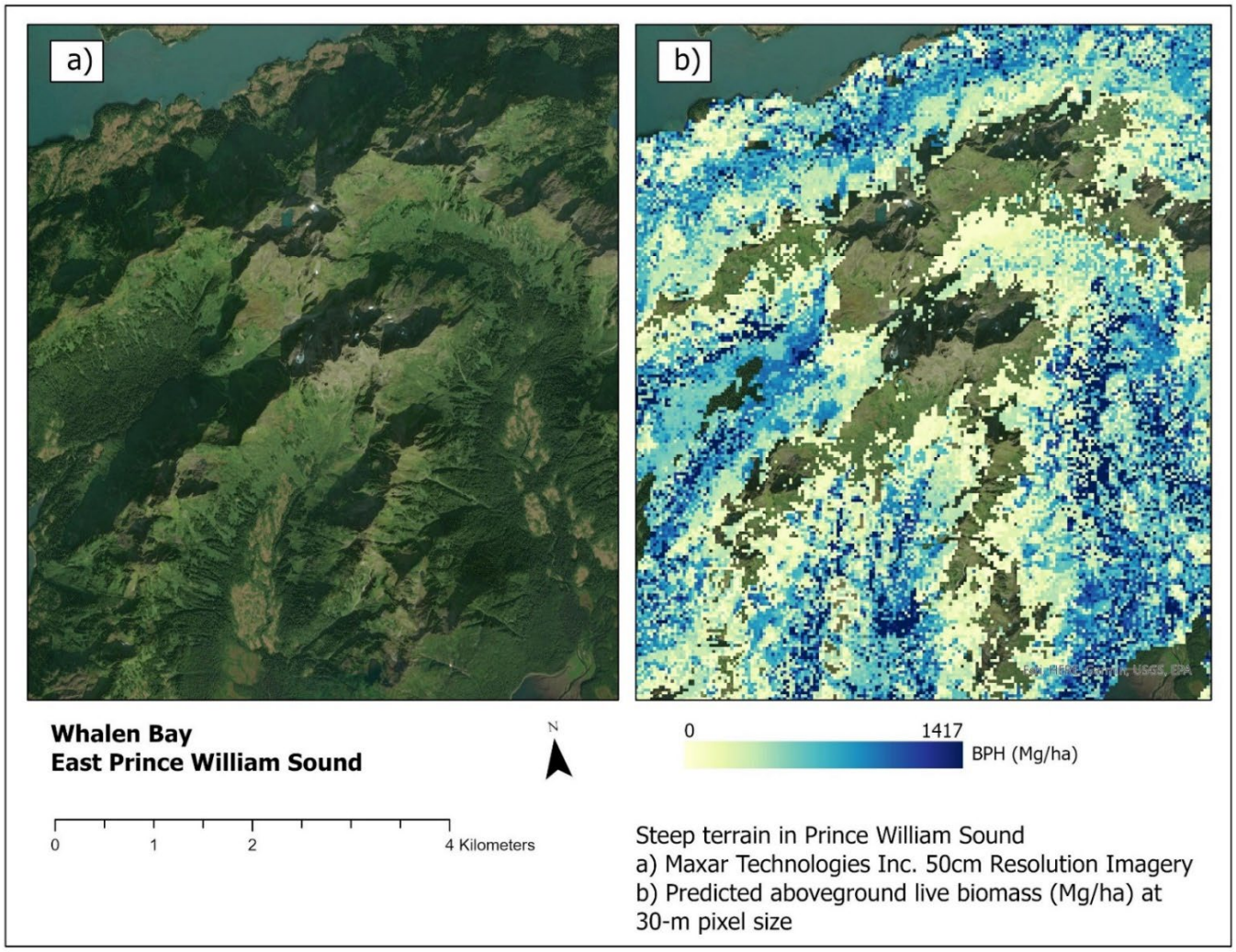

Figure 17. Distribution of neighbor distances (Euclidean) across study area

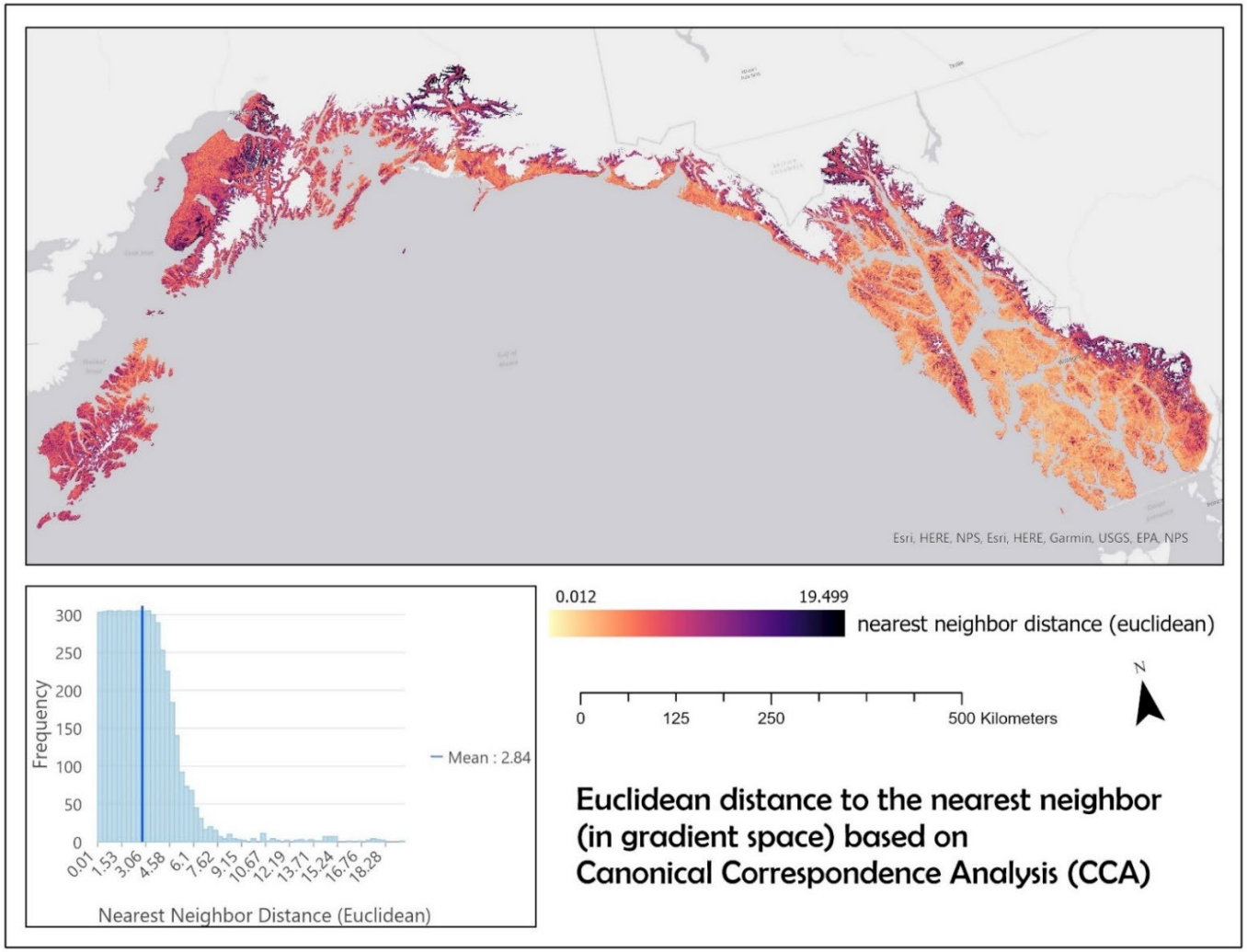

Appendix 1. Image Processing & LandTrendr Script

All code used to process Landsat Timeseries and create fitted image stacks available at:
https://code.earthengine.google.com/fcf51ecc63c7ca021b473ef920e2ed89

Appendix 2. Species presence: observed vs. predicted

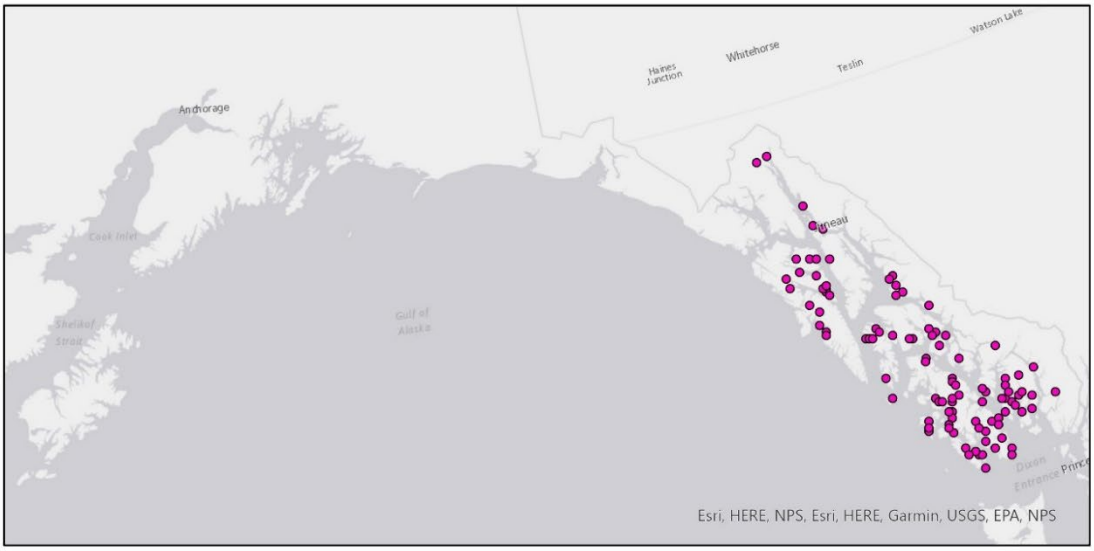

Observed Present

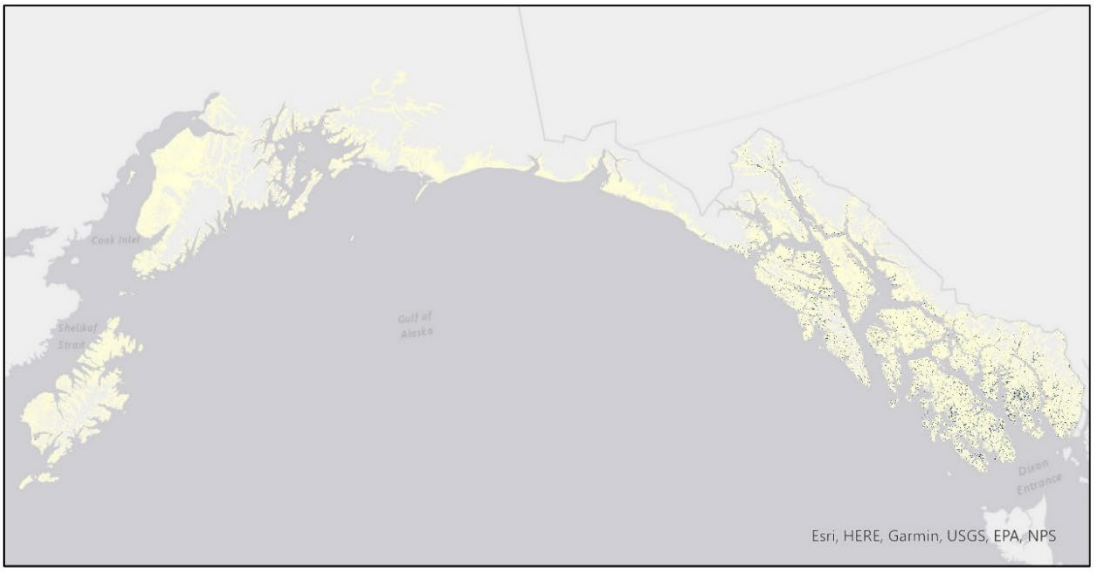

Predicted Present

N

0 175 350 700 Kilometers

Alnus rubra

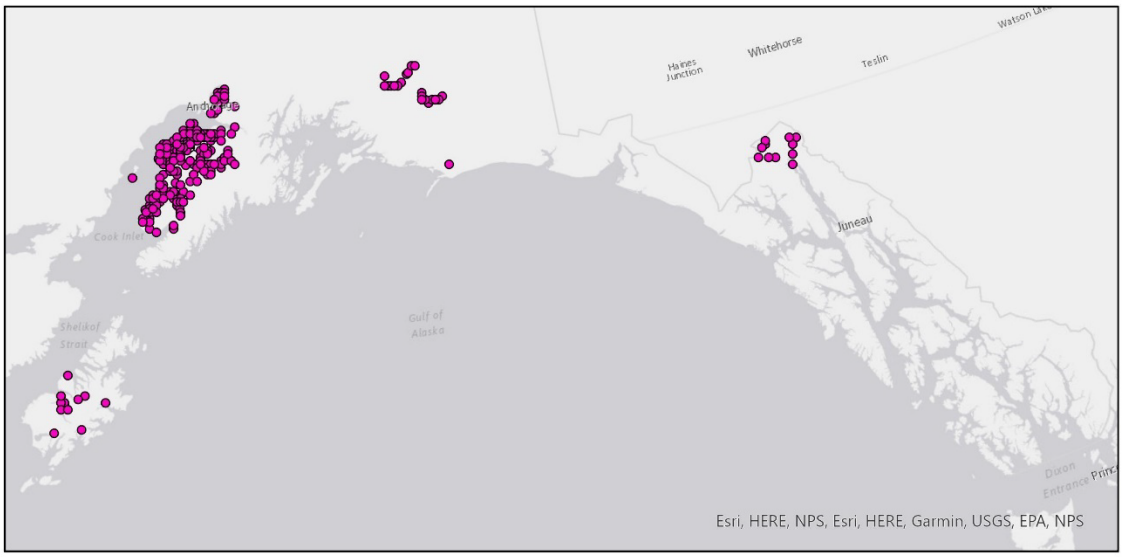

Observed Present

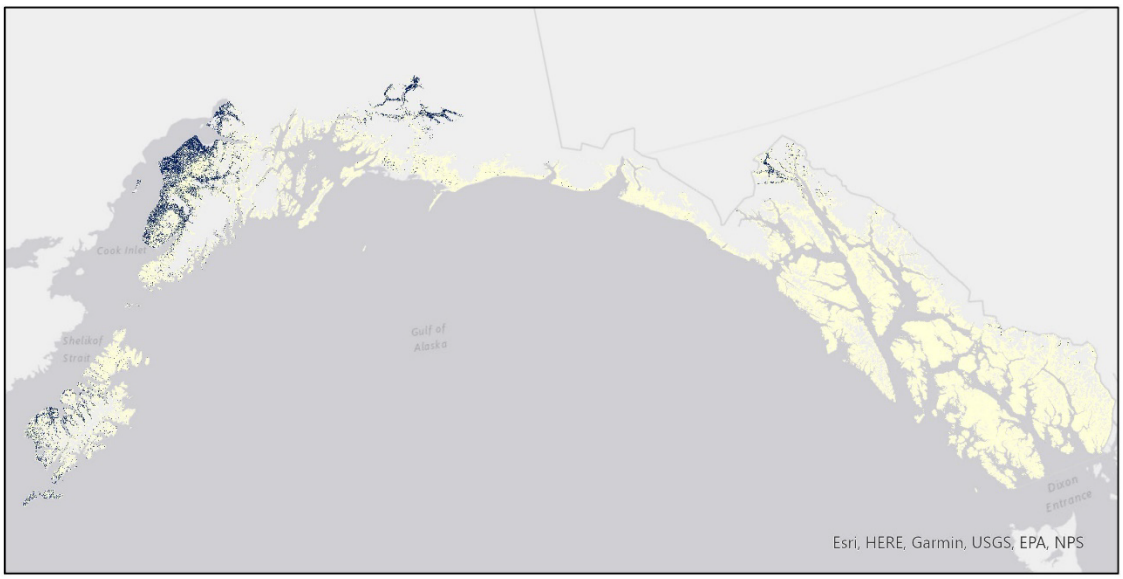

Predicted Present

N

0 162.5 325 650 Kilometers

Betula neoalaskana

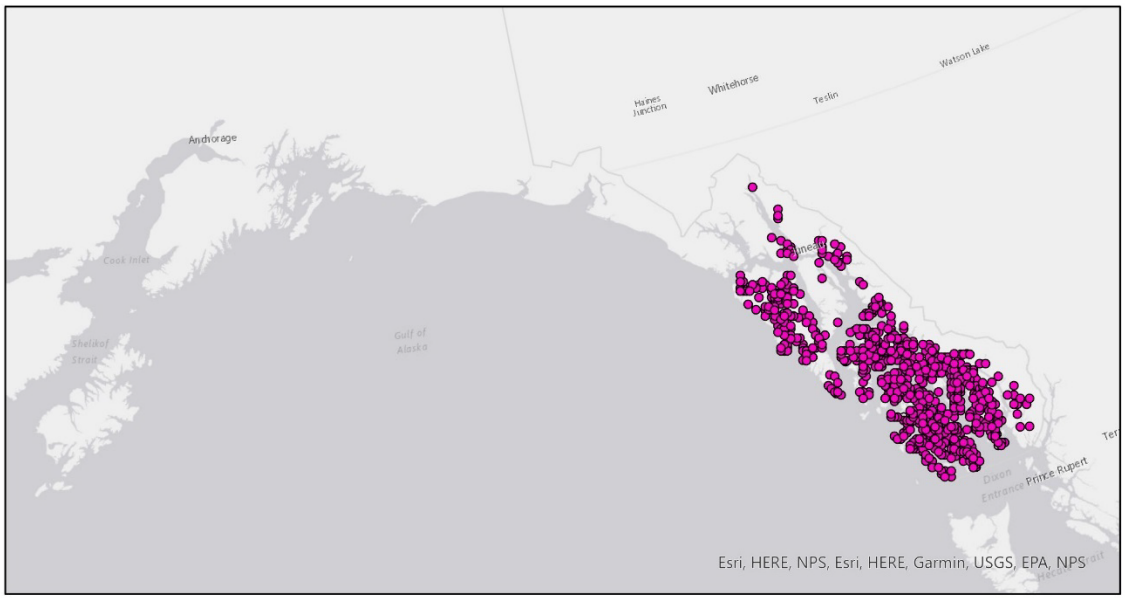

Observed Present

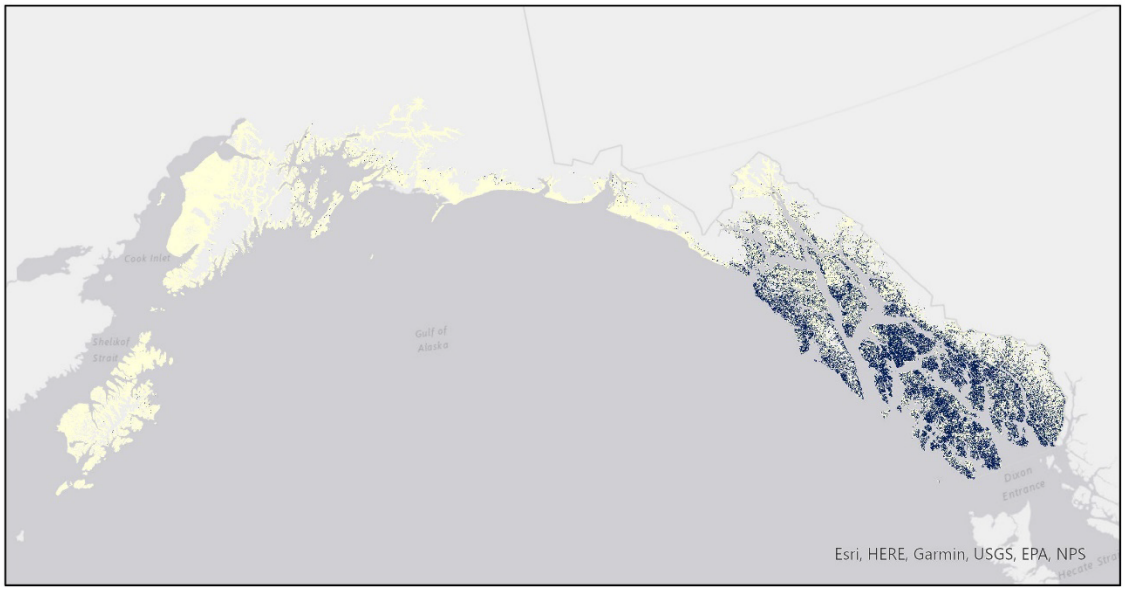

Predicted Present

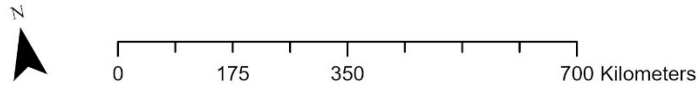

Callitropsis nootkatensis

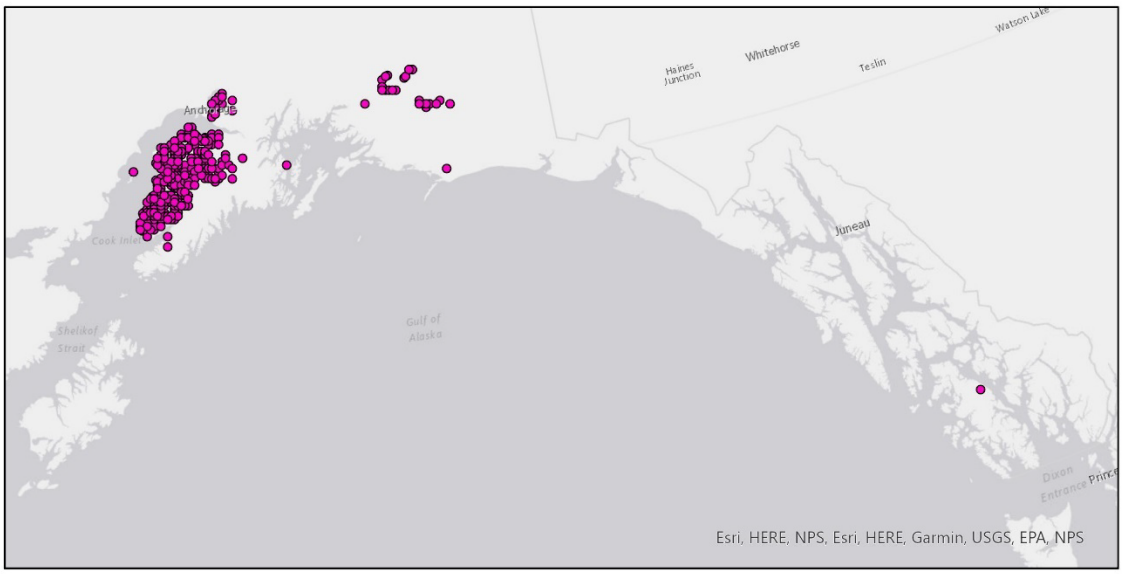

Observed Present

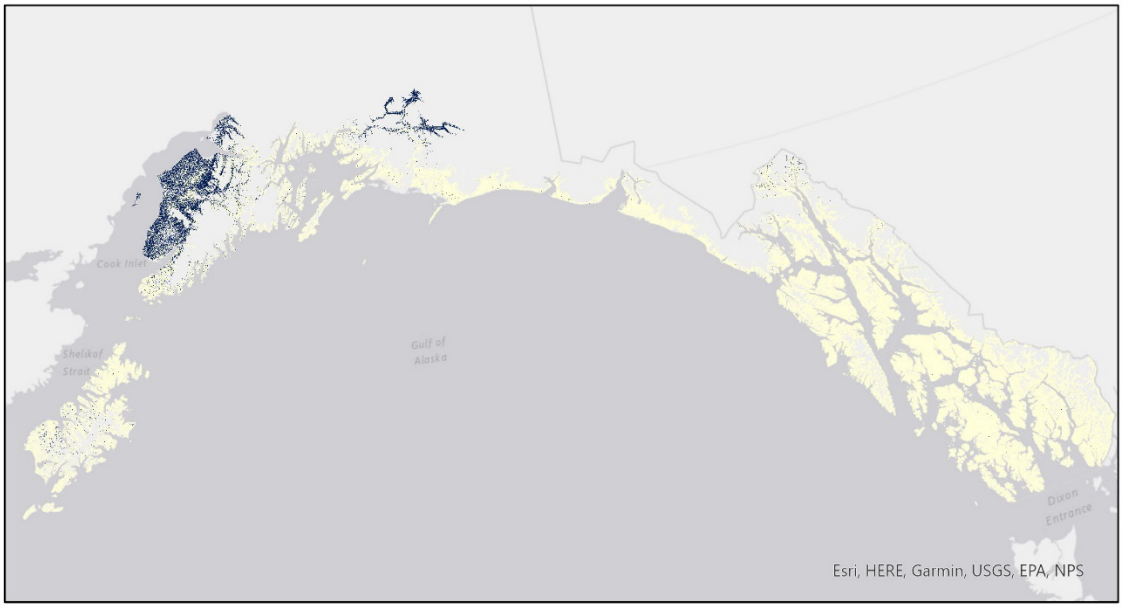

Predicted Present

N

0 175 350 700 Kilometers

Picea glauca

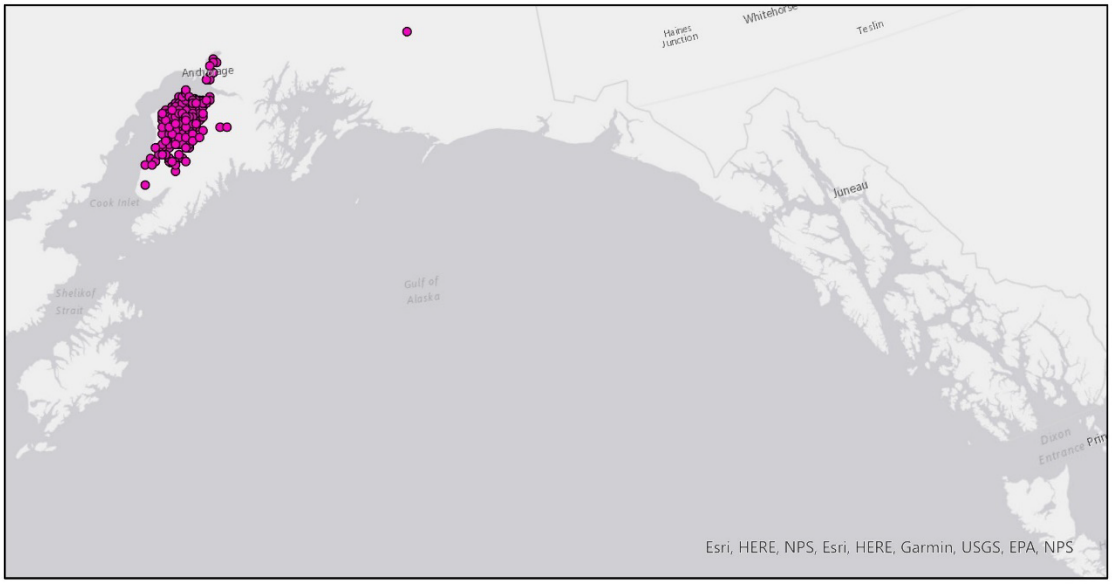

Observed Present

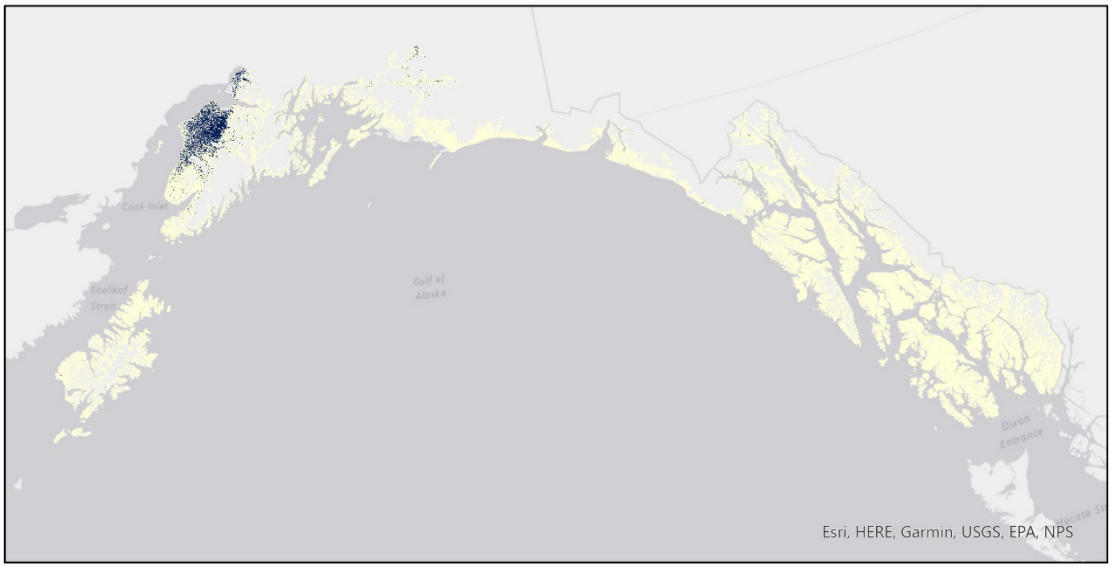

Predicted Present

Picea mariana

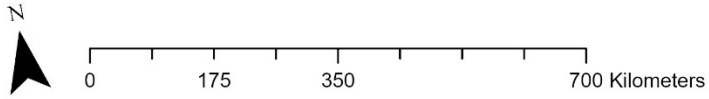

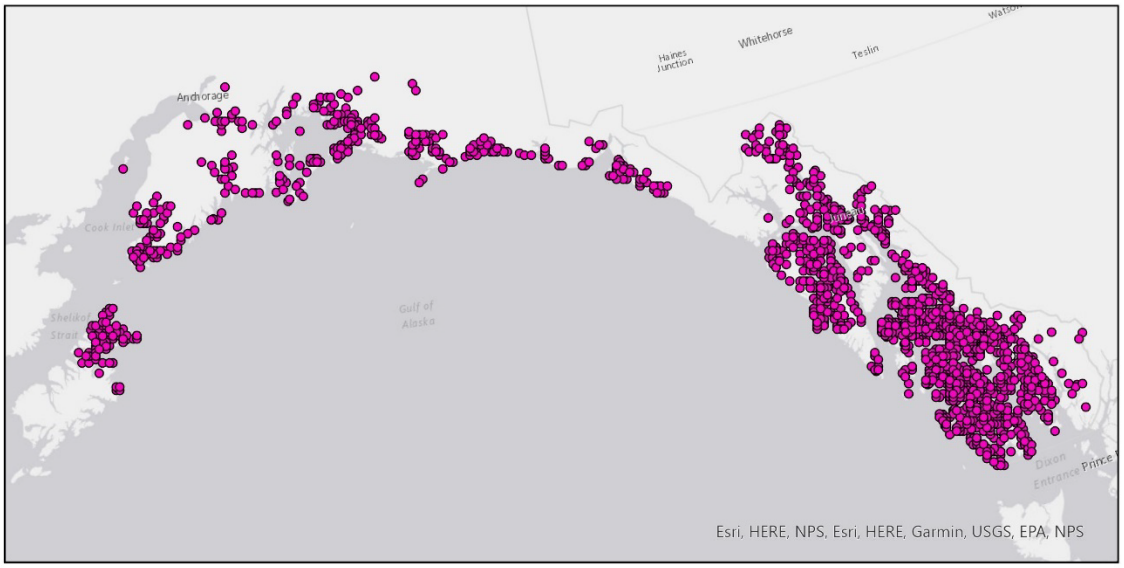

Observed Present

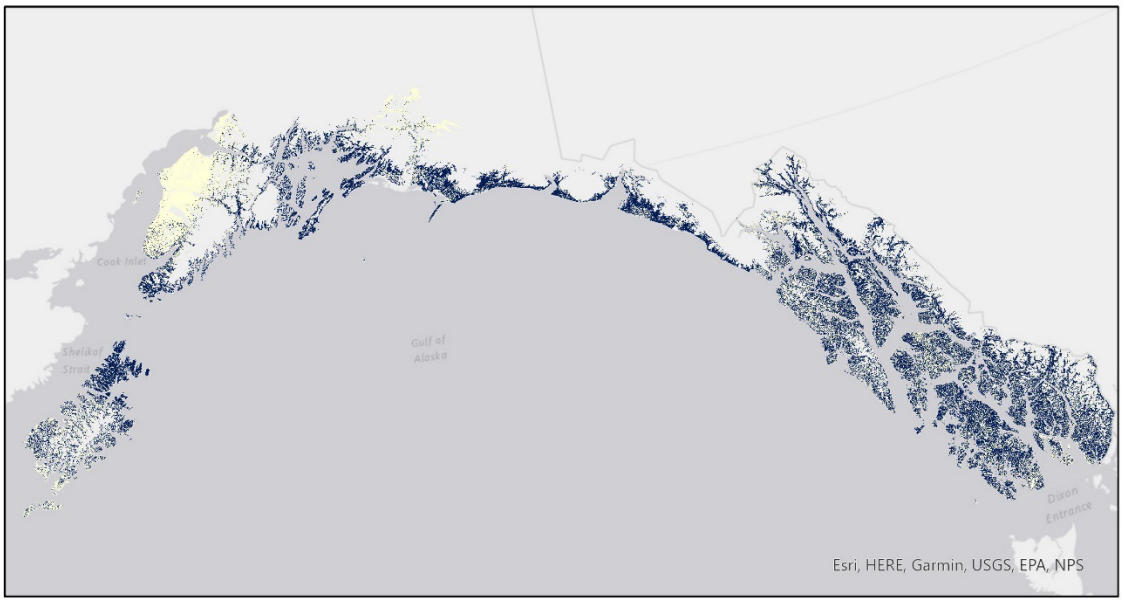

Predicted Present

Picea sitchensis

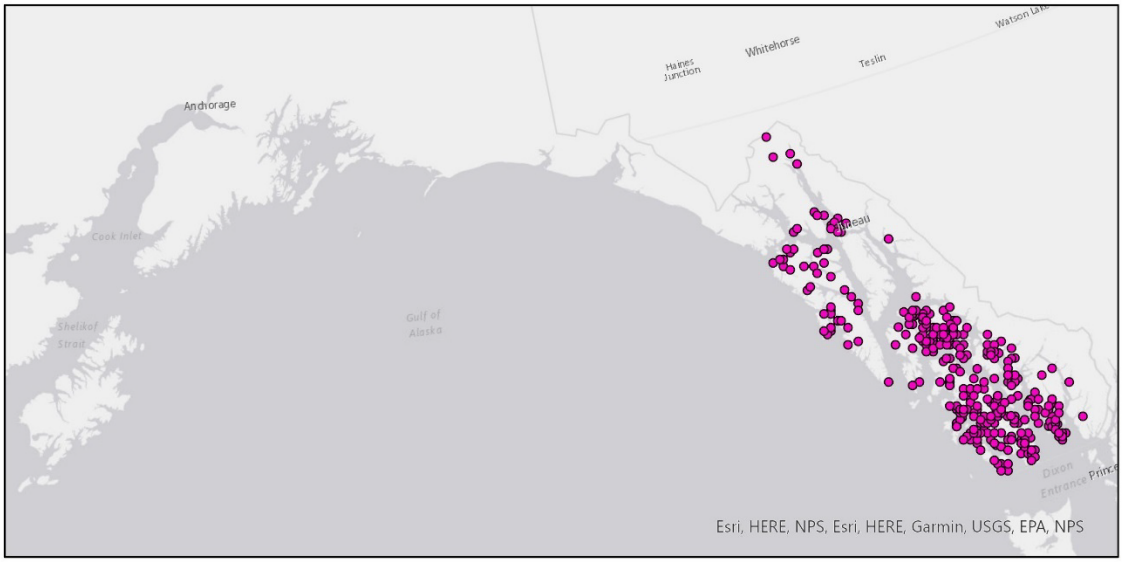

Observed Present

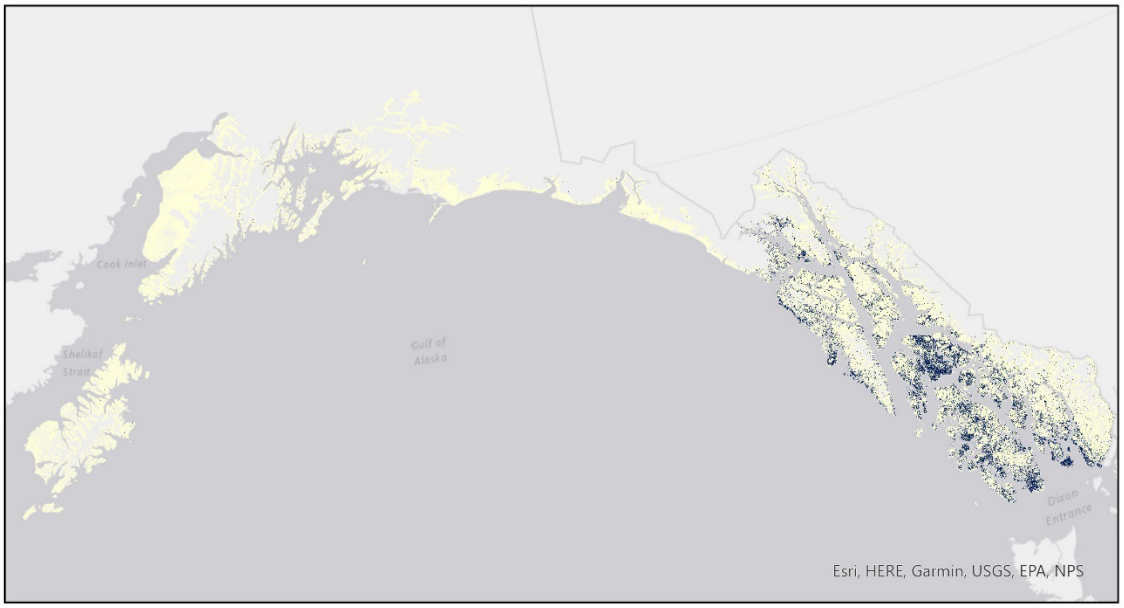

Predicted Present

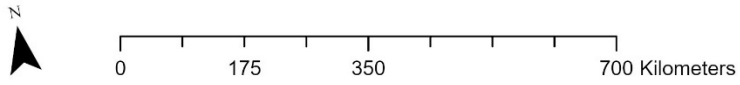

Pinus contorta

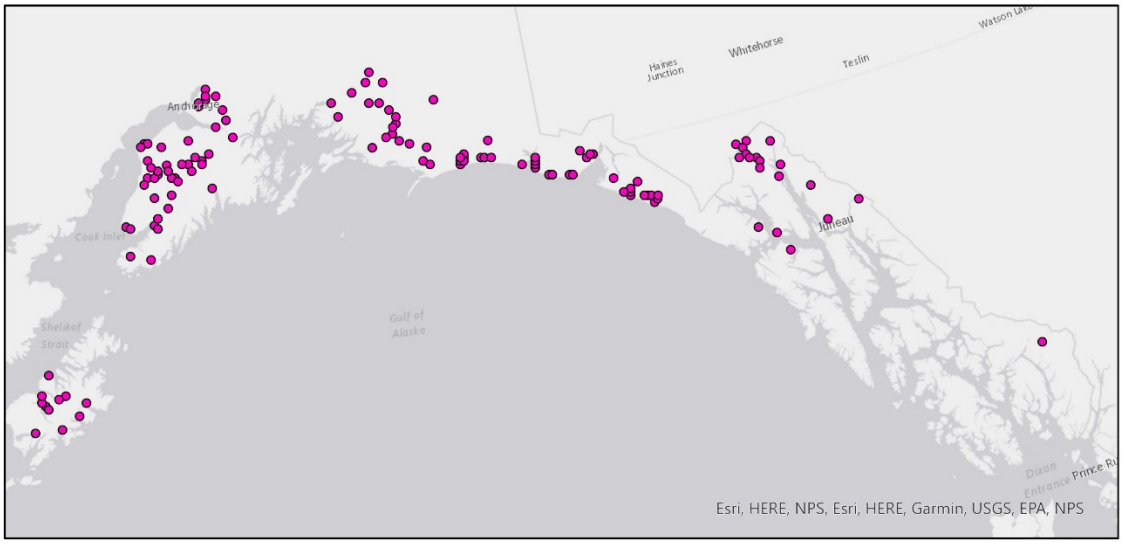

Observed Present

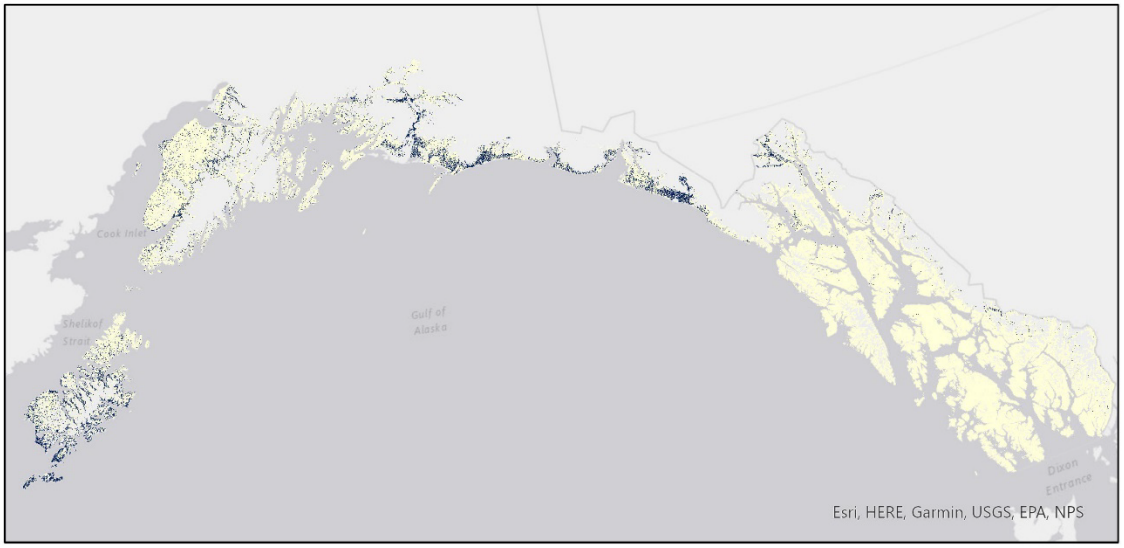

Predicted Present

N

0 175 350 700 Kilometers

Populus balsamifera ssp. trichocarpa

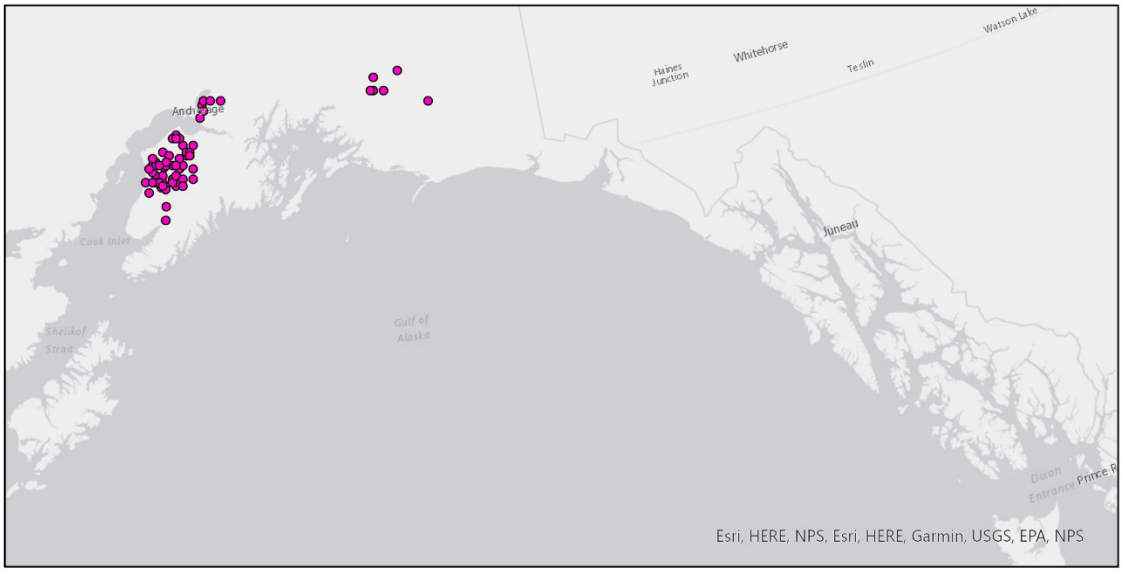

Observed Present

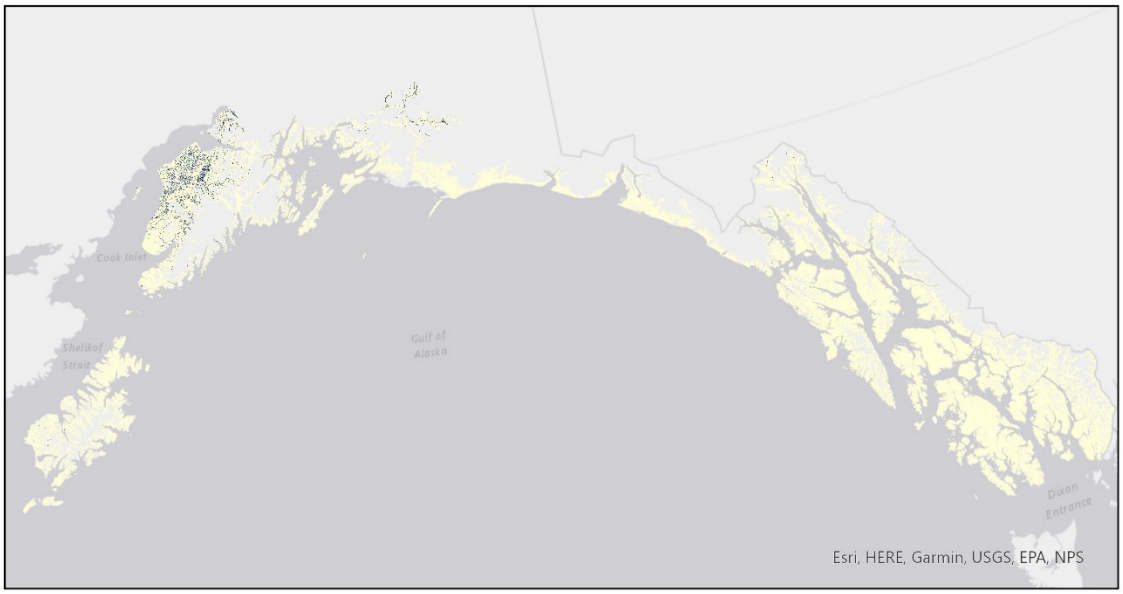

Predicted Present

N

0 150 300 600 Kilometers

Populus tremuloides

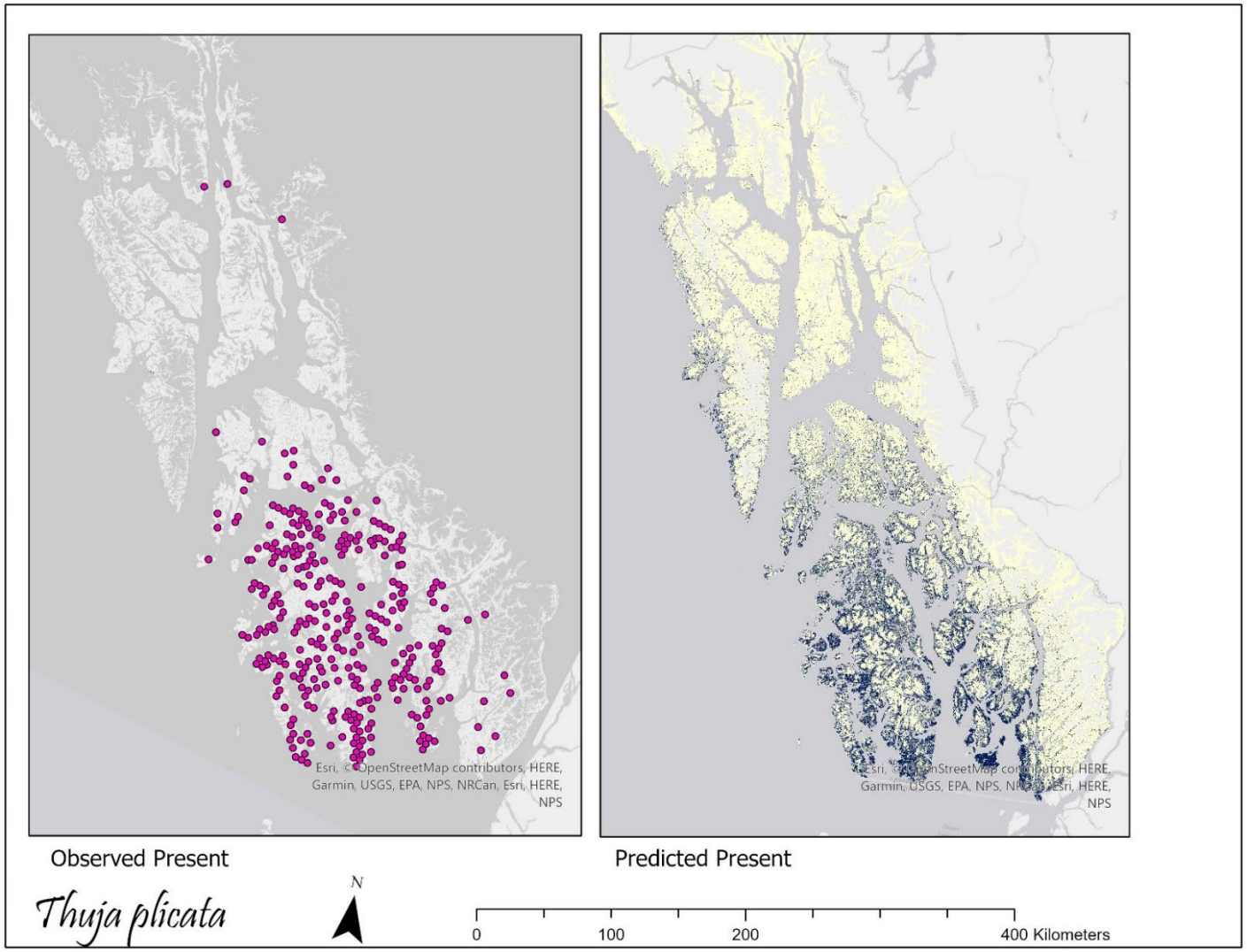
Esri, © OpenStreetMap contributors, HERE, Garmin, USGS, EPA, NPS, NRCan, Esri, HERE, NPS
Esri, © OpenStreetMap contributors, HERE, Garmin, USGS, EPA, NPS, NRCan, Esri, HERE, NPS
Observed Present
Predicted Present
Thuja plicata
N
0
100
200
400 Kilometers

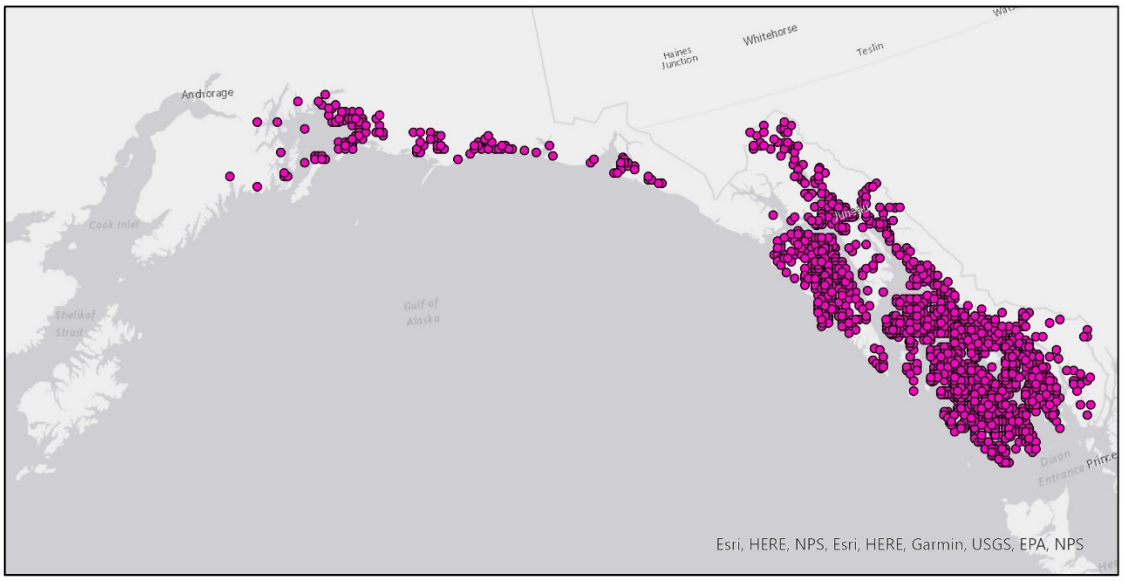

Observed Present

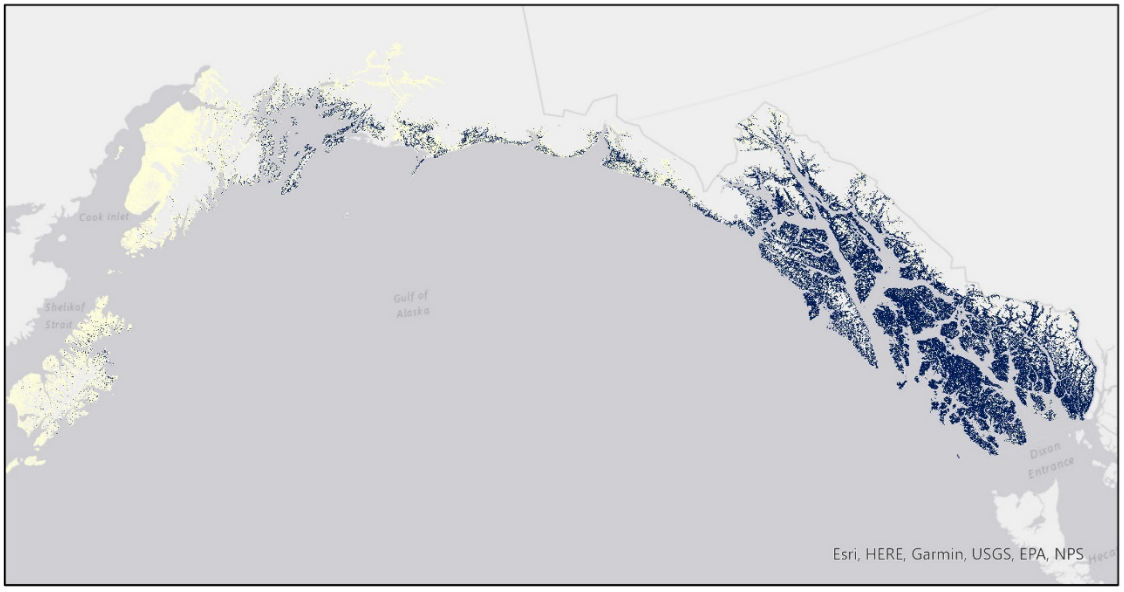

Predicted Present

N

0 175 350 700 Kilometers

Tsuga heterophylla

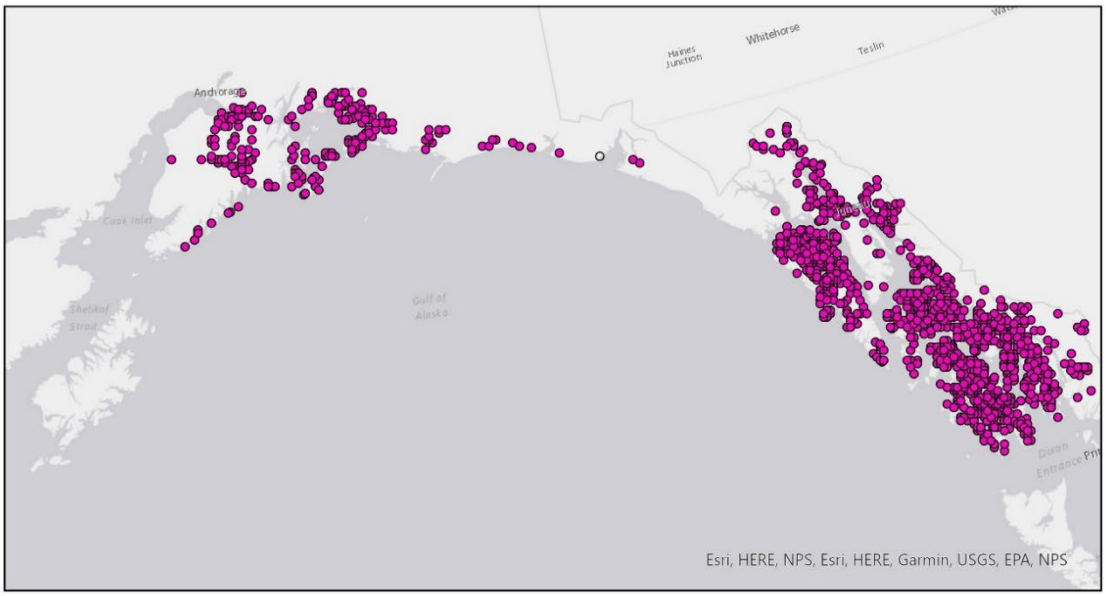

Observed Present

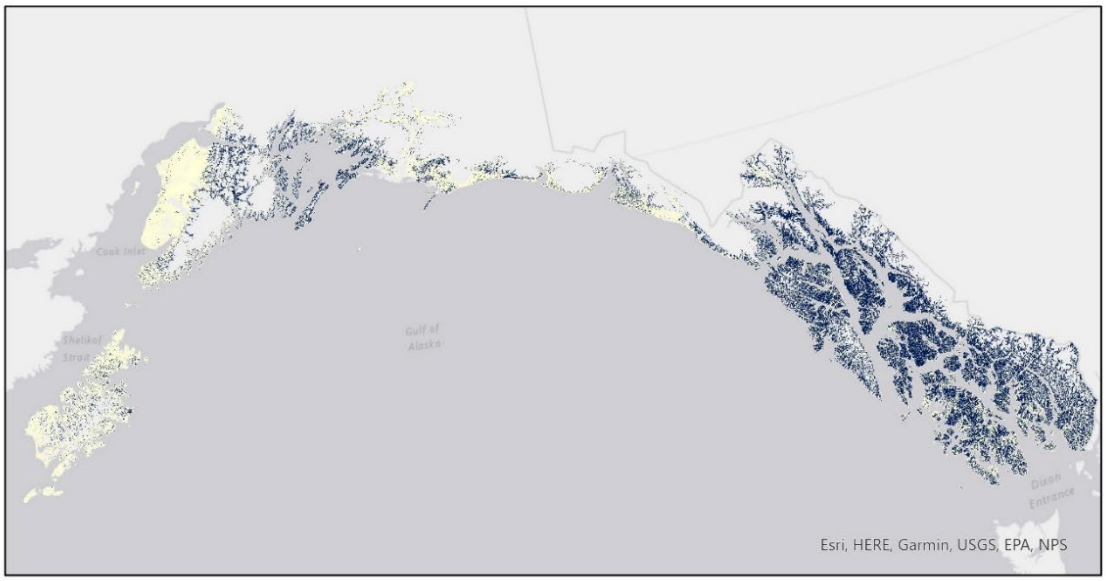

Predicted Present

N

0 175 350 700 Kilometers

Tsuga mertensiana

Appendix 3. Comparison of TC indices, high resolution satellite imagery, *k*=1 prediction, and *k*=7 prediction across study area

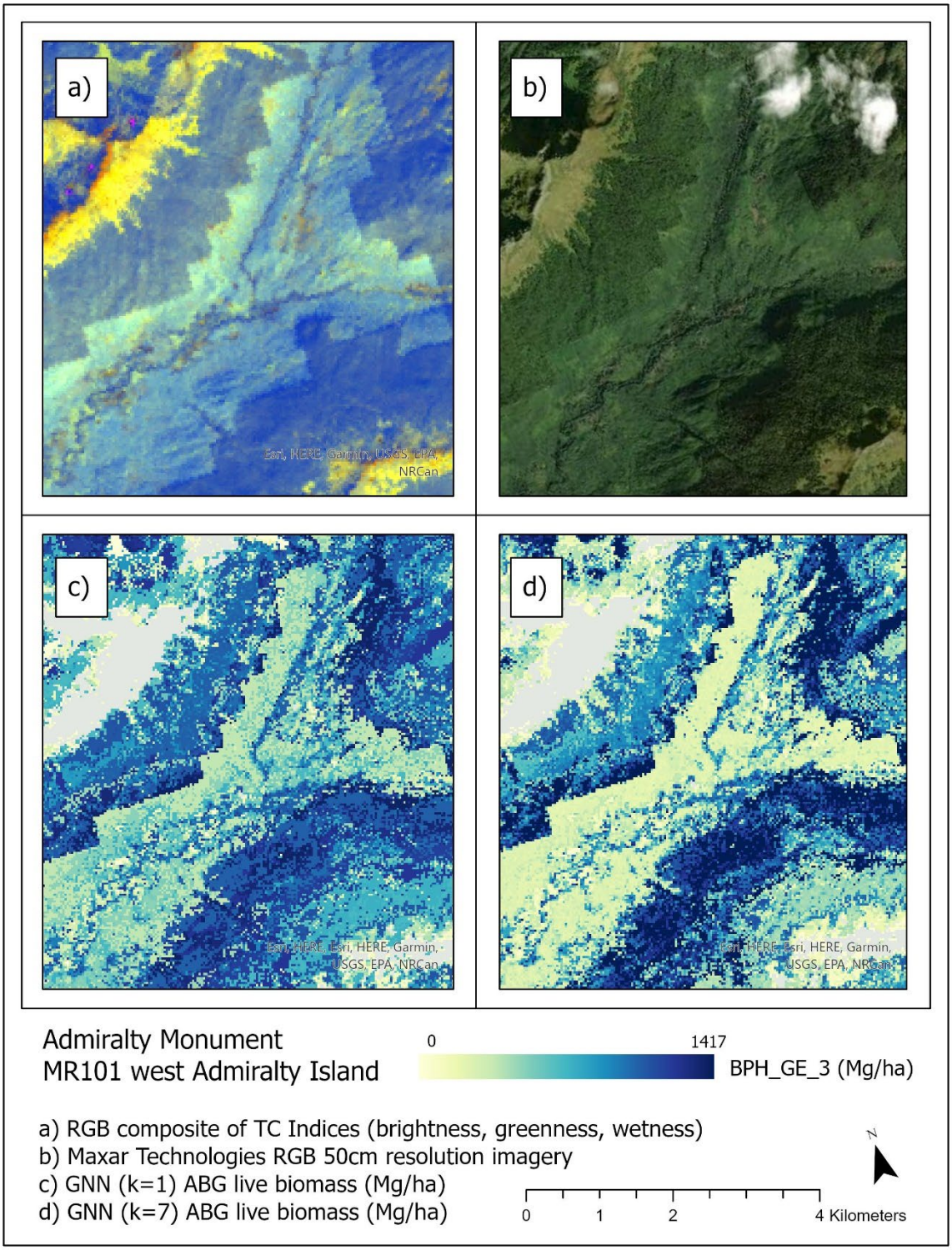

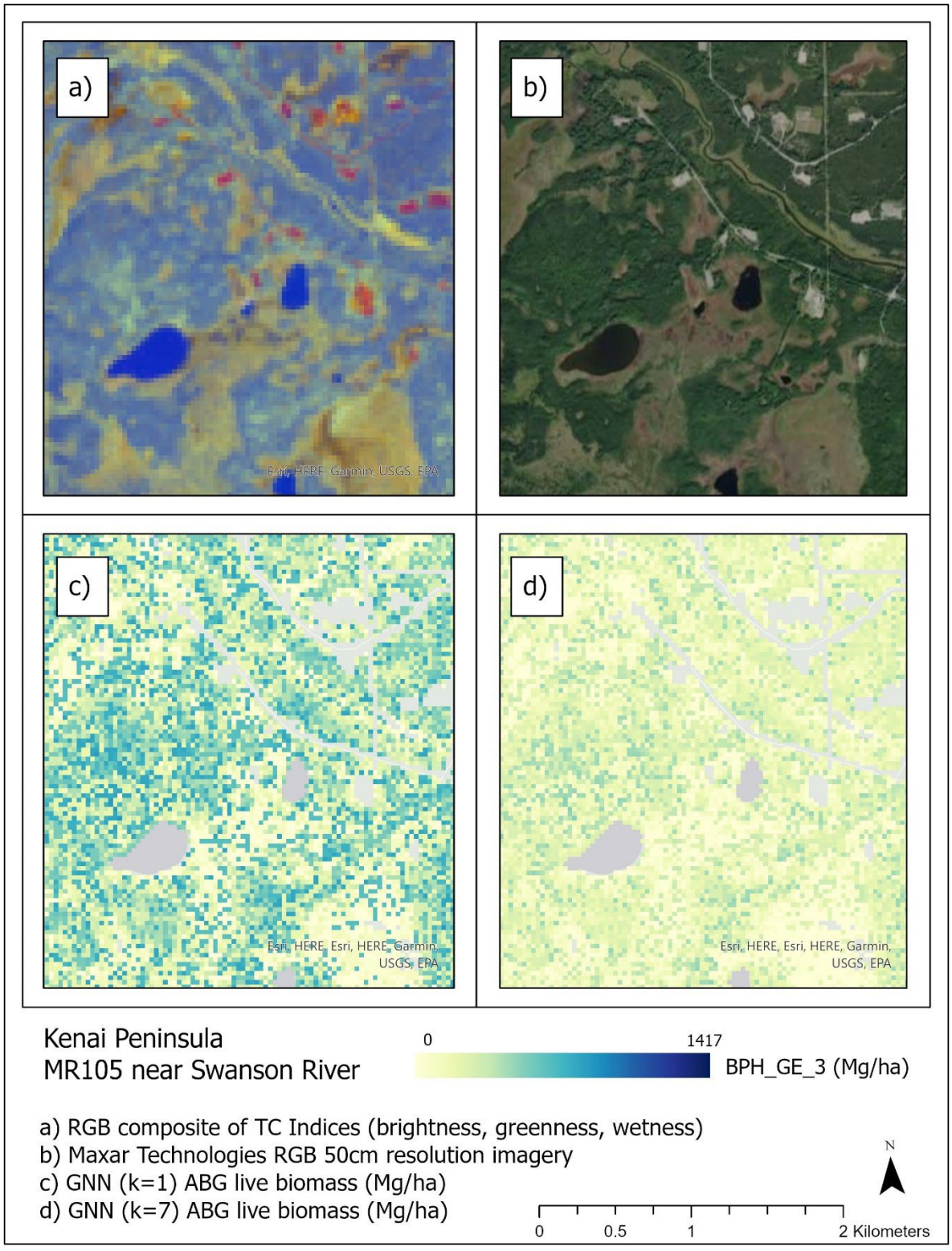
a)
b)
c)
d)
Esri, HERE, Garmin, USGS, EPA
Esri, HERE, Esri, HERE, Garmin, USGS, EPA
Esri, HERE, Esri, HERE, Garmin, USGS, EPA
Kenai Peninsula
MR105 near Swanson River
0
1417
BPH_GE_3 (Mg/ha)
a) RGB composite of TC Indices (brightness, greenness, wetness)
b) Maxar Technologies RGB 50cm resolution imagery
c) GNN (k=1) ABG live biomass (Mg/ha)
d) GNN (k=7) ABG live biomass (Mg/ha)
N
0
0.5
1
2 Kilometers

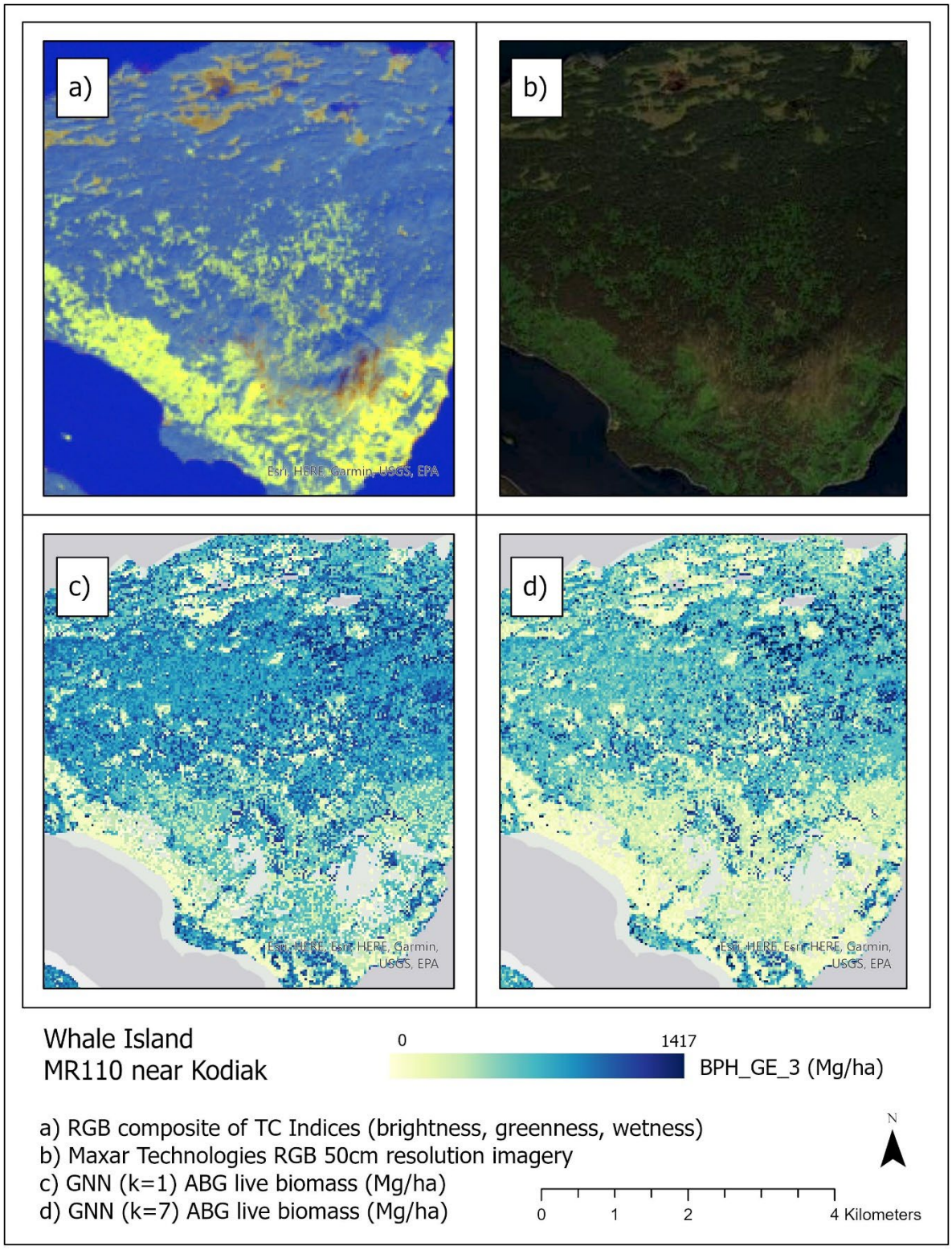
a)
b)
c)
d)
Esri, HERE, Garmin, USGS, EPA
Esri, HERE, Esri, HERE, Garmin, USGS, EPA
Whale Island
MR110 near Kodiak
0
1417
BPH_GE_3 (Mg/ha)
a) RGB composite of TC Indices (brightness, greenness, wetness)
b) Maxar Technologies RGB 50cm resolution imagery
c) GNN (k=1) ABG live biomass (Mg/ha)
d) GNN (k=7) ABG live biomass (Mg/ha)
N
0
1
2
4 Kilometers

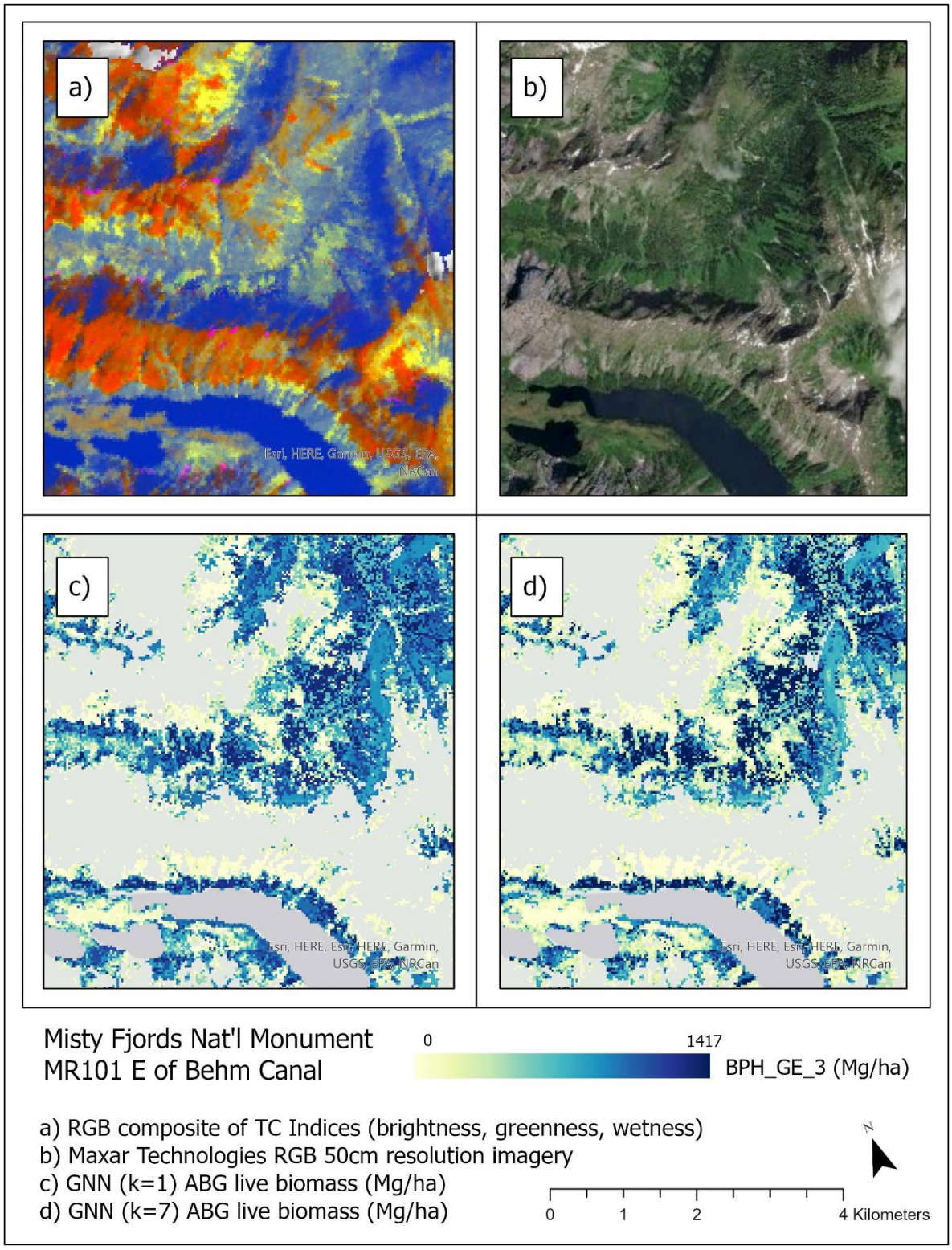
a)
b)
c)
d)
Esri, HERE, Garmin, USGS, EPA, NRCan
Misty Fjords Nat'l Monument
MR101 E of Behm Canal
0
1417
BPH_GE_3 (Mg/ha)
a) RGB composite of TC Indices (brightness, greenness, wetness)
b) Maxar Technologies RGB 50cm resolution imagery
c) GNN (k=1) ABG live biomass (Mg/ha)
d) GNN (k=7) ABG live biomass (Mg/ha)
N
0
1
2
4 Kilometers

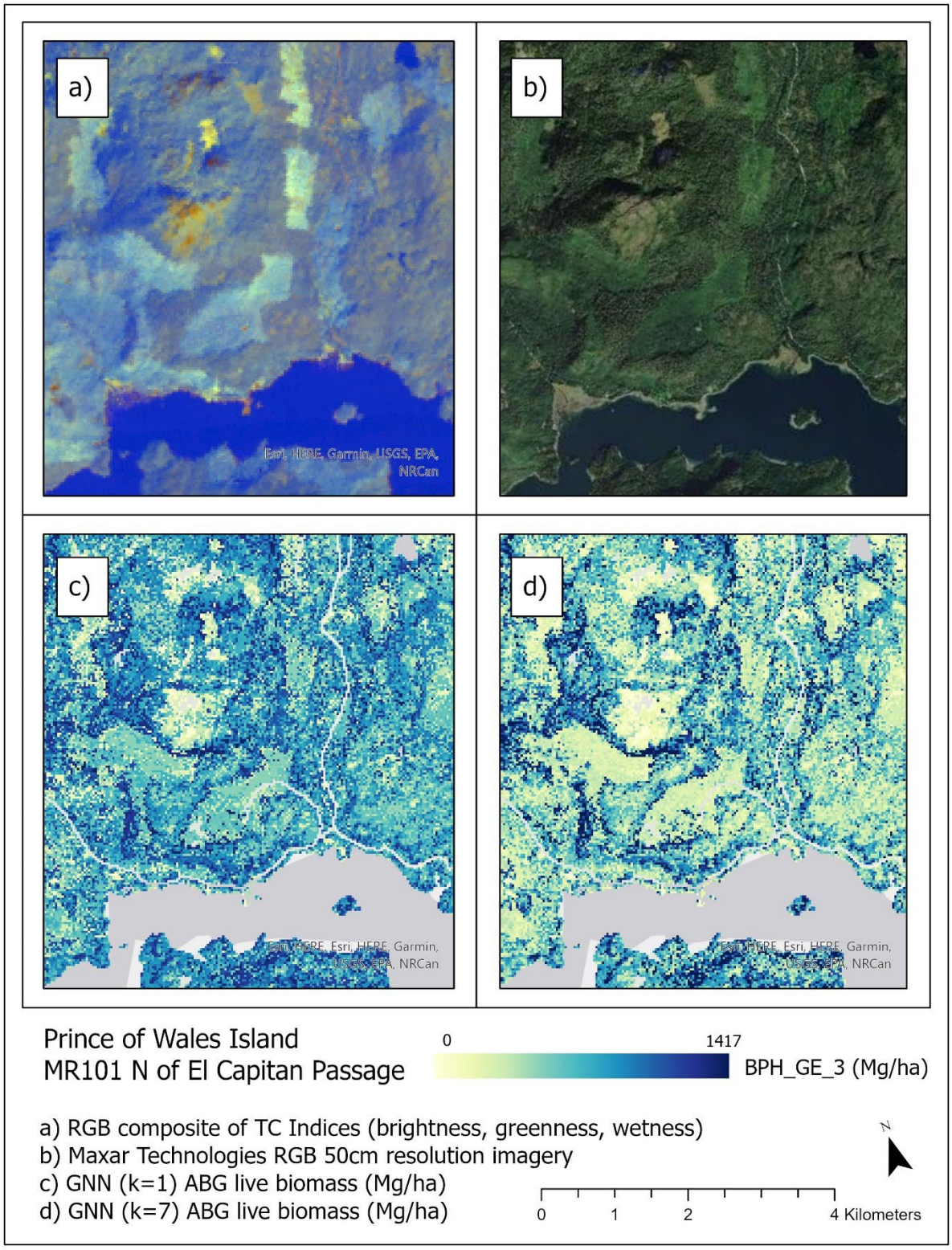
a)
b)
c)
d)
Esri, HERE, Garmin, USGS, EPA, NRCan
Prince of Wales Island
MR101 N of El Capitan Passage
0
1417
BPH_GE_3 (Mg/ha)
a) RGB composite of TC Indices (brightness, greenness, wetness)
b) Maxar Technologies RGB 50cm resolution imagery
c) GNN (k=1) ABG live biomass (Mg/ha)
d) GNN (k=7) ABG live biomass (Mg/ha)
N
0
1
2
4 Kilometers

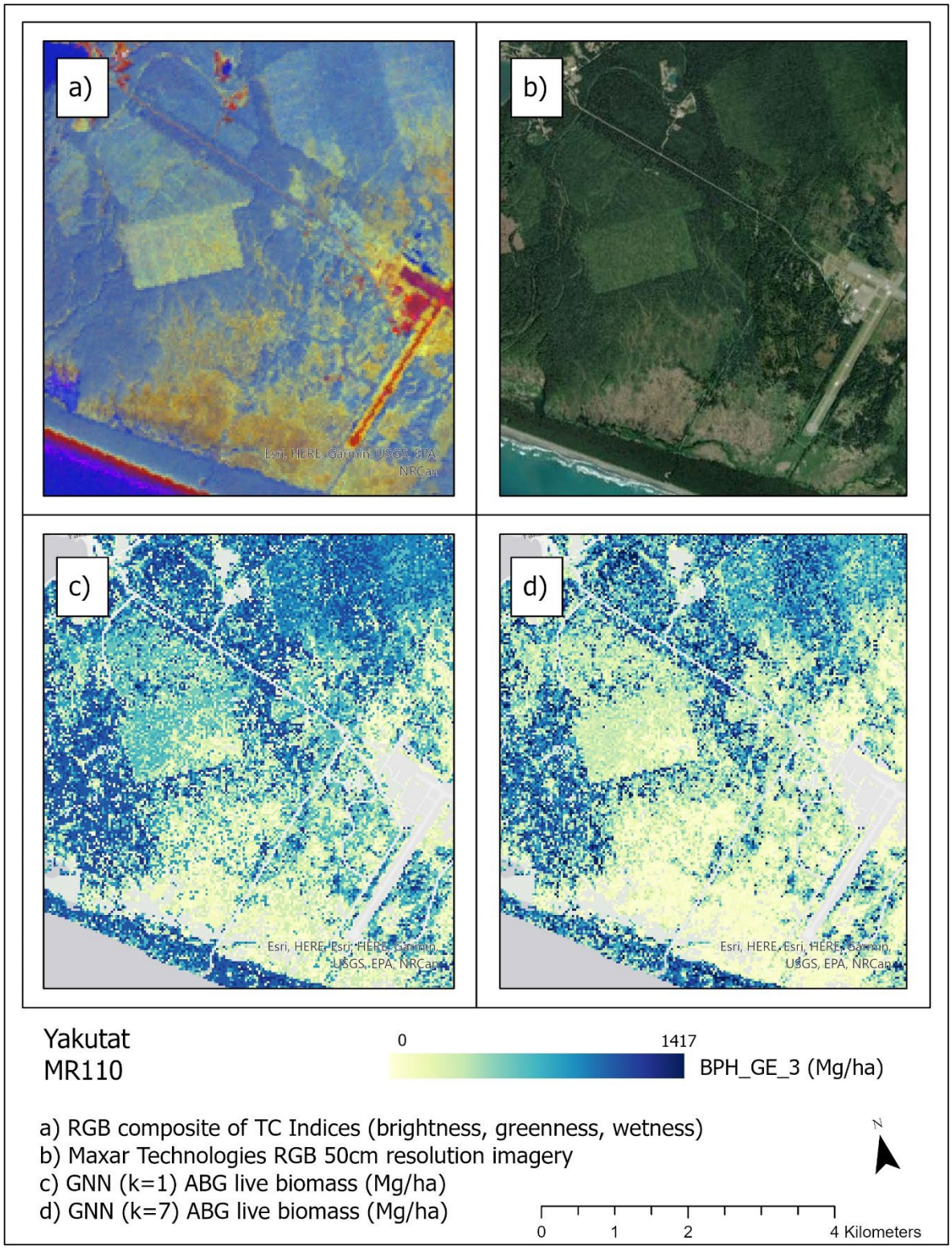
a)
b)
c)
d)
Esri, HERE, Garmin, USGS, EPA, NRCan
Esri, HERE, Esri, HERE, Garmin, USGS, EPA, NRCan
Yakutat
MR110
0
1417
BPH_GE_3 (Mg/ha)
a) RGB composite of TC Indices (brightness, greenness, wetness)
b) Maxar Technologies RGB 50cm resolution imagery
c) GNN (k=1) ABG live biomass (Mg/ha)
d) GNN (k=7) ABG live biomass (Mg/ha)
N
0
1
2
4 Kilometers

Sources Cited

Abatzoglou, J., and T. Brown. 2011. A comparison of statistical downscaling methods suited for wildfire applications. International Journal of Climatology 32(5): 772-780. https://doi.org/10.1002/joc.2312.

Adams, M., C. Kelly, J. Kabrick, and J. Schuler. 2019. Temperate forests and soils. *In:* Busse, M., C. Giardina, D. Morris, and D. Page-Dumroese (Eds.). Global Change and Forest Soils: Cultivating Stewardship of a Finite Natural Resource. 83-108.

Alaback, P. 1984. Plant succession following logging in the Sitka spruce-western hemlock forests of southeast Alaska: implications for management. Gen. Tech. Rep. PNW-173. Portland, OR: U.S. Department of Agriculture, Forest Service, Pacific Northwest Forest and Range Experiment Station; 1984. 26 p.

Alaback, P. 1991. Comparative ecology of temperate rainforest of the Americas along analogous climatic gradients. Revista Chelena de Historia Natural. 64: 399-412.

Alaback, P. 1996. Biodiversity patterns in relation to climate: the coastal temperate rainforests of North America. *In:* Lawford, R., P. Alaback, E. Fuentes, (Eds.). 1996. High-latitude rainforest and associated ecosystems of the west coast of the Americas: Climate, hydrology, ecology, and conservation. Ecological Studies vol. 116. Springer-New York.

Alaback, P. 2015. The southeastern Alaska rainforest in a global context. *In:* A conservation assessment and resource synthesis for the Coastal Forests and Mountains Ecoregion in the Tongass National Forest and southeast Alaska, chapter 5.1. The Nature Conservancy. Accessed 13 February 2022. https://www.conservationgateway.org/ConservationByGeography/NorthAmerica/UnitedStates/alaska/seak/era/cfm/Pages/RS-AKCFM.aspx.

Alaska Department of Fish and Game. Featured Species-Associated Forest Habitat. https://www.adfg.alaska.gov/static/species/wildlife_action_plan/appendix5_forest_habitats.pdf. Accessed 06 February 2022.

Alaska Forest Association. Alaska Timber Industry History: Southeast Alaska. https://www.akforest.org/Alaska%20Timber%20Industry%20History.pdf. Accessed 10 December 2021.

Alaska Roadless Rulemaking. 2020. USDA Forest Service, Alaska Region. https://www.fs.usda.gov/detail/roadless/alaskaroadlessrule/?cid=fseprd672388. Accessed May 29, 2020.

Albert, D., and J. Schoen. 2012. Use of historical logging patterns to identify disproportionately logged ecosystems within temperate rainforests of southeastern Alaska. Conservation Biology. 27(4): 774-784. https://doi.org/10.1111/cobi.12109.

Alexander, S., E. Henderson, and R. Coleman. 2010. Economic Analysis of Southeast Alaska: Envisioning a Sustainable Economy with Thriving Communities. Forest Service, Alaska Region Publication R10-MB-725, Juneau, AK, 93 p.

Andersen, H., R. Pattison, A. Gray, A., B. Schulz, S. Jovan, R. Smith, K. Manis, and T. Thompson. 2019. Section 2: Forest resources of Interior Alaska and U.S.-affiliated jurisdictions of the Insular

Caribbean and Pacific. [In] S. N. Oswalt, W. B. Smith, P. D. Miles, and S. A. Pugh, editors. Forest resources of the United States, 2017: A technical document supporting the Forest Service 2020 RPA assessment. U.S. Department of Agriculture, Forest Service, Washington Office General Technical Report WO-97, Washington, D.C. https://doi.org/10.2737/WO-GTR-97.

Babcock, C., A. Finley, H. Andersen, R. Pattison, B. Cook, D. Morton, M. Alonzo, R. Nelson, T. Gregoire, L. Ene, T. Gobakken and E. Naesset. 2018. Geostatistical estimation of forest biomass in interior Alaska combining Landsat-derived tree cover, sampled airborne lidar and field observations. Remote Sensing of Environment. 212: 212-230. https://doi.org/10.1016/j.rse.2018.04.044.

Barrett, T., and A. Gray. 2011. Potential of a national monitoring program for forests to assess change in high-latitude ecosystems. Biological Conservation 144: 1285-1294. https://doi.org/10.1016/j.biocon.2010.10.015.

Barrett, T. and G. Christensen, tech. (Eds.). 2011. Forests of southeast and south-central Alaska, 2004–2008: five-year forest inventory and analysis report. Gen. Tech. Rep. PNW-GTR-835. Portland, OR: U.S. Department of Agriculture, Forest Service, Pacific Northwest Research Station. 156 p.

Baughman, R. Loehman, D. Margness, L. Saperstein, and R. Sherriff. 2020. Four decades of land-cover change on the Kenai Peninsula, Alaska: detecting disturbance-influenced vegetation shifts using Landsat legacy data. Land 9(382). https://doi.org/10.3390/land9100382.

Beamish, A., M. Raynolds, H. Epstein, G. Frost, M. Macander, H. Bergstedt, A. Bartsch, S. Kruse, V. Miles, C. M. Tanis, B. Heim, M. Fuchs, S. Chabrillat, I. Shevtsova, M. Verdonen, J. Wagner. 2020. Recent trends and remaining challenges for optical remote sensing of Arctic tundra vegetation: a review and outlook. Remote Sensing of Environment 246: 111872. https://doi.org/10.1016/j.rse.2020.111872.

Bechtold, W., and P. Patterson (Eds.). 2005. The enhanced forest inventory and analysis program—national sampling design and estimation procedures. General Technical Report SRS-80. USDA Forest Service, Southern Research Station, Asheville, NC, USA.

Beier, C., S. Sink, P. Hennon, D. D'Amore, and G. Juday. 2008. Twentieth-century warming and the dendroclimatology of declining yellow-cedar forests in southeastern Alaska. Canadian Journal of Forest Research 38: 1319-1334. https://doi.org/10.1139/cjfr-2016-0041.

Bell, D., S. Acker, M. Gregory, R. Davis, and B. Garcia. 2021. Quantifying regional trends in large live tree and snag availability in support of forest management. Forest Ecology and Management 479:118554. https://doi.org/10.1016/j.foreco.2020.118554.

Bell, D., M. Gregory, and J. Ohmann. 2015a. Imputed forest structure uncertainty varies across elevational and longitudinal gradients in the western Cascade Mountains, Oregon, USA. Forest Ecology and Management 358: 154-164. https://doi.org/10.1016/j.foreco.2015.09.007.

Bell, D., M. Gregory, H. Roberts, R. Davis, and J. Ohmann. 2015b. How sampling and scale limit accuracy assessment of vegetation maps: A comment on Loehle et al. Forest Ecology and Management 358: 361-364. https://doi.org/10.1016/j.foreco.2015.07.017.

Bell, D., and D. Schlaepfer. 2016. On the dangers of model complexity without ecological justification in species distribution modeling. Ecological Modelling. 330: 50-59. https://doi.org/10.1016/j.ecolmodel.2016.03.012.

Bell, D., B. Wilson, C. Werstak, Jr., C. Oswalt, C. Perry. *In Press.* Understanding uncertainty in k-nearest neighbor small area estimation across scales using national forest inventory data. Submitted to *Frontiers in Forests and Global Change.*

Bidlack, A., S. Bisbing, B. Buma, D. D'Amore, P. Hennon, T. Huette, J. Krapek, R. Mulvey, and L. Oakes. 2017. Alternative interpretation and scale-based context for "No evidence of recent (1995-2013) decrease of yellow-cedar in Alaska" (Barrett and Pattison 2017). Canadian Journal of Forest Research 47: 1145-1151. https://doi.org/10.1139/cjfr-2017-0070.

Bidlack A., S. Bisbing, B. Buma, H. Diefenderfer, J. Fellman, W. Floyd, I. Giesbrecht, A. Lally, K. Lertzman, S. Perakis, D. Butman, D. D'Amore, S. Fleming, E. Hood, B. Hunt, P. Kiffney, G. McNicol, B. Menounos, and S. Tank. 2021. Climate-mediated changes to linked terrestrial and marine ecosystems across the northeast Pacific coastal temperate rainforest margin. Bioscience 71(6): 581-595. https://doi.org/10.1093/biosci/biaa171.

Bisbing, S., D. Cooper, D. D'Amore, and K. Marshall. 2016. Determinants of conifer distributions across peatland to forest gradients in the coastal temperate rainforest of southeast Alaska. Ecohydrology. 9: 354-367pp. https://doi.org/10.1002/eco.1640.

Bisbing, S., and D. D'Amore. 2018. Nitrogen dynamics vary across hydrologic gradients and by forest community composition in the perhumid coastal temperate rainforest of southeast Alaska. Canadian Journal of Forest Research. 48: 180-191. https://doi.org/10.1139/cjfr-2017-0178.

Blackard, J., M. Finco, E. Helmer, G. Holden, M. Hoppus, D. Jacobs, A. Lister, G. Moisen, M. Nelson, R. Riemann, B Ruefenacht, D. Salajanu, D. Weyermann, K. Winterberger, T. Brandeis, R. Czaplewski, R. McRoberts, P. Patterson, and R. Tymcio. 2008. Mapping US forest biomass using nationwide forest inventory data and moderate resolution information. Remote Sensing of Environment 112: 1658-1677. https://doi.org/10.1016/j.rse.2007.08.021.

Bonan, G. 1991. A biophysical surface energy budget analysis of soil temperature in the boreal forests of interior Alaska. Water Resources Research. 27(5): 767-781.

Braaten, J., W. Cohen, and Z. Yang. 2015. Automated cloud and cloud shadow identification in Landsat MSS imagery for temperate ecosystems. Remote Sensing of Environment. 169: 128-138. https://doi.org/10.1016/j.rse.2015.08.006.

Brackley, A., R. Haynes, and S. Alexander. 2009. Timber Harvests in Alaska: 1910–2006. Research Note PNW-RN-560. Portland, OR: U.S. Department of Agriculture, Forest Service, Pacific Northwest Research Station. 26 p.

Brannoch, S., and J. Moan, (Eds.). 2020. FS-R10-FHP. Forest Health Conditions in Alaska 2020. Anchorage, Alaska. U.S. Department of Agriculture, Forest Service, Alaska Region. Publication R10-PR-46. 76pp.

Breiman, L. 2001. Random Forests. Machine Learning 45: 5-32.

Buma, B., and T. Barrett. 2015. Spatial and topographic trends in forest expansion and biomass change, from regional to local scales. Global Change Biology. https://doi.org/10.1111/gcb.12915

Buma, B., J. Krapek, and R. Edwards. 2016. Watershed-scale forest biomass distribution in a perhumid temperate rainforest as driven by topographic, soil, and disturbance variables. Canadian Journal of Forest Research 46: 1-11pp. https://doi.org/10.1139/cjfr-2016-0041.

Buma, B., P. Hennon, C. Harrington, J. Popkin, J. Krapek, M. Lamb, L. Oakes, S. Saunders, and S. Zeglen. 2017. Emerging climate-driven disturbance processes: widespread mortality associated with snow-to-rain transitions across 10' of latitude and half the range of a climate-threatened conifer. Global Change Biology 23: 2903-2914. https://doi.org/10.1111/gcb.13555.

Buma, B., and T. Thompson. 2019. Long-term exposure to more frequent disturbances increases baseline carbon in some ecosystems: Mapping and quantifying the disturbance frequency-ecosystem C relationship. PLoS One 14(2). https://doi.org/10.1371/journal.pone.0212526.

Cahoon, S., O. Kuegler, G. Christensen, tech. (Eds.). 2020. Coastal Alaska's forest resources, 2004–2013: Ten-year Forest Inventory and Analysis report. Gen. Tech. Rep. PNW-GTR-979. Portland, OR: U.S. Department of Agriculture, Forest Service, Pacific Northwest Research Station. 73 p.

Caouette, J., and E. DeGayner. 2005. Predictive mapping for tree sizes and densities in southeast Alaska. Landscape and Urban Planning. 72: 49-63. https://doi.org/10.1016/j.landurbplan.2004.09.012.

Caouette, J. and E. DeGayner. 2008. Broad-scale classification and mapping of tree size and density attributes in productive old-growth forests in southeast Alaska's Tongass National Forest. Western Journal of Applied Forestry. 23(2).

Caouette, J., E. Steel, P. Hennon, P. Cunningham, C. Pohl, and B. Schrader. 2015. Influence of elevation and site productivity on conifer distributions across Alaskan temperate rainforests. Canadian Journal of Forest Research. 46: 249-261. https://doi.org/10.1139/cjfr-2015-0283.

Carrara, P., T. Ager, and J. Baichtal. Possible refugia in the Alexander Archipelago of southeastern Alaska during the late Wisconsin glaciation. Canadian Journal of Earth Science. 44: 229-244.

Cohen, J. 1960. A coefficient of agreement for nominal scales. Educational and Psychological Measurement. XX(1). https://doi.org/10.1177/001316446002000104.

Cohen, W., and T. Spies. 1992. Estimating structural attributes of Douglas-fir/western hemlock forest stands from Landsat and SPOT imagery. Remote Sensing of Environment. 41(1):17.

Cohen, W., and S. Goward. 2004. Landsat's role in ecological applications of remote sensing. Bioscience 54(6).

Cohen, W., Z. Yang, S. Healey, R. Kennedy, N. Gorelick. 2018. A LandTrendr multispectral ensemble for forest disturbance detection. Remote Sensing of Environment. 205(2018): 131-140. https://doi.org/10.1016/j.rse.2017.11.015.

Crist, E., and R. Cicone. 1984. A physically based transformation of thematic mapper data – the TM tasseled cap. IEEE Transactions on Geoscience and Remote Sensing. 22(3).

Daly, C., J. Smith, and M. Halbleib. 2018. PRISM Climate Group, Oregon State University. http://prism.oregonstate.edu. 1981-2010 High-Resolution Temperature and Precipitation Maps for Alaska. Created October 2018.

Daniels, J., M. Paruszkiewicz, and S. Alexander. 2016. Tongass National Forest timber demand: projections for 2015 to 2030. Gen. Tech. Rep. PNW-GTR-934. Portland, OR: U.S. Department of Agriculture, Forest Service, Pacific Northwest Research Station. 53 p.

Davis, R., B. Hollen, J. Hobson, J. Gower, and D. Keenum. 2016. Northwest Forest Plan—the first 20 years (1994–2013): status and trends of northern spotted owl habitats. Gen. Tech. Rep. PNW-GTR-929. Portland, OR: U.S. Department of Agriculture, Forest Service, Pacific Northwest Research Station. 54 p.

Davis, R., J. Ohmann, R. Kennedy, W. Cohen, M. Gregory, Z. Yang, H. Roberts, A. Gray, and T. Spies. 2015. Northwest Forest Plan–the first 20 years (1994-2013): status and trends of late-successional and old-growth forests. Gen. Tech. Rep. PNW-GTR-911. Portland, OR: U.S. Department of Agriculture, Forest Service, Pacific Northwest Research Station. 112 p.

Day, R. 2011. Evaluating Population Trends of Kittlitz's Murrelets in Alaska. Prepared for Alaska Department of Fish and Game, Division of Wildlife Conservation. 68p.

DellaSala, D., F. Moola, P. Alaback, P. Paquet, J. Schoen, and R. Noss. 2011. Temperate and boreal rainforests of the Pacific Coast of North America. Pp. 42–81 *in* DellaSala (ed.) Temperate and boreal rainforests of the world: ecology and conservation. Island Press, Washington, D.C.

Dewitz, J. 2019. National Land Cover Dataset (NLCD) 2016 Products [Data set]. U.S. Geological Survey. https://doi.org/10.5066/P96HHBIE.

Dubayah, R., J. Blair, S. Goetz, L. Fatoyinbo, M. Hansen, S. Healy, M. Hofton, G. Hurtt, J. Kellner, S. Luthcke, J. Armston, H. Tang, L. Duncanson, S. Hancock, P. Jantz, S. Marselis, P. Patterson, W. Qi and C. Silva. 2020. The global ecosystem dynamics investigation: high-resolution laser ranging of the Earth's forests and topography. Science of Remote Sensing. 1: 1000002. https://doi.org/10.1016/j.srs.2020.100002.

Dunleavy, M. Alaska Office of Governor. 2021. https://gov.alaska.gov/newsroom/2021/11/19/governor-dunleavy-criticizes-usda-plan-to-reinstate-the-roadless-rule/. Accessed 13 February 2022.

Dunleavy, M. Alaska Office of Governor. 2022. https://gov.alaska.gov/newsroom/2022/01/17/governor-dunleavy-announces-completed-land-exchange-in-southeast-alaska/. Accessed 20 January 2022.

Engler, R., A. Guisan, and L. Rechsteiner. 2004. An improved approach for predicting the distribution of rare and endangered species from occurrence and pseudo-absence data. Journal of Applied Ecology 41: 263-274.

Eskelson, B., H. Temesgen, V. Lemay, T. Barrett, N. Crookston, and A. Hudak. 2009. The roles of nearest neighbor methods in imputing missing data in forest inventory and monitoring databases. Scandinavian Journal of Forest Research. 24: 235-246. https://doi.org/10.1080/02827580902870490.

Federal Register 2021. Bears Ears National Monument. Proclamation 10285. Vol 86. No 197. https://www.govinfo.gov/content/pkg/FR-2021-10-15/pdf/2021-22672.pdf. Accessed 06 February 2022.

Fellman, J., D. D'Amore, E. Hood, P. Cunningham. 2017. Vulnerability of wetland soil carbon stocks to climate warming in the perhumid coastal temperate rainforest. Biogeochemistry. 133: 165-179. doi 10.1007/s10533-017-0324-y.

Fennel, A. 2016. Tongass National Forest: Forest Service's Actions Related to Its Planned Timber Program Transition. GAO-16-456. Government Accountability Office, 441 G St. N.W. Washington, DC 20548. 42 p.

Fenster, D. 2022. Tongass National Forest Young Growth Inventory Portal Story Map. https://usfs.maps.arcgis.com/apps/MapJournal/index.html?appid=e748ce92139c4100a65ad8b12510d620#. Accessed 06 February 2022.

Flood, N. 2013. Seasonal composite Landsat TM/ETM+ images using the medoid (a multi-dimensional median). Remote Sensing 5:6481-6500. https://doi.org/10.3390/rs5126481.

Gatziolis, D., and H. Andersen. 2008. A guide to LIDAR data acquisition and processing for the forests of the Pacific Northwest. Gen. Tech. Rep. PNW-GTR-768. Portland, OR: U.S. Department of Agriculture, Forest Service, Pacific Northwest Research Station. 32 p.

Genet, H., Y. He, Z. Lyu, A. D. McGuire, Q. Zhuang, J. Clein, D. D'Amore, A. Bennett, A. Breen, F. Biles, E. Euskirchen, K. Johnson, T. Kurkowski, S. Schroder, N. Pastick, T. S. Rupp, B. Wylie, Y. Zhang, X Zhou, Z. Zhu. 2017. The role of driving factors in historical and projected carbon dynamics of upland ecosystems in Alaska. Ecological Applications 28:1. 5-27pp. https://doi.org/10.1002/eap.1641.

Giles, P. 2001. Remote Sensing and Cast Shadows in Mountainous Terrain. Photogrammetric Engineering and Remote Sensing. 67:7. 833-839pp.

Google Simple Cloud Score. 2022. https://developers.google.com/earth-engine/apidocs/ee-algorithms-landsat-simplecloudscore. Repurposed in accordance with Google's Creative Commons 4.0 Attribution License. Accessed January 9, 2022.

Grasser, E., D. Vincent-Lang, and T. Schumacher. 2020. Trappers Harvest Record Number of Wolves on Prince of Wales and Associated Islands in 2019/2020. Alaska Department of Fish and Game, Division of Wildlife Conservation. Advisory Announcement 5 March, 2020. http://www.adfg.alaska.gov/static/applications/webintra/wcnews/2020/releases/03-05-2020.pdf

Gregory, M., J. Ohmann, H. Roberts, and R. Riemann. 2011. Nearest neighbor vegetation maps for landscape analysis and conservation planning: are they good enough, and how will I know? Poster.

Gregory, M. and H. M. Roberts. 2020. Pynnmap: Nearest-neighbor vegetation mapping with Python tools. https://github.com/lemma-osu/pynnmap. Accessed 08 February 2022.

Griscom, B., J. Adams, P. Ellis, R. Houghton, G. Lomax, D. Miteva, W. Schlesinger, D. Shoch, J. Siikamaki, P. Smith, P. Woodbury, C. Zganjar, A. Blackman, J. Campari, R. Conant, C. Delgado, P. Elias, T. Gopalakrishna, M. Hamsik, M. Herrero, J. Kiesecker, E. Landis, L. Laestadius, S. Leavitt, S. Minnemeyer, S. Polasky, P. Potapov, F. Putz, J. Sanderman, M. Silvius, E. Wollenberg, and J. Fargione. 2017. Natural climate solutions. Proceedings of the National Academy of Sciences. 114(44): 11645-11650. Doi: 10.1073/pnas.1710465114.

Gu, D., and A. Gillespie. 1998. Topographic Normalization of Landsat TM Images of Forest Based on Subpixel Sun-Canopy-Sensor Geometry. Remote Sensing of Environment 64: 166-175.

Hantson, S., and E. Chuvieco. 2011. Evaluation of different topographic correction methods for Landsat imagery. International Journal of Applied Earth Observation and Geoinformation 13: 691-700. https://doi.org/10.1016/j.jag.2011.05.001.

Hastings, K. 1997. When trees fall in the forest: stand structure following partial disturbance in the spruce-hemlock forests of southeast Alaska. Graduate Student Theses, Dissertations, and Professional Papers. 4652. University of Montana. https://scholarworks.umt.edu/etd/4652.

Hayward, G, S. Colt, M. McTeague, T. Hollingsworth, (Eds.). 2017. Climate change vulnerability assessment for the Chugach National Forest and the Kenai Peninsula. Gen. Tech. Rep. PNW-GTR-950. Portland, OR: U.S. Department of Agriculture, Forest Service, Pacific Northwest Research Station. 340 p.

Healy, S., W. Cohen, Z. yang, C. K. Brewer, E. Brooks, N. Gorelick, A. Hernandez, C. Huang, M. J. Hughs, R. Kennedy, R. Loveland, G. Moisen, T. Schroeder, S. Stehman, J. Vogelmann, C. Woodcock, L. Yang, Z. Zhu. 2018. Mapping forest change using stacked generalization: an ensemble approach. Remote Sensing of Environment. 204: 717-728. https://doi.org/10.1016/j.rse.2017.09.029.

Henderson, E., J. Ohmann, M. Gregory, H. Roberts, and H. Zald. 2014. Species distribution modelling for plant communities: stacked single species or multivariate modelling approaches? Applied Vegetation Science. 17: 516-527. Doi: 10.1111/avsc.12085.

Herz, N. 2021. Alaska Public Media. https://www.alaskapublic.org/2021/12/07/a-historic-settlement-turns-50-but-questions-linger-over-whether-it-was-fair/. Accessed 07 December 2021.

Hjerpe, E., and A. Hussain. 2016. Willingness to pay for ecosystem conservation in Alaska's Tongass National Forest: a choice modeling study. Ecology and Society 21(2):8. http://dx.https://doi.org/10.5751/ES-08122-210208.

Hoffman, K., B. Starzomki, K. Lertzman, I. Giesbrecht, and A. Trant. 2021. Old-growth forest structure in a low-productivity hypermaritime rainforest in coastal British Columbia, Canada. Ecosphere 12(5). Doi: 10.1002/ecs2.3513.

Hulten, E. 1968. Flora of Alaska and Neighboring Territories. A Manual of the Vascular Plants. Stanford University Press. 1032pp.

Jin, S., C. Homer, L. Yang, P. Danielson, J. Dewitz, C. Li, Z. Shu, G. Xian, and D. Howard. 2019. Overall methodology design for the United States National Land Cover Database 2016 products. Remote Sensing 11(2971). https://doi.org/10.3390/rs11242971.

Johnson, A., A. Clavijo, G. Hamar, D. Head, A. Thoms, W. Price, A. Lapke, J. Crotteau, L. Cerveny, H. Wilmer, L. Petershoare, A. Cook, and S. Reid. 2021. Wood Products for Cultural Uses: Sustaining Native Resilience and Vital Lifeways in Southeast Alaska, USA. Forests 12:90. https://doi.org/10.3390/f12010090.

Johnson, A., J. Bellmore, S. Haught, and R. Medel. 2019. Quantifying the Monetary Value of Alaska National Forests to Commercial Pacific Salmon Fisheries. North American Journal of Fisheries Management 39:1119–1131. https://doi.org/10.1002/nafm.10364.

Julin, K., and J. Caouette. 1997. Options for defining old-growth timber volume strata: a resource assessment. *In:* Julin, Kent R., comp. Assessments of wildlife viability, old-growth timber volume

estimates, forested wetlands, and slope stability. Gen. Tech. Rep. PNW-GTR-392. Portland, OR: U.S. Department of Agriculture, Forest Service, Pacific Northwest Research Station: 24-37. (Shaw, C. G., III, tech.coord.; Conservation and resource assessments for the Tongass land management plan revision).

Kane, V., A. Gillespie, R. McGaughey, J. Lutz, K. Ceder, and J. Franklin. 2008. Interpretation and topographic compensation of conifer canopy self-shadowing. Remote Sensing of Environment. 112: 3820-3832. https://doi.org/10.1016/j.rse.2008.06.001.

Kane, V., R. McGaughey, J. Bakker, R. Gersonde, J. Lutz, and J. Franklin. 2010. Comparisons between field- and LiDAR-based measures of stand structural complexity. Canadian Journal of Forest Research. 40: 761-773. https://doi.org/10.1139/X10-024.

Kauth, R., and G. Thomas. 1976. The tasselled cap – a graphic description of the spectral-temporal development of agricultural crops as seen by Landsat. Laboratory for Applications of Remote Sensing (LARS) Symposia. 159.

Keenan, R., G. Reams, F. Achard, J. de Freitas, A. Grainger, E. Lindquist. 2015. Dynamics of global forest area: Results from the FAO Global Forest Resources Assessment 2015. Forest Ecology and Management 352: 9-20. https://doi.org/10.1016/j.foreco.2015.06.014.

Kelly, D. 2013. Climate Change on the Tongass National Forest. Flyer. www.fs.fed.us/r10/tongass. Accessed 13 February 2022.

Kennedy, R. Z. Yang and W. Cohen. 2010. Detecting trends in forest disturbance and recovery using yearly Landsat time series: 1. LandTrendr -- Temporal segmentation algorithms. Remote Sensing of Environment 114(2010): 2897-2910.

Kennedy, R., J. Ohmann, M. Gregory, H. Roberts, Z. Yang, D. Bell, V. Kane, M. J. Hughes, W. Cohen, S. Powell, N. Neeti, T. Larrue, S. Hooper, J. Kane, D. Miller, J. Perkins, J. Braaten, and R. Seidl. 2018a. An empirical, integrated forest biomass monitoring system. Ecological Research Letters 13(2018): 025004. https://doi.org/10.1088/1748-9326/aa9d9e.

Kennedy R., Z. Yang, N. Gorelick, J. Braaten, L. Cavalcante, W. Cohen, and S. Healey. 2018b. Implementation of the LandTrendr Algorithm on Google Earth Engine. Remote Sensing 10(691). https://doi.org/10.3390/rs10050691.

Keyser, C., comp. 2008 (revised October 2, 2019). Southeast Alaska and Coastal British Columbia (AK) Variant Overview – Forest Vegetation Simulator. Internal Rep. Fort Collins, CO: U. S. Department of Agriculture, Forest Service, Forest Management Service Center. 40p.

Krankina, O., D. Dellasala, J. Leonard, and M. Yatskov. 2014. High-biomass forests of the pacific northwest: who manages them and how much is protected? Environmental Management. doi 10.1007/s00267-014-0283-1.

Krauss, M., G. Holton, J. Kerr, and C. West. 2011. Indigenous Peoples and Languages of Alaska. Fairbanks and Anchorage: Alaska Native Language Center and UAA Institute of Social and Economic Research. Online: https://www.uaf.edu/anla/collections/map/. Accessed 21 February 2022.

LaBau, V. 2013. History of Forest Survey in Alaska. Part II of a History of Forest Research in Alaska.

Leonawicz, M., M. Lindgren, T. Kurkowski, S. Rupp, J. Walsh. Historical Monthly and Derived Precipitation Products - 771m CRU TS 1901-2009. Revised 01 May 2015. Scenarios Network for Alaska and Arctic Planning, International Arctic Research Center, University of Alaska, Fairbanks. http://data.snap.uaf.edu/data/Base/AK_771m/historical/CRU_TS/Historical_Monthly_and_Derived_Precipitation_Products_771m_CRU_TS/. Accessed 10 May 2020.

Li, T. 1926. Soil Temperature as Influenced by Forest Cover. Yale School of Forestry Bulletin 18. 92.

Lister, A., M. Hoppus, and R. Czaplewski. 2005. K-Nearest neighbor imputation of forest inventory variables in New Hampshire. Remote Sensing for Field Users: Proceedings of the Tenth Forest Service Remote Sensing Applications Conference. Salt Lake City, Utah. 5-9 April, 2004.

Lister, A., H. Andersen, T. Frescino, D. Gatziolis, S. Healey, L. Heath, G. Liknes, R. McRoberts, G. Moisen, M. Nelson, R. Riemann, K. Schleeweis, T. Schroeder, J. Westfall, and B. Wilson. 2020. Use of remote sensing data to improve efficiency of national forest inventories: a case study from the United States national forest inventory. Forests 11:1364. https://doi.org/10.3390/f11121364.

Little, E. Jr. 1971. Atlas of United States trees, volume 1, conifers and important hardwoods: Misc. Pub. 1146. Washington, D.C.: U.S. Department of Agriculture. 9 p., 200 maps.

Lorenz, T., M. Raphael, R. Young, D. Lynch, S. Nelson, W. McIver. 2021. Status and trend of nesting habitat for the marbled murrelet under the Northwest Forest Plan, 1993 to 2017. Portland, OR: U.S. Department of Agriculture, Forest Service, Pacific Northwest Research Station. 64 p.

Lu, D., Q. Chen, G. Wang, L. Liu, G. Li, and E. Moran. 2016. A survey of remote sensing-based aboveground biomass estimation methods in forest ecosystems. International Journal of Digital Earth 9(1): 63-105. https://doi.org/10.1080/17538947.2014.990526.

Marcille, K., E. Berg, T. Morgan, and G. Christensen. 2021. Alaska's Forest Products Industry and Timber Harvest, 2015. Resource Bulletin. PNW-RB-271. Portland, OR: U.S. Department of Agriculture, Forest Service, Pacific Northwest Research Station.

Masek, J., M. Wulder, B. Markham, J. McCorkel, C. Crawford, J. Storey, and D. Jenstrom. 2020. Landsat 9: Empowering open science and applications through continuity. Remote Sensing of Environment 248:111968. https://doi.org/10.1016/j.rse.2020.111968.

Massey, F. 1951. The Kolmogorov–Smirnov test for goodness of fit. Journal of the American Statistical Association 46: 68–78.

McCune, B., and D. Keon. 2002. Equations for potential annual direct incident radiation and heat load. Journal of Vegetation Science. 13(4): 603-606.

McGuire, A., H. Genet, Z. Lyu, N. Pastick, S. Stackpoole, R. Birdsey, D. D'Amore, Y. He, T. S. Rupp, R. Striegl, B. Wylie, X. Zhou, Q. Zhuang, and Z. Zhu. 2018. Assessing historical and projected carbon balance of Alaska: A synthesis of results and policy / management implications. Ecological Applications 28:6. 1396-1412.

McNicol, G., C. Bulmer, D. D'Amore, P. Sanborn, S. Saunders, I. Giesbrecht, S. Gonzalez Arriola, A. Bidlack, D. Butman and B. Buma. 2019. Large, climate-sensitive carbon stocks mapped with pedology-informed machine learning in the North Pacific coastal temperate rainforest. Environmental Research Letters. https://doi.org/10.1088/1748-9326/ aaed52.

McRoberts, R., E. Tomppo, A. Finley, and J. Heikkinen. 2007. Estimating areal means and variances of forest attributes using the k-Nearest Neighbors technique and satellite imagery. Remote Sensing of Environment. 111: 466-480. https://doi.org/10.1016/j.rse.2007.04.002.

McRoberts, R. 2010. The effects of rectification and Global Position System errors on satellite image-based estimates of forest area. Remote Sensing of Environment. 114: 1710-1717. https://doi.org/10.1016/j.rse.2010.03.001.

McRoberts, R., S. Magnussen, E. Tomppo, and G. Chirici. 2011. Parametric, bootstrap, and jackknife variance estimators for the k-Nearest Neighbors technique with illustrations using forest inventory and satellite image data. Remote Sensing of Environment. 115: 3165-3174. https://doi.org/10.1016/j.rse.2011.07.002.

McRoberts, R., E. Naesset, and T. Gobakken. 2016. The effects of temporal differences between map and ground data on map-assisted estimates of forest area and biomass. Annals of Forest Science. 73:839-847. doi 10.1007/s13595-015-0485-6.

Megown, K. 2016. USFS Tree Canopy Cover, Coastal Alaska. USDA Forest Service Remote Sensing Applications Center (RSAC), 2222 West 2300 South Salt Lake City, Utah 84119 USA. https://data.fs.usda.gov/geodata/rastergateway/treecanopycover/. Accessed 13 February 2022.

Moisen, G., K. McConville, T. Schroeder, S. Healey, M. Finco, and T. Frescino. 2020. Estimating Land Use and Land Cover Change in North Central Georgia: Can Remote Sensing Observations Augment Traditional Forest Inventory Data? Forests 11:856. https://doi.org/10.3390/f11080856.

NASA/METI/AIST/Japan Space systems, and U.S./Japan ASTER Science Team. *ASTER Global Digital Elevation Model V003*. 2018, distributed by NASA EOSDIS Land Processes DAAC, https://doi.org/10.5067/ASTER/ASTGTM.003

Natural Resources Conservation Service, USDA. 2022. Web Soil Survey. https://websoilsurvey.nrcs.usda.gov/. Accessed 06 February 2022.

Neiland, B. 1971. The Forest-Bog Complex of Southeast Alaska. Vegetatio 22(1/3): 1-64.

Nelson, M., J. Garner, B. Tavernia, S. Stehman, R. Riemann, A. Lister, C. Perry. 2021. Assessing map accuracy from a suite of site-specific, non-site specific, and spatial distribution approaches. Remote Sensing of Environment. 260: 112442. https://doi.org/10.1016/j.rse.2021.112442.

Nowacki, G., Spencer, P., Fleming, M, Brock, T., Jorgenson, T., 2002. Unified Ecoregions of Alaska: 2001. U.S. Geological Survey Open-File Report 02-297 (map). http://agdc.usgs.gov/data/usgs/erosafo/ecoreg/index.html

Ohmann, J. and M. Gregory. 2002. Predictive mapping of forest composition and structure with direct gradient analysis and nearest neighbor imputation in coastal Oregon, U.S.A. Canadian Journal of Forest Research (32): 725–741.

Ohmann, J., M. Gregory, E. Henderson, H. Roberts. 2011. Mapping gradients of community composition with nearest-neighbor imputation: extending plot data for landscape analysis. Journal of Vegetation Science (22): 660–676.

Ohmann, J., M. Gregory, H. Roberts, W. Cohen, R. Kennedy, and Z. Yang. 2012. Mapping change of older forest with nearest-neighbor imputation and Landsat time-series. Forest Ecology and Management 272: 13-25pp. https://doi.org/10.1016/j.foreco.2011.09.021.

Ohmann, J., M. Gregory, and H. Roberts. 2014. Scale considerations for integrating forest inventory plot data and satellite image data for regional forest mapping. Remote Sensing of Environment. 151: 3-15pp. https://doi.org/10.1016/j.rse.2013.08.048.

Olofsson, P., G. Foody, S. Stehman, and C. Woodcock. 2013. Making better use of accuracy data in land change studies: Estimating accuracy and area and quantifying uncertainty using stratified estimation. Remote Sensing of Environment. 129: 122-131. https://doi.org/10.1016/j.rse.2012.10.031.

Olofsson, P., G. Foody, M. Herold, S. Stehman, C. Woodcock, and M. Wulder. 2014. Good practices for estimating area and assessing accuracy of land change. Remote Sensing of Environment. 148: 42-57. https://doi.org/10.1016/j.rse.2014.02.015.

Ott, R., and G. Juday. 2002. Canopy gap characteristics and their implications for management in the temperate rainforests of southeast Alaska. Forest Ecology and Management. 159: 271-291.

Palmer, M. 1993. Putting things in even better order: the advantages of canonical correspondence analysis. Ecology 74(8): 2215-2230.

Pendleton, B., R. Monahan, F. Cole, P. O'Connor. 2013. Leader's Intent: Forest Stewardship and Young Growth Management on the Tongass National Forest. R10-MB-777.

Person, D., M. Kirchhoff, V. Van Ballenberghe, G. Iverson, and E. Grossman. 1996. The Alexander Archipelago wolf: a conservation assessment. Gen. Tech. Rep. PNW-GTR-384. Portland, OR: U.S. Department of Agriculture, Forest Service, Pacific Northwest Research Station. 42 p.

Piatt, J., K. Kuletz, A. Burger, S. Hatch, V. Friesen, T. Birt, M. Arimitsu, G. Drew, A. Harding, and K. Bixler. 2007. Status review of the Marbled Murrelet (*Brachyramphus marmoratus*) in Alaska and British Columbia: U.S. Geological Survey Open-File Report 2006-1387. 258 p.

Pierce, K., T. Lookingbill, and D. Urban. 2005. A simple method for estimating potential relative radiation (PRR) for landscape-scale vegetation analysis. Landscape Ecology. 20: 137-147. https://doi.org/10.1007/s10980-004-1296-6.

Pierce, K., J. Ohmann, M. Wimberly, M. Gregory, and J. Fried. 2009. Mapping wildland fuels and forest structure for land management: a comparison of nearest neighbor imputation and other methods. Canadian Journal of Forest Research 39:1901-1916. https://doi.org/10.1139/X09-102.

R Core Team. 2019. R: A language and environment for statistical computing. R Foundation for Statistical Computing, Vienna, Austria. http://www.R-project.org/.

Ricker, W. 1984. Computation and uses of central trend lines. Canadian Journal of Zoology, 62, 1897−1905.

Riemann, R., B. Wilson, A. Lister, and S. Parks. 2010. An effective assessment protocol for continuous geospatial datasets of forest characteristics using USFS Forest Inventory and Analysis (FIA) data. Remote Sensing of Environment. 114: 2337-2352. https://doi.org/10.1016/j.rse.2010.05.010.

Roy, D., V. Kovalskyy, H. Zhang, E. Vermote, L. Yan, S. Kumar, and A. Egorov. 2016. Characterization of Landsat-7 to Landsat-8 reflective wavelength and normalized difference vegetation index continuity. Remote sensing of Environment, 185, 57-70.

Sabol, D. Jr., A. Gillespie, J. Adams, M. Smith, and C. Tucker. 2002. Structural stage in Pacific Northwest forests estimated using simple mixing models of multispectral images. Remote Sensing of Environment. 80(1): 1-16. https://doi.org/10.1016/S0034-4257(01)00245-0.

Schleeweis, K., G. Moisen, T. Schroeder, C. Toney, E. Freeman, S. Goward, C. Huang, and J. Dungan. 2020. US National Maps Attributing Forest Change: 1986-2010. Forests 11:653. https://doi.org/10.3390/f11060653.

Schneider, E., and A. Larson. 2017. Spatial aspects of structural complexity in Sitka spruce – western hemlock forests, including evaluation of a new canopy gap delineation method. Canadian Journal of Forest Research. 47: 1033-1044. https://doi.org/10.1139/cjfr-2017-0029.

Sealaska 11 January 2021. Sealaska transitioning out of logging operations. https://www.sealaska.com/mysealaska/sealaska-transitioning-out-of-logging-operations/. Accessed 13 February 2022.

Sexton, J., X. Song, M. Feng, P. Noojipady, A. Anand, C. Huang, D, Kim, K. Collins, S. Channan, C. DiMiceli, and J. Townshend. 2013. Global, 30-m resolution continuous fields of tree cover: Landsat-based rescaling of MODIS vegetation continuous fields with lidar-based estimates of error. International Journal of Digital Earth 6(5): 427-448. https://doi.org/10.1080/17538947.2013.786146.

Shanley, C., S. Pyare, M. Goldstien, P. Alaback, D. Albert, C. Beier, T. Brinkman, R. Edwards, E. Hood, A. MacKinnon, M. McPhee, T. Patterson, L. Suring, D. Tallmon, M. Wipfli. 2015. Climate change implications in the northern coastal temperate rainforest of North America. Climatic Change. 130: 155-170. doi 10.1007/s10584-015-1355-9.

Sisk, J. 2007. The Southeastern Alaska Timber Industry: Historical Overview and Current Status. The Nature Conservancy. https://www.conservationgateway.org/ConservationByGeography/NorthAmerica/UnitedStates/alaska/seak/era/cfm/Documents/9.6_TimberIndustry.pdf. Accessed Nov 01, 2019.

Smith, R., and A. Gray. 2021. Strategic monitoring informs wilderness management and socioecological benefits. Conservation Science and Practice. 3:e482. https://doi.org/10.1111/csp2.482.

Stage, A., and N. Crookston. 2007. Partitioning error components for accuracy assessment of near-neighbor methods of imputation. Forest Science. 53(1).

Stow, D., A. Hope, D. McGuire, D. Verbyla, J. Gamon, F. Huemmrich, S. Houston, C. Racine, M. Sturm, K. Tape, L. Hinzman, K. Yoshikawa, C. Tweedie, B. Noyle, C. Silapaswan, D. Douglas, B. Griffith, G. Jia, H. Epstien, D. Walker, S. Daeschner, A. Petersen, L. Zhou, and R. Myneni. 2004. Remote sensing of vegetation and land-cover change in arctic tundra ecosystems. Remote Sensing of Environment 89: 281-308. https://doi.org/10.1016/j.rse.2003.10.018.

Southeast Alaska by the Numbers 2019. Rain Coast Data. Southeast Conference, 612 West Willoughby Avenue, Suite B Juneau, AK 99801. www.seconference.org. Accessed Nov 1, 2019.

ter Braak, C. 1987. The analysis of vegetation-environment relationships by canonical correspondence analysis. Vegetatio 69: 69-77.

Taylor, K., R. Stouffer, and G. Meehl. 2012. An overview of CMIP5 and the Experiment Design. Bulletin of the American Meteorological Society 93(4): 485-298. https://doi.org/10.1175/BAMS-D-11-00094.1.

Thompson, R.; K. Anderson, P. Bartlein, 1999. Digital representations of tree species range maps from "Atlas of United States trees" by Elbert L. Little, Jr. (and other publications). In: Atlas of relations between climatic parameters and distributions of important trees and shrubs in North America. Denver, CO: U.S. Geological Survey, Information Services (Producer). On file at: U.S. Department of Agriculture, Forest Service, Rocky Mountain Research Station, Fire Sciences Laboratory, Missoula, MT; FEIS files. [82831]

University of Alaska Fairbanks. Federal Indian Law for Alaska Tribes. https://www.uaf.edu/tribal/112/index.php. Accessed 06 February 2022.

USDA 2001. Federal Register Vol 66, No. 9. US Department of Agriculture, US Forest Service. 36 CFR Part 294. Special Areas; Roadless Area Conservation: Final Rule.

USDA 2008. Helicopter access to conduct forest inventory and analysis (FIA) in wilderness. Record of Decision. USDA Forest Service – Alaska Region.

USDA 2012. Tongass National Forest Timber Classification, 1978. https://www.sciencebase.gov/catalog/item/51d440dde4b09630fbdc52d5. Accessed 13 February 2022.

USDA 2014. Forest inventory and Analysis Fiscal Year 2014 Business Report. United States Department of Agriculture, Forest Service. FS-1053.

USDA 2021a. Special Areas; Roadless Area Conservation; National Forest System Lands in Alaska. Notice of Proposed Rulemaking: Request for Comment. Federal Register Volume 86, No 223. 23 November 2021.

USDA 2021b. USDA Announces Southeast Alaska Sustainability Strategy, Initiates Action to Work with Tribes, Partners and Communities. https://www.usda.gov/media/press-releases/2021/07/15/usda-announces-southeast-alaska-sustainability-strategy-initiates. Accessed 06 February 2022.

USDA Forest Service Forest Inventory and Analysis National Program Library. 2021c. Field Guides, Methods, and Procedures. https://www.fia.fs.fed.us/library/field-guides-methods-proc/. Accessed 06 February 2022.

USEPA 2021. Inventory of US Greenhouse Gas Emissions and Sinks 1990-2019.

US Forest Service Alaska Region. 1997. Tongass National Forest Land Management Plan. USDA, Forest Service, Alaska Region. PO Box 21628 Juneau, Alaska 99802. https://www.fs.usda.gov/detail/tongass/landmanagement/planning/?cid=stelprdb5445359. Accessed 13 February 2022.

US Forest Service Alaska Region R10-MB-769j December 2016. Tongass National Forest Land and Resource Management Plan. USDA, Forest Service, Alaska Region, PO Box 21628 Juneau, Alaska 99802 516p.

US Geological Survey. Landsat 7 ETM+. https://www.usgs.gov/land-resources/nli/landsat/data-tools. Accessed 10 May 2020.

Van Rossum, G. and F. Drake. 2009. Python 3 Reference Manual, Scotts Valley, CA: CreateSpace.

Viereck, L., and E. Little. 1986. Alaska Trees and Shrubs. University of Alaska Press. 265pp.

Vynne, C., E. Dovichin, N. Fesco, N. Dawson, A. Joshi, B. Law, K. Lertzman, S. Rupp, F. Schmiegelow, and E. J. Trammell. 2021. The importance of Alaska for climate stabilization, resilience, and biodiversity conservation. Frontiers in Forests and Global Change 4:701277. https://doi.org/10.3389/ffgc.2021.701277.

Wang, J., D. Sulla-Menashe, C. Woodcock, O. Sonnentag, R. Keeling, and M. Friedl. 2019. ABoVE: Landsat-derived Annual Dominant Land Cover Across ABoVE Core Domain, 1984-2014. ORNL DAAC, Oak Ridge, Tennessee, USA. https://doi.org/10.3334/ORNLDAAC/1691.

Weiss, A. 2001. Topographic Position and Landforms Analysis. The Nature Conservancy. Poster.

Wells, J., N. Dawson, N. Culver, F. Reid, and S. Siegers. 2020. The state of conservation in North America's boreal forest: issues and opportunities. Frontiers in Forests and Global Change 3:90. https://doi.org/10.3389/ffgc.2020.00090.

Wilson, B., C. Woodall, and D. Griffith. 2013. Imputing forest carbon stock estimates from inventory plots to a nationally continuous coverage. Carbon Balance and Management 8:1. https://doi.org/10.1186/1750-0680-8-1.

Wolken, J., T. Hollingsworth, T. Rupp, F. Chapin III, S. Traincor, T. Barrett, P. Sullivan, A. McGuire, E. Euskirchen, P. Hennon, E. Beever, J. Conn, L. Crone, D. D'Amore, N. Fresco, T. Hanley, K. Kielland, J. Kruse, T. Patterson, E. Schuur, D. Verbyla, and J. Yarie. 2011. Evidence and implications of recent and projected climate change in Alaska's forest ecosystems. Ecosphere 2(11):124. https://doi.org/10.1890/ES11-00288.1.

Yatskov, M., M. Harmon, T. Barrett, K. Dobelbower. 2019. Carbon pools and biomass stores in the forests of Coastal Alaska: Uncertainty of estimates and impact of disturbance. Forest Ecology and Management (434): 303-317.

Young, N., R. Anderson, S. Chignell, A. Vorster, R. Lawrence, and P. Evangelista. 2017. A survival guide to Landsat preprocessing. Ecology. 98(4): 920-932. https://doi.org/10.1002/ecy.1730.

Zald, H., J. Ohmann, H. Roberts, M. Gregory, E. Henderson, R. McGaughey, J. Braaten. 2014. Influence of lidar, Landsat imagery, disturbance history, plot location accuracy, and plot size on accuracy of imputation maps of forest composition and structure. Remote Sensing of Environment. 143: 26-38. https://doi.org/10.1016/j.rse.2013.12.013.

Zhao, F., C. Huang, S. Goward, K. Schleeweis, K. Rishmawi, M. Lindsey, E. Denning, L. Keddell, W. Cohen, Z. Yang, J. Dungan, A. Michaelis. Development of Landsat-based annual US forest disturbance history maps (1986-2010) in support of the North American Carbon Program (NACP). Remote Sensing of Environment 209: 312-326. https://doi.org/10.1016/j.rse.2018.02.035.

Zhao, P., D. Lu, G. Wang, C. Wu, Y. Huang, S. Yu. 2016. Examining Spectral Reflectance Saturation in Landsat Imagery and Corresponding Solutions to Improve Forest Aboveground Biomass Estimation. Remote Sensing 8:469. https://doi.org/10.3390/rs8060469.

Zhu, Z., and A. McGuire (Eds.). 2016. Baseline and projected future carbon storage and greenhouse-gas fluxes in ecosystems of Alaska: U.S. Geological Survey Professional Paper 1826, 196. https://doi.org/10.3133/pp1826.

Zhu, Z., and C. Woodcock. 2011. Object-based cloud and cloud shadow detection in Landsat imagery. Remote Sensing of Environment 118: 83-94. https://doi.org/10.1016/j.rse.2011.10.028.

Zhu, Z., and C. Woodcock. 2014. Automated cloud, cloud shadow, and snow detection in multi-temporal Landsat data: An algorithm designed specifically for monitoring land cover change. Remote Sensing of Environment 152: 217-234pp. https://doi.org/10.1016/j.rse.2014.06.012.